2014-01-29

The role of synovial progenitor cells in cartilage repair

Mak, Joyce

UNIVERSITY OF CALGARY

The role of synovial progenitor cells in cartilage repair

by

Joyce Mak

A THESIS

SUBMITTED TO THE FACULTY OF GRADUATE STUDIES

IN PARTIAL FULFILMENT OF THE REQUIREMENTS FOR THE

DEGREE OF MASTER OF SCIENCE

DEPARTMENT OF MEDICAL SCIENCE

CALGARY, ALBERTA

JANUARY, 2014

Abstract

In this study, we have isolated a Sca-1 positive population of mouse synovial cells that contains progenitors capable of chondrogenesis. Intra-articular injection of Sca-1^{+}-GFP^{+} synovial cells preserved proteoglycan content in the cartilage following cartilage injury but GFP expression could not be detected in the injury sites. Histological analysis suggests that *in vivo* mechanical stimulation of the injected cells due to joint loading results in the secretion of GAGs by the exogenous cells and thereby protects the joints from further degradation. Furthermore, progressive changes in cell morphology were observed in Sca-1^{+} synovial cells in response to injury, changing from a flatten, fibroblast-like appearance to a spherical and detached morphology 48 hours after injury. The presented study provides insight as to how endogenous synovial cells might act in response to injury as well as a mechanism by which the cells could protect the joint from degradation.

Acknowledgements

I would like to thank Roman Krawetz for giving me the opportunity to work on such an exciting project and for the invaluable guidance that he has given me.

The Dynamic Duo (aka Dave Rushforth and Tad Foniok) working at the Experimental Imaging Centre for their help and expertise in MRI as well as their willingness to accommodate my timed experiments and my endless list of questions.

Catherine Leonard for her willingness to help me with the animal surgeries and the histological analysis.

My committee members, Jeff Dunn and John Matyas, for their willingness to take part in my academic journey. Their guidance was crucial in shaping and streamlining the project.

The current and past lab members as well as my officemates for providing advice, support, and encouragement in the times that I have struggled.

Table of Contents

ABSTRACT I

ACKNOWLEDGEMENTS II

TABLE OF CONTENTS III

LIST OF FIGURES AND ILLUSTRATIONS VI

LIST OF SYMBOLS, ABBREVIATIONS AND NOMENCLATURE XI

CHAPTER ONE: INTRODUCTION 12
1.1 OVERVIEW 12
1.2 SYNOVIAL JOINT 13
1.2.1 Cartilage Biology 14
1.2.2 Extracellular Matrix (ECM) 15
1.2.3 Synovial Tissue 16
1.2.4 Synovial Fluid 17
1.3 STEM CELL BASICS 17
1.3.1 Adult Stem Cells – Mesenchymal Stem Cells (MSCs) 19
1.3.2 Synovial MSCs 21
1.3.3 Intra-articular injection of exogenous MSCs 22
1.4 Mouse Model- MRL/MpJ (Superhealer) mice 23
1.5 Rationale of project 24
1.6 Hypothesis 25
1.7 Aims 25

CHAPTER TWO: CHARACTERIZING MOUSE SYNOVIUM 26
2.1 BACKGROUND 26
2.2 MATERIALS AND METHODS 30
2.2.1 Histology 30
2.2.1.1 Decalcification 30
2.2.1.2 Safranin- O/Fast-green 30
2.2.1.3 Prussian Blue 31
2.2.1.4 Immunohistochemistry 31
2.2.2 Isolating murine synovial cells 32
2.2.3 In vitro detection of Sca-1 expressing cells 33
2.2.4 Sca-1 selection of cells 33
2.2.5 Tri-lineage (Adipo-, Osteo-, and Chondrogenic) Differentiation 34
2.3 RESULTS 35
2.3.1 PDGFRα is universally expressed while Sca-1 is localized to the synovium 35
2.3.2 Sca-1 expressing cells are found in mouse synovium 36

2.3.3 Sca-1 purified synovial cells display tri-differentiation potential 36
2.4 DISCUSSION 40

CHAPTER THREE: CHARACTERIZING ENDOGENOUS RESPONSE TO CARTILAGE INJURY 47
3.1 BACKGROUND 47
3.2 MATERIALS AND METHODS 50
3.2.1 Creating surgical apparatus- stopped needle 50
3.2.2 Inducing cartilage defect 51
3.2.3 Experimental outline 52
3.2.4 Magnetic Resonance Imaging (MRI) 52
3.2.5 Characterizing defect size by image analysis 53
3.2.6 Histological Analysis 53
3.2.6.1 Decalcification 53
3.2.6.2 Safranin-O/Fast-green 54
3.2.6.3 Immunohistochemistry 54
3.2.7 Cartilage grading 55
3.3 RESULTS 55
3.3.1 Characterization of defect with MRI and histology. 55
3.3.2 Defects can be visualized with MRI up to 4 weeks post-injury in both strains56
3.3.3 MRL/MpJ mice display superior repair compared to C57BL/6 mice 56
3.3.4 C57 mice display extensive infiltration by various cell types into injury site.61
3.3.5 MRL mice display minimal cell infiltration into defect site 67
3.4 DISCUSSION 67

CHAPTER FOUR: EVALUATING THE ROLE OF EXOGENOUS SYNOVIAL PROGENITOR CELLS IN A CARTILAGE INJURY MODEL SYSTEM 74
4.1 BACKGROUND 74
4.2 MATERIALS AND METHODS 75
4.2.1 Isolating murine synovial cells 75
4.2.2 Sca-1 Selection of cells 76
4.2.3 GFP Lentiviral Transduction 77
4.2.4 Toxicity Assay 78
4.2.5 Receptor Internalization 78
4.2.6 Animal experimental outline 79
4.2.7 Injection Apparatus 80
4.2.8 Intra-articular injection 80
4.2.9 Inducing cartilage defect 81
4.2.10 Magnetic Resonance Imaging 82
4.2.11 Histological Analysis 83
4.2.11.1 Decalcification 83
4.2.11.2 Safranin-O/ Fast-green 83
4.2.11.3 Immunohistochemistry 83

4.2.11.4 Prussian Blue 85
4.2.12 Scratch-wound assay 85
4.3 RESULTS 86
4.3.1 Sca-1 cell population is heterogenous and GFP lentiviral transduction was not efficient 86
4.3.2 Labelling of primary C57BL/6 synovial cells with BioMag Streptavidin beads were not toxic.....86
4.3.3 Maximum internalization of magnetically bound Sca-1 receptor is reached in 30 minutes.....90
4.3.4 Intra-articular injection of magnetically labelled cells results in localized hypointense signaling.....90
4.3.5 Minimal difference between MRL and C57 derived Sca-1^+ cell treatment of focal cartilage injury as assessed by MRI.....91
4.3.6 No observable difference in cartilage grading between C57 and MRL Sca-1^+ cell treated joints.....91
4.3.7 Cells remain viable following intra-articular injection 94
4.3.8 Injected Sca-1^+-GFP^+ synovial cells, irrespective of mouse strain and time point, are absent in the defect.....98
4.3.9 Sca-1^+-GFP^+ synovial cells do not participate in active migration 98
4.4 DISCUSSION.....101

CHAPTER FIVE: DISCUSSION.....109
5.1 Large quantities of purified MSCs may not be required for joint protection 109
5.2 Intra-articular injection of exogenous synovial progenitors leads to the production of GAGs 110
5.3 In response to *in vitro* injury, cells change morphology and detach 111
5.4 No observable difference between animals treated with C57 and MRL cells – C57 synovial cells are not overtly deficient in repair.....112
5.5 Summary.....113
5.6 Limitations.....114

APPENDICES 116
Appendix A: QPCR analysis of Tri-lineage Differentiation 116
Appendix B: MRI Sample Preparation.....118
Appendix C: Setup for Intra-articular Injections.....120
Appendix D: Positive and Negative controls for Sca-1, F4/80 and c-Kit.....121
References.....123

List of Figures and Illustrations

Figure 2-1 Histological assessment of PDGFRα. Mouse embryo at dpc 15 (A-C) was used as the positive control. Staining for PDGFRα was present in the mesenchyme (M) of the embryo (B) but was absent in the negative control (C). In the mouse knee joint (E), staining for PDGFRα was present in the synovium (S) as well as in the cartilage (C). Staining in the knee joint was absent in the negative control (F). A hematoxylin and eosin stained embryo (A) as well as a Safranin-O stained knee joint (D) are provided for reference. 37

Figure 2-2 Histological assessment of Sca-1. Periosteum (A, B) was used as the positive control. Positive staining is seen only in the cambium (Cm) layer and not in the fibrous (F) layer of the periosteum. Staining is absent in the periosteum in the negative control (B). In the knee joint (C), positive staining was seen in the synovium (S) but was not seen cartilage (Cr). Staining was not seen in the knee joint of the negative control (D). 38

Figure 2-3 Sca-1 expressing cells exist in mouse synovium. Primary cells isolated from C57BL/6 mouse synovium (A) using the outgrowth method display healthy, rounded morphology. Incubation with magnetic particles alone for 30 minutes resulted in minimal unspecific labelling (B). Incubation with magnetically bound Sca-1 antibody for 30 minutes revealed Sca-1 expressing cells, as detected by Prussian Blue stain (B) and counterstained with nuclear fast red (C). 39

Figure 2-4 Adipogenic differentiation with C57BL/6 synovium derived Sca-1^+ cells. At the end of 21 days, control wells (A, B) as well as experimental wells (E, F) contained oil droplets as detected by Oil Red O. Experimental wells fixed at the midpoint of 21 days contained fewer oil droplets (C, D). 41

Figure 2-5 Osteogenic differentiation with C57BL/6 synovium derived Sca-1^+ cells. At the end of 21 days, both control (A, B) and experimental wells (E, F) contained nodules that stained positive with Alizarin Red, indicative of calcium deposits. At the midpoint of 21 days (C, D), experimental wells seem to contain more nodules compared to wells at the end of 21 days but nodules were smaller. 42

Figure 2-6 Chondrogenic differentiation with C57BL/6 synovium derived Sca-1^+ cells. At the end of 21 days, control wells (A, B) did not stain blue with Alcian blue. At the midpoint of 21 days, cell bodies in the experimental wells (C, D) stained blue, indicative of proteoglycan production. At the end of 21 days (E, F), proteoglycan deposits could be detected although overall staining was low. 43

Figure 3-1 Characterization of defect. A 26G stopped needle (A) was created to induce focal defects in mice. The surgical apparatus as a diameter of 45 μm and a bead-to-needle tip

distance of approximately 1450 µm. To confirm injury, the injured leg was disarticulated and india ink was used to increase contrast for visualization of defect (B), which is seen in the yellow box. When defect size was measured from the MRI scans (C), the defect measurements were 375 µm in diameter and 1125 µm in length. The yellow lines on the MRI scan indicate the dimentions in which the measurements were taken. Sample scanned in the MRI was also analyzed histologically (D) and the defect opening, as indicated by the yellow line, was measured to be 441.7 µm. 57

Figure 3-2 MRI evaluation of cartilage defect in C57BL/6 mice at 0, 2, and 4 weeks post-injury. Evidence of a defect, as indicated in the yellow box, can be seen at each time point in the MRI as well as in the corresponding Safranin-O stained sections. 58

Figure 3-3 MRI evaluation of cartilage defect in MRL/MpJ mice at 0, 2, and 4 weeks post-injury. Evidence of a defect, as indicated in the yellow box, can be seen at each time point in the MRI as well as in the corresponding Safranin-O stained sections. 59

Figure 3-4 Correlation of signal intensity with histology. In both strains, repair tissue is observed to be hypointense when proteoglycan production has begun (red arrows). Areas with lack of proteoglycans are observed to display higher signal intensity (yellow arrows), which can be due to the magic angle effect or due to increased fluid content. Areas of low signal intensity do not always correlate with proteoglycan content. Low signal intensity can be seen in a region of the patella (purple arrow) where proteoglycan content, as assessed by Safranin-O, is low..... 60

Figure 3-5 Comparison of total joint morphology in the poorest healers at 4 weeks post injury. Level of repair was assessed by blinded cartilage grading. In both MRI and histology, the C57 sample displayed extensive changes in tissue morphology, especially at the patella tendon. A diminished growth plate as well as the loss of proteoglycan content in the surrounding articular cartilage are also seen in the C57 sample. In contrast, the MRL sample display a robust growth plate and no gross changes in patella tendon morphology. Proteoglycan content in the cartilage surrounding the defect is also diminished in the MRL sample. 62

Figure 3-6 Statistical analysis of cartilage gradings at 4 weeks post injury in both C57 and MRL mice. MRL mice display significantly superior repair compared to C57 animals. 63

Figure 3-7 Sca-1 analysis during early cartilage repair in C57BL/6 mice at 0, 2 and 4 weeks post surgery. Defects are indicated in the yellow boxes. Sca-1, a marker for undifferentiated cells, is strongly localized in the defects at both 2 and 4 weeks. P- patella; C- cartilage. See appendix for positive and negative controls for Sca-1 staining.... 64

Figure 3-8 F4/80 analysis during early cartilage repair in C57BL/6 mice at 0, 2 and 4 weeks post surgery. Defects are indicated in the yellow boxes. F4/80, a macrophage marker can be seen at 0 weeks but is strongly localized in the defects at both 2 and 4 weeks. P-

patella; C- cartilage; M-marrow. See appendix for positive and negative controls for F4/80 staining..... 65

Figure 3-9 C-Kit analysis during early cartilage repair in C57BL/6 mice at 0, 2 and 4 weeks post surgery. Defects are indicated in the yellow boxes. C-kit, a marker for cells of hematopoietic origin, can be seen to localize to the defect only at 4 weeks. P- patella; C- cartilage. See appendix for positive and negative controls for c-Kit staining. 66

Figure 3-10 Sca-1 analysis during early cartilage repair in MRL/MpJ mice at 0, 2 and 4 weeks post surgery. Defects are indicated in the yellow boxes. Sca-1, a marker for undifferentiated cells, is absent all time points. P- patella; C- cartilage. See appendix for positive and negative controls for Sca-1 staining. 68

Figure 3-11 F4/80 analysis during early cartilage repair in MRL/MpJ mice at 0, 2 and 4 weeks post surgery. Defects are indicated in the yellow boxes. F4/80, a macrophage marker, is present at only 2 weeks. P- patella; C- cartilage. See appendix for positive and negative controls for F4/80 staining..... 69

Figure 3-12 C-Kit analysis during early cartilage repair in MRL/MpJ mice at 0, 2 and 4 weeks post surgery. Defects are indicated in the yellow boxes. C-Kit, a marker for cells of hemtopoeitc origin, is absent all time points. P- patella; C- cartilage. See appendix for positive and negative controls for c-Kit staining. 70

Figure 4-1 Evaluation of GFP lentiviral transduction efficiency with flow cytometry. Absence of clusters with Sca-1^{+}-GFP^{-} cells (A) indicate heterogeneity in the cells purified for Sca-1. Analysis of Sca-1^{+}-GFP^{+} cells (B) resulted in a two-peak histogram. R2 peak represents GFP^{-} cells and is similar to the peak shown in (A). R3 peak represents GFP^{+} cells. Gating the individual peaks revealed that of the live cells counted, only approximately 18% of the cells counted expressed GFP. 87

Figure 4-2 Determining the toxicity of magnetic particles using Sca-1^{+}-GFP^{+} cells derived from C57BL/6 synovium. At time = 0, cells labelled with magnetic beads (E) displayed similar levels of cell death compared to the controls (C). A slight increase in EthD-1 staining was observed in treated cells 48 hours later (F) though levels were comparable to negative controls (D). Cells treated with DMSO displayed the most cell death at both time points (G,H). 88

Figure 4-3 Assessing the rate of internalization and the level of retention of magnetically bound Sca-1 receptor. Maximum internalization was reached at 30 minutes after incubation of biotinylated anti-Sca-1 and BioMag streptavidin beads. Although the number of sorted cells appear to decrease at 9 hours, there was no significant difference in % cell sorted between each of the time points. 89

Figure 4-4 MRI visualization of 10 000 magnetically labelled cells. Intra-articular injection of sterile PBS (A) resulted in an increase in signal intensity between the patella and the articular surface (purple arrow). Imaging 0 hours post-injection (P.I) of labelled cells (B) resulted in hypointense signal appearing below the patella (red arrow) and appears to trail off at the needle entry point (yellow arrow). Imaging 24 hours after injection (C) showed hypointense signaling along the synovium (red arrow). Imaging 24 hours after injection and an injury (defect in yellow box) revealed hypointense signaling below the femur (red arrow). Hypointense band appears to be thicker compared to (B) and (C), and appears to be in the fat pad..... 92

Figure 4-5 MRI evaluation of intra-articular injection of either C57BL/6 or MRL/MpJ derived synovial progenitor cells. Corresponding Safranin-O stain of the same sample is shown. 93

Figure 4-6 Safranin-O stains of the surgical shams and controls after 4 weeks. Proteoglycan content was preserved in samples that either had patella displaced and no injection, patella displaced with PBS injection, and patella displaced with C57BL/6 cells injection. Some of the samples that received PBS injection displayed surface irregularity despite the preservation of proteoglycan content. 95

Figure 4-7 Mean histological score for cartilage repair at 2 and 4 weeks. The grading scheme used was previously published by Fitzgerald et al. where a score of 14 represented complete repair and 0 represented no repair. 96

Figure 4-8 Presence of cellular debris in the joint space after intra-articular injection of C57BL/6 derived Sca-1^{+}-GFP^{+} cells. Cellular debris was detected in the joint space at 0 hours after injection (A, B) as indicated by the red arrows. At 24 hours after injection (C, D), debris was also detected in the joint space (red arrows). Positive Safranin-O staining was also detected surrounding the debris. 97

Figure 4-9 Characterization of magnetically labelled C57BL/6 derived Sca-1^{+}-GFP^{+} cells 24 hours after intra-articular injection. Cellular debris was detected throughout the joint (A, D) 24 hours after injection. Detection of GFP using immunohistochemistry on serial sections revealed positive staining on the debris (B) as indicated with the green arrows. The debris seen in the negative control (C), however, did no stain positive, as indicated by the green arrow. Magnetic particles could be detected by Prussian Blue (E) as indicated by the red arrows. Iron detection, however, was low and did not overlap with GFP staining (F; cell staining positive for GFP is indicated by the red arrow). 99

Figure 4-10 GFP detection at 2 and 4 weeks post injury (representative figures). GFP staining was absent at both time points, irrespective of whether the progenitor cells were isolated from MRL/MpJ or C57BL/6 mice (B, D). Cartilage defects are indicated in the yellow boxes. 100

Figure 4-11 A lack of migration was seen in both magnetically labelled (A) and labelled (B) cells at 48 hours post-scratch. Attempts at fixation at 12 hours (C) and 24 hours (D) was not successful due to cellular detachment. 102

Figure 4-12 Progressive changes in morphology observed at 0, 12, 24, and 48 hours post-scratch. At 0 hours (A), cells display a flatten, fibroblast-like morphology. At 48 hours (D), cells display a detached, spherical morphology. 103

Figure 4-13 Live/dead assay performed at 48 hours post-scratch using Calcein AM and Ethidium homodimer-1. Majority of the cells were alive (D, G) despite changes in morphology. Dead cells could be detected (G, H) though to a lesser degree compared to live cells. 104

List of Symbols, Abbreviations and Nomenclature

Symbol	Definition
Ab-Bd	Antibody-bead complex
ACI	Autologous chondrocyte implantation
BM-MSC	Bone marrow derived MSCs
BrdU	5-bromo-2-deoxyuridine
BSA	Bovine serum albumin
CIdU	Chlorodeoxyuridine
CFDA-SE	Carboxyfluorescein diacetate succinimidyl ester
Col2	Type 2 collagen
DAB	3,3′-Diaminobenzidine
DMSO	Dimethyl sulfoxide
DPC	Days post coitum
ECM	Extracellular Matrix
EDTA	Ethylenediaminetetraacetic acid
EthD-1	Ethidium Homodimer-1
GAG	Glycosaminoglycan
GFP	Green fluorescent protein
HA	Hyaluronic Acid
HRP	Horse radish peroxidase
HSC	Hematopoietic Stem Cell
IdU	Iododeoxyuridine
MRI	Magnetic Resonance Imaging
MSC	Mesenchymal Stem Cell
NBF	Neutral Buffered Formalin
OA	Osteoarthritis
PBS	Phosphate buffered saline
PDGF	Platelet Derived Growth Factor
PDGFRα	Platelet Derived Growth Factor Receptor alpha
PFA	Paraformaldehyde
RARE	Rapid Acquisition with Relaxation Enhancement
Sca-1	Stem Cell Antigen-1
SM-MSC	Synovial membrane derived MSCs
UC-MSC	Umbilical cord MSCs
SD	Standard deviation
SE	Standard error

Chapter One: **Introduction**

1.1 OVERVIEW

Osteoarthritis (OA), the most common form of arthritis, affects approximately 1 in 8 Canadians and impacts not only quality of life but also the labor force **[http://www.arthritisnetwork.ca/downloads/20111022_Impact_of_arthritis.pdf].** OA is characterized by the progressive loss of articular cartilage, possibly due to the inability of cartilage to heal itself. Further aggravating the problem, the lack of nerves in cartilage prevents early detection of injury until the nerve containing bone tissue beneath the cartilage has been exposed.

Current strategies include pain management and surgery. The latter encompasses a range of techniques such as microfracture and autologous chondrocyte implantation (ACI). The microfracture procedure includes the creation of tiny holes or channels to the subchondral bone marrow so that mesenchymal stem cells (MSCs) are released into the defect to form new cartilage. Fibrocartilage, the resulting cartilage that forms, is not a suitable replacement for articular cartilage as it does not have the mechanical properties to sustain long term durability within the synovial joint [1]. In an ACI, chondrocytes from a non-load bearing location are isolated, expanded *in vitro*, and implanted into the injury site. Studies involving 20 year follow-ups have shown that the technique is effective in repairing large surface lesions on the whole [1,2] but structurally, inconsistencies have been documented as fibrocartilage have been observed in the repair tissue [1]. Furthermore, due to significant donor-site comorbidity associated with removing cartilage from the already injured joint, an increasingly popular strategy is osteochondral allograft transplantation, in which fresh donor tissue is transplanted [3]. While the

techniques is effective in cartilage resurfacing of large osteochondral lesions, donor tissue is limited and expensive.

It is important to note that all of the current methods for treating OA are quite invasive as most, if not all, OA disease modifying (and not simply symptom management) treatments available require surgical intervention. Although behavioural modification (e.g. weight loss) is thought to reduce the risk of OA onset and/or progression, no studies have demonstrated that behavioural modification can repair cartilage after damage has already occurred. A pharmaceutical intervention would be ideal as it would be less invasive provided that the side effects are minimal. Before drug-based therapeutics can occur, however, the natural healing process post cartilage injury needs to be understood. As mentioned, this is a large hurdle since cartilage does not normally heal in mammals after injury. The majority of current research is focused on the application of cell-based therapeutics for cartilage repair, but few focus on highlighting and characterizing the events that occur after injury in a non-pathological joint. To advance the field of cartilage repair/regeneration, it is necessary to first understand the natural progression of repair post injury before potential therapeutic targets can be identified. Thus, the goal of this project is to understand the healing process of cartilage after injury using a model system that demonstrates endogenous cartilage repair. Subsequent sections will outline the biology of the joint and cartilage as well as the hypothesis and the specific aims of the project.

1.2 SYNOVIAL JOINT

A joint can be defined as a point at which different parts of a skeleton are connected. Two different types of joints exist: synarthroses and diarthrosis joints. Synarthroses joints include bones that are joined by fibrous or cartilage tissues where movement is limited, such as the joints

in the vertebrae. In contrast, diarthrosis joints, also known as synovial joints, allow dynamic range of movement and are associated with limbs. In a synovial joint, the joint itself is contained within a fibrous capsule. The two bones involved do not actually meet but are connected to each other via the capsule. The articulating ends of the bones are covered in a specialized type of cartilage termed hyaline cartilage. Lining the inner side of the capsule is the synovium, a thin membrane that secretes lubricating fluid, also known as synovial fluid, into the joint cavity [4].

1.2.1 Cartilage Biology

Articular cartilage is avascular, lacks nerves as well as lymphatics, and is composed largely of extracellular matrix (ECM). Chondrocytes are the only resident cell type in cartilage and is thought to maintain the anabolic/catabolic processes within the cartilage matrix. The ECM is composed mostly of type 2 collagen fibers which are parallel to the joint surface while in the intermediate and deep zone, fibers are in a vertical alignment. The fibers contain proteoglycans with negatively charged polysaccharide chains that function to retain water [5,6].

As cartilage is avascular, uptake of nutrients by chondrocytes occur via diffusion. Specifically, blood plasma is filtered from the capillaries and through the synovium into the synovial fluid. Nutrients then need to diffuse down through the ECM to the chondrocytes. Additionally, due to lack of vasculature, chondrocytes are exposed to low oxygen concentrations and rely on anaerobic metabolism [7].

As mentioned previously, chondrocytes are the only cell type in the cartilage and maintain the homeostasis of the ECM. Each chondrocyte resides within a lacunae and thus, are thought to be secluded from one another. The isolation of each cell limits the ability for cell

migration. The isolation coupled with the lack of vasculature are thought to be some of the main reasons contributing to low healing potential in cartilage [8].

With respect to the structure of cartilage, there are 4 distinct zones that make up the tissue: superficial, transition, deep, and calcified. In the superficial zone, the collagen fibers are arranged parallel to the articular surface and chondrocytes have a distinct "flattened" morphology. Due to the low levels of proteoglycans, water retention is the greatest in the superficial zone. Transitioning from the superficial zone to the deep zone, chondrocytes become progressively rounder in shape. In the deep zone, the chondrocytes are now spherical and are oriented in columns. Due to the high levels of proteoglycans, the water content in the deep zone is the lowest. The final zone is the stiff calcified zone which separates the articular cartilage from the underlying bone and restricts nutritional transport between the bone and cartilage [9].

1.2.2 Extracellular Matrix (ECM)

As previously mentioned, articular cartilage is composed mainly of ECM. The three major components of ECM are water, collagen, and proteoglycan. In fact, due to the water retention of the tissue, water can make up 65-80% of the total weight of the cartilage while collagen makes up about 60% of the dry weight. The most abundant type of collagen found in cartilage is type 2, and it is in part responsible for the strength and stiffness of the tissue. Trapped within the matrix of collagen fibers are proteoglycans, which are macromolecules with a protein core and negatively charged glycosaminoglycan (GAG) side chains. Secreted by chondrocytes, aggrecan is made up of cartilage-specific proteoglycans that bind to hyaluronan to form proteoglycan aggregates [9]. Taken altogether, the interaction between water, collagens, and proteoglycans is responsible for protecting cartilage from shear forces when compressed. The

tissue is able to store energy upon deformation and dissipate energy upon decompression. Cartilage protects against compressive pressure through the interaction of the water and proteoglycan components.

The ECM is porous and allows water to flow in and out of the cartilage during compression. Due to the negative charge on the GAG side chains, the chains repel each other and allow positively charged water molecules to intercalate between the chains. When cartilage is compressed, the water is pushed out while the GAG side chains are pushed together. The closer the side chains are to one another, the more resistance there is due to the negative charges. When cartilage decompresses, water content is restored to the tissue as the molecules flow back towards the GAG side chains. The water in the matrix provides protection in the form of fluid pressure which shields the matrix from the stress of the compressive load. [9]

1.2.3 Synovial Tissue

The synovium (also known as synovial membrane) is located along the inner side of the capsule that separates the soft tissues that surround the joint (capsule and muscle) from the inter-articular space. Cells within the synovium are responsible for secreting synovial fluid which lubricates and acts as a medium for nutrients. The latter diffuses from the blood and into the joint environment. The fluid also transport waste products back to the synovium, which are then removed via the lymphatic system. The synovium contains fat cells, mesenchymal progenitor cells, synoviocytes (synovial fibroblasts) and macrophages. There are three types of synoviocytes: the macrophage-like Type A synoviocytes, the fibroblast-like Type B synoviocytes which are also responsible for hyaluronan synthesis, and Type C synoviocytes, which are also called transition cells but the function of which are unknown at this time [10].

Structurally, the synovium can be partitioned into two sections, the intimal layer and the deeper, vascularized subintima. Cells residing in the intima are mostly macrophages and fibroblasts while the subintima houses a more diverse cell population including macrophages, fibroblasts, adipocytes, and mast cells [11].

1.2.4 Synovial Fluid

Synovial fluid is found within the joint cavity and functions to lubricate the joint and provide nutrients. The latter is especially important to chondrocytes as cartilage is avascular and therefore receives nutrients via diffusion from the synovium and synovial fluid. Nutrients are then carried into the cartilage through convective transport when joint motion occurs [12]. The fluid itself is composed of hyaluronan and plasma ultrafiltrate. Hyaluronan is a GAG that is made by the type B synoviocytes while the ultrafiltrate is plasma from the blood that filters through the synovium capillary system [13].

1.3 STEM CELL BASICS

There are three main criteria that a cell must meet before it can be defined as a stem cell: The ability to self-renew, differentiate into at least one other cell type, and demonstrate the ability to remain unspecialized (retain potency). The ability to self-renew means the cell must be able to generate a cell identical to the first. Differentiation refers to the ability of the stem cell to commit to a certain lineage and eventually turn into a specialized cell that can no longer self-renew. To remain unspecialized speaks to the stem cell's ability to retain some level of differentiation capacity while existing in a quiescent state. The concept of potency is a measure of the degree to which a stem cell can differentiate. A totipotent cell can differentiate into any

cell derived from the three germ layers (mesoderm, ectoderm, and mesoderm) as well as tissues that support the development of the embryo *in utero* but are not part of the embryo itself e.g. placenta. A zygote resulting from the union of a sperm and egg would be totipotent. Pluripotent cells are able to differentiate into cells from all three germ layers but not extraembryonic tissues. Embryonic stem cells are pluripotent cells. Multipotent cells are usually lineage restricted, meaning they are only able to different into cells that make up the tissues from the germ layer that the stem cell was derived from. An example would be the ability of bone marrow MSCs, which are derived from the mesodermal germ layer, to only differentiate into cells present in tissues formed from mesoderm (e.g. bone, cartilage, fat). MSCs will be described in fuller detail in the subsequent section. Unipotent cells are stem cells that can only differentiate into one other cell type but are also able to self-renew [14].

Another point that requires introduction is the concept of a stem cell niche, which refers to the local micro-environment that a particular stem cell population resides within. The niche provides specific factors and cues for stem cell maintenance, modulation, and activation. It is important to note that without the niche, the function of a stem cell may be limited or altered. Hematopoietic stem cells (HSC) that reconstitute the immune system are found in circulation at very low levels, but the HSC stem cell niche is present in the bone marrow. In this niche environment, the HSCs are able to self-renewal and/or undergo unequal cell division to produce progenitor cells which can dynamically respond to environmental cues when the cells are required in the peripheral blood system. [15].

The niche concept was initially described as a ‘regulatory unit that maintains and directs HSC (hematopoietic stem cell) self-renewal and differentiation’ [16]. This hypothesis has been supported by studies in worms, flies, and more recently in the bone marrow of mammalian

model organisms [16]. The majority of stem cell niche research has been focused on the MSC population as a niche cell type for hematopoietic stem cells (HSCs), with only recent studies looking for the niche cell populations that support the MSCs [17]. A number of 'criteria' for niche cells have been proposed [18]: **1.)** *Rarity*. Since MSCs are a rare cell population (<1% of total cells in a given tissue), genuine niche cells are also expected to be rare. **2.)** *Physical proximity*. The distance between the niche cell and MSC is directly proportional to the active range of the factors expressed by the niche cell to regulate the MSC. In some cases this might require direct contact, while in other instances, secreted morphogens, which are molecules that direct cell fate and tissue patterning during development, can be active over many cell diameters. **3.)** *Synthesis of MSC maintenance products*. Several factors influence MSC function, such as chemokines (CCLs, CXCs), growth factors (FGFs, BMPs) and other ligands (Notch, Wnts). These factors may control MSC quiescence, adhesion, maintenance, self-renewal and other cellular functions [19,20]. **4.)** *Selective regulation of MSC functions by the niche*. The MSC niche is required to sense the need to induce migration, division, or differentiation, and therefore niche cells should be regulated differently and possibly independently from other tissue resident cells [17,18].

1.3.1 Adult Stem Cells – Mesenchymal Stem Cells (MSCs)

Stem cells found in adult tissue are usually either multipotent or unipotent and have been thought to function in wound healing and tissue homeostasis. Examples of adult stem cells that have been isolated and characterized include gut stem cells, follicular hair stem cells, neural stem cells, as well as MSCs [21]. As MSCs are the focus of this project, other stem cell types will not be discussed. [22]

MSCs are stem cells found in soft and connective tissues and have the capability of differentiating into cell types that are of the mesenchymal lineage such as fat, bone, and cartilage [22]. According to the International Society for Cellular Therapy [23], the criteria for human MSCs are as follows:

1) Cells must adhere to plastic
2) Cells must be able to undergo chondrogensis, osteogenesis, and adipogenesis
3) Human derived cells must express CD73+, CD90+, CD105+, CD34-, CD45-, HLA-DR-. CD14-, CD79a-, or CD19-

Despite the fact that MSC populations have been derived from multiple sources within the adult, it should be noted that MSCs appear to demonstrate some level of differentiation bias depending on what tissue they were harvested from, e.g. bone marrow MSCs have a greater capacity to differentiate into osteoblasts [24–26]. Coupled with these biases in function, differences in gene expression have also been observed. Panepucci et al. performed gene expression analysis between umbilical cord MSCs (UC-MSCs) and bone-marrow derived MSCs (BM-MSCs), and the latter was observed to have higher expression of genes relating to antimicrobial activity and osteogenesis while UC-MSCs had higher expressions of genes related to matrix remodelling through metalloproteinase and angiogenesis [27]. It is important to note that tissue bias and gene expression differences between MSC populations have been independently confirmed and documented in other studies [24,28].

1.3.2 Synovial MSCs

With respect to the joint environment and the surrounding tissues, MSCs have been isolated in bone marrow [29], adipose tissue [30], synovium and synovial fluid [31] and periosteum [32]. While, the use of BM-MSCs in studies involving cartilage repair or in cartilage tissue engineering is still prevalent and remains the gold standard [33–37] due to the abundance and ease of access to tissue sources, small phenotypic differences between MSCs harvested from distinct tissues could possibly determine the effectiveness of these MSC-based strategies. If this is the case, it might be more effective to utilize a progenitor/stem cell that is more developmentally related to cartilage. During the development of synovial joints in mice and humans, the synovium and cartilage originate from a common pool of cells [38]. As mentioned earlier, MSC populations have been derived from the synovial membrane as well as synovial fluid and there is compelling evidence that these cells possess cartilage repair potential [39,40]. Evidence from *in vivo* studies have shown that cells from synovial membrane contribute to repair of partial-thickness cartilage defects [41,42].

Due to the presence of MSCs in the synovial tissue and the close proximity of these cells to cartilage, it is likely that SM-MSCs would be the ideal cell source for cartilage repair. In fact, in a number of comparative studies, MSCs derived from the synovial membrane (SM-MSCs) was observed to have higher chondrogenic potential than MSCs derived from adipose tissue or bone marrow [25,43]. SM-MSCs have been observed to express higher levels of chondrogenic mRNA after chondrogenic induction compared to BM-MSCs [24].

It should be noted that in addition to SM-MSCs, studies have also suggested additional progenitor populations are present within the articular joint. In 2009, Koelling et al. discovered a chondrogenic progenitor population specific to late-stage osteoarthritis articular cartilage. In

the study, the authors isolated the cells based on migratory potential from repair tissue. These cells were able to migrate and populate diseased tissues as well. The authors determined that the progenitors were distinct from mesenchymal stem/stromal cells (MSCs), osteoblasts, and chondrocytes but the origins of these progenitors remains unknown. As the progenitors were solely committed to chondrogenesis, it is possible that these cells are an intermediate cell type derived from an MSC population or that they may be the product of chondrocyte de-differentiation [44].

1.3.3 Intra-articular injection of exogenous MSCs

Intra-articular injection of exogenous progenitor/stem cells have been performed in numerous studies, yet the role or function of the injected cells remains unclear. In one study, GFP- transduced bone marrow MSCs resuspended in a solution containing hyaluronic acid (HA) was injected intra-articularly 6 weeks after induction of OA in goats [45]. Twenty weeks post transplantation, the authors observed tissue repair in the stem cell injected joints, while control joints displayed extensive cartilage degradation and loss of ECM as well as osteophyte formation GFP cells were also detected in various tissues including meniscus and synovial capsule. The authors noted that the results were not depended on the HA, as the same positive outcome measures were observed for animals treated with cells resuspended in PBS.

In another study, human MSCs were labelled with carboxyfluorescein diacetate succinimidyl ester (CFDA-SE), suspended in either PBS or hyaluronic acid (HA), and injected into the knees of Hartley strain guinea pigs, which are prone to spontaneous OA [46]. Interestingly, Safranin-O staining for proteoglycan content was reduced for all groups except for animals treated with HA + MSCs. Animals treated with the latter also had labelled cells scattered from

superior to transition zone and displayed columnar formation, suggesting differentiation of the injected MSCs. However, engraftment was not observed when cells were suspended in PBS, suggesting that engraftment would not occur in the absence of HA, clouding the functional capacity of the stem cells themselves.

Taken together, these studies suggest that when injected, MSCs are able to migrate to the site of injury and affect some level of tissue repair. Although it is still unknown if MSCs contribute to direct repair (becoming the tissue itself), indirect repair (secreting factors which enhance the repair capacity of endogenous cells) or a combination of both.

1.4 Mouse Model- MRL/MpJ (Superhealer) mice

Animal models are widely used for the study of cartilage biology, repair, and regeneration. Rabbit, dog, horse and sheep models remain the most popular animal models [47]. Defects made in larger animals can be more clinically relevant to humans but smaller animals are more cost-effective and readily available. Specifically with mice, the availability of various transgenic animals and genetic tools available make murine models an attractive alternative to other animal models.

In our research project, we use the MRL/MpJ (MRL) mouse, also known as the Superhealer mouse. They were first documented in 1998 as having superior ability to heal wounds by day 25, where ear notches were completely closed with normal tissue architecture and absence of scarring as compared to control C57BL/6 (C57) mice [48]. Evidence suggests that MRL mice, compared to C57, express higher levels of MMP2 and MMP9 during the inflammatory response which allow for the breakdown of ECM by day 5. Epithelial-mesenchymal interactions initiate and lead to the formation of blastema similar to amphibian

limb regeneration [49]. In 2008, it was reported that MRL mice were able to repair full thickness lesions that were made in the articular cartilage of the trochlear groove [50]. Specifically, lesions in MRL mice displayed ample chondrocytes, proteoglycan, collagen 2 and collagen VI whereas lesions in BL6 mice exhibited lower levels of proteoglycan and collagen II. Interestingly, the heightened ability to regenerate cartilage was observed only in male MRLs, with females displaying little to no regeneration capacity. However, our lab has found that female MRL mice do display tissue regeneration, suggesting some level of heterogeneity in healing capacity, or possibly issues with the previous studies experimental design or follow through. However, since our results and that of the field agree that male MRLs exhibit enhanced regenerative capacity (including cartilage repair), this project will use only male MRLs.

1.5 Rationale of project

Currently, studies that investigate the cellular mechanism that occurs after cartilage injury is lacking. We believe that in order to understand how to best treat degenerative cartilage diseases, we need to first characterize the endogenous repair process. To study the latter, we used MRL mice as they have been documented to repair cartilage, and we compared these mice to the C57 mice to gain insight as to why MRL mice are permissive to cartilage repair. As synovial derived MSCs have been shown to have superior chondrogenic potential, we focused on studying these progenitors in MRL and C57 mice and how these cells might be different between the two strains as well as the role of the synovial derived progenitors in repairing cartilage injury. Furthermore, we also looked at the interplay between inflammation and MSCs/progenitors as recent studies suggest the two factors can interact to impact wound healing.

1.6 Hypothesis

Mesenchymal stem/progenitor cells in the synovial membrane will demonstrate the ability to differentiate into chondrocytes (*in vitro*), migrate/home to the site of injury (*in vivo*) and effect cartilage repair when exogenously injected into a cartilage injury model system (*in vivo*).

1.7 Aims

My hypothesis will be testing using the following specific aims:

1. Isolating and characterizing synovial progenitors from mouse synovium using known markers for murine MSC.
2. Characterizing endogenous repair (or lack thereof) in MRL/MpJ and C57BL/6 mice following a reproducible focal cartilage injury.
3. Performing intra-articular injections of synovial progenitor cells and assessing the role of progenitor cells in response to injury.

Chapter Two: **Characterizing Mouse Synovium**

2.1 BACKGROUND

Mesenchymal stem cells (MSCs) were first discovered in human synovial membrane (SM) in 2001 [51]. The discovery and independent validation by other studies [24,25,52] suggests the possibility of an innate healing mechanism in the joint as adult stem cells are thought to play a role in tissue repair. Interestingly and potentially related is that SM often becomes hyperplastic in response to injury [53,54]. Most studies since the initial discovery of synovial MSCs focus on characterizing the MSC population and investigating the potential of these cells for therapeutic use and/or tissue engineering [55]. Few studies have attempted to characterize the mechanism of repair (direct vs. indirect) of synovial MSCs after exogenous transplantation. Engraftment of MSCs does not always occur and even when it does, transplanted MSCs can be found in the adjacent uninjured tissues, signifying that they do not completely localize to the site of injury [46].

While research characterizing the role of exogenous stem cells is lacking, studies examining the role of endogenous stem cells in relation to cartilage repair are non-existent. To address this shortcoming, this study will utilize a mouse model system that demonstrates the capacity for cartilage regeneration/repair so we can study the natural healing process of an arguably unnatural ability to determine if synovial stem cells can play a role in the healing of cartilage. Unlike human MSCs, there is a lack of standardized cellular markers that define murine MSCs and markers present on human MSCs do not readily translate to MSCs found in other animals [56,57]. Recently, however, studies have shown that platelet derived growth factor receptor-α (PDGFRα) and stem cell antigen-1 (Sca-1) can be used in conjunction with negative selection to isolate murine MSCs. Specifically, PDGFR-α^{+}Sca-$1^{+}$$CD45^{-}$$TER119^{-}$ cells from adult murine bone marrow were able to differentiate into 3 different mesenchymal lineages [58].

Furthermore, >70% of these cells were in the G_0 phase, an important characteristic as stem cells are traditionally thought to be quiescent *in vivo*. While PDGFR-α and/or Sca-1 have been previously shown to be expressed by murine MSCs [57,59,60], Morikawa et al. were the first to use the PDGFR-α+Sca-1+ combination for murine MSC isolation [61]. Emerging studies have provided further evidence that PDGFR- α and Sca-1 are efficient and reproducible markers for isolating progenitors of mesenchymal origins [62–64].

Platelet derived growth factor (PDGF) is a molecule that promotes motility and growth of connective tissue. In adults, PDGF signaling plays a role in wound healing as well as regulation of blood vessel contractions/relaxation. Pathologically, it has been associated with disorders involving malignancies and fibrotic conditions due to uncontrolled or excess cell growth. The dimeric molecule, consisting of A and B polypeptide chains, can exist as homodimers (PDGF-AA and PDGF-BB) as well as heterodimers (PDGF-AB) isoforms. Due to the dimeric nature of the molecule, each PDGF binds to two receptors. The α-receptor is able to bind to both A- and B-chains while the β-receptor is only able to bind to the B-chains. Each receptor consists an intracellular tyrosine kinase domain and five extracellular immunoglobulin domains where the three outermost domains are involved with ligand binding. Upon activation, the receptors dimerize and autophosphorylation occurs, initiating various downstream signaling pathways that regulate cell motility, growth, differentiation, and apoptosis [65].

With respect to PDGF signaling and stem cells, MSCs are known to abundantly express both types of receptors and have been observed to be crucial for directing lineage commitment. In a 2012 study, Ball et al. used small molecular inhibitors to block PDGFRs which induced a rounded morphology in the MSCs as well as an upregulation of the transcription factors Oct4 and Nanog, both of which play an important role in maintaining pluripotency of embryonic stem

cells. Specifically, knockdown of PDGFRα resulted in approximately 2.7 fold increase in Oct4A, the nuclear localized isoform that is responsible for regulating pluripotency, and a 1.4 fold increase in Nanog though knockdown of PDGFRβ elicited greater fold responses for both transcription factors [66]. When comparing human PDGFRα expression in human bone marrow MSCs with synovial derived MSCs, Nimura et al. (2008) observed a mean rate of PDGFRα expression of 42% on synovial MSCs and 6% on bone marrow derived MSCs. When PDGF signaling was abolished via anti-PDGF antibody, the proliferation of both bone marrow MSCs and synovial MSCs decreased though the effect was greater in the latter [59].

Stem cell antigen-1 (Sca-1), also known as lymphocyte activation protein 6-A (Ly-6A), is a mouse-specific cell surface protein belonging to the *Ly6* gene family which encodes approximately 18 homologous genes, some with greater than 80% sequence similarity with Sca-1. Along with other markers, Sca-1 has been traditionally associated with mouse hematopoietic stem cells (HSCs) enrichment. Upon differentiation of HSCs, expression of Sca-1 is downregulated though Sca-1 is upregulated in peripheral T cells and activated lymphocytes. In addition to HSCs, Sca-1 is expressed on stem and progenitor cells in a number of tissues and organs including dermis, skeletal system, skeletal muscle, and liver. It has been hypothesized that the alteration of lipid raft composition by Sca-1 can favor or inhibit cell signaling in the local vicinity of the protein. Functionally, however, the mechanism of action of Sca-1 is less clear as no specific ligand has been identified [67].

With specific regards to synovial progenitors and marker expression, there have been reports that Sca-1 and PDGFRα have been found in the synovium after injury. In 2011, a paper was published that used iododeoxyuridine (IdU) and chlorodeoxyuridine (CIdU) to label slow cycling cells in a mouse model of cartilage repair [40]. Label-retaining cells are traditionally

associated with stem cells due to their quiescent nature *in vivo*. The authors were able to show that double-labelled slow cycling cells became activated in response to full thickness cartilage lesion and that these slow cycling cells were localized in the synovium. With respect to PDGFRα and Sca-1, both markers were found on IdU positive cells. Interestingly, the authors of this study observed that the population they identified as stem/progenitor cells was very heterogeneous. When double labeling the IdU positive cells with MSC markers, the authors found that not all IdU positive cells stained positive for all MSC markers tested and even cells IdU negative stained positive with some MSC markers. They also found that over time, fluorescent IdU+ cells had decreased fluorescence in response to the cartilage defect, suggesting quiescent cells in the synovium become activated in response to injury.

While the authors used the double-labeling technique and surface markers to implicate the role of MSCs, the study did not provide conclusive evidence regarding the identity of the activated cells. Retention of DNA labels has traditionally been used as a marker for stemness but studies have shown the method to be unreliable [68]. In fact, in a 2007 paper by Kiel et al., it was shown 70 days post labelling with 5-bromo-2-deoxyuridine (BrdU), less than 5% of all BrdU positive cells were hematopoietic stem cells. It is possible that the results observed by Kiel et al. are not universal to all stem cells but the findings suggest that the use of DNA label retention can result in the labelling of a heterogeneous population of cells, a finding that seems to be supported by the results in the Kurth et al. paper as well. When combined with the lack of functional tests of the labeled cells such as tri-lineage differentiation, the identity of the activated cells remains inconclusive.

Due to the growing body of evidence suggesting that a local population of MSCs resides within the synovium and that the markers PDGFRα and Sca-1 are potentially markers of this

population of cells [69], we have undertaken a series of experiments to determine whether progenitor cells could be isolated from mouse synovium using PDGFRα and/or Sca-1. As the third aim of this thesis project involves tracking injected exogenous synovial progenitors, we did not look into the markers used for the negative selection of mouse MSCs e.g. CD45 and TER119. Instead, we focused our attention on markers used for positive selection i.e. PDGFR α and Sca-1, and identifying which marker out of the two could best select for a progenitor population and be utilized for cell tracking.

2.2 MATERIALS AND METHODS

2.2.1 Histology

2.2.1.1 Decalcification

Rear legs from MRL and C57 mice were fixed for 3 days in 10% neutral buffered formalin (NBF; Sigma) after which tissue samples were washed with water. For the first week of decalcification, legs were submerged in 10% EDTA (in double distilled water, pH 7.4; Sigma) and solution was changed every day. After the first week, the solution was changed once per week for the second and third week. After decalcification was completed, samples were washed with water and underwent tissue processing and embedding. Paraffin-embedded tissue blocks were sectioned at 7 μm.

2.2.1.2 Safranin- O/Fast-green

Slides were deparaffinized and rehydrated with an ethanol series to distilled water. Slides were placed in Gill's hematoxylin (Fisher) for 20 minutes followed by 15 minutes in running tap water. Slides were transferred to fast green (Fisher) for 10 minutes followed by 1 minute in 1%

acetic acid. Slides were quickly rinsed with distilled water and then stained with Safranin-O (Fisher) for 2 minutes. With quick dips, slides were dehydrated with a progressive ethanol series to 100% ethanol after which they were cleared and mounted.

2.2.1.3 Prussian Blue

For the iron staining, adherent primary synovial cells were fixed in 4% paraformaldehyde (PFA) at room temperature for 15 minutes after which the samples were washed 3 times in PBS. The working solution (1:1 ratio of 20% hydrochloric acid and 10% potassium ferrocyanide) was added to each well and left to rest for 20 minutes. Working solution was then removed and the wells were rinsed three times with distilled water. Samples were then counterstained with nuclear fast red for 5 minutes, washed twice in distilled water, and then covered with PBS.

2.2.1.4 Immunohistochemistry

The following primary antibodies were used: biotin-conjugated anti-mouse CD140a (also known as PDGFRα; eBioscience) and biotin-conjugated anti-mouse Ly-6A/E (also known as Sca-1; eBioscience).

Slides were deparaffinized and rehydrated with a decreasing ethanol series to distilled water. Slides were then incubated with 20 µg/mL of proteinase K (Invitrogen) in distilled water at 37 ° C for 15 minutes followed by 2 washes in distilled water, 2 minutes each. Endogenous peroxidase was quenched by incubating cells with 0.3% hydrogen peroxide in methanol for 30 minutes at room temperature. Slides were rinsed with PBS for 5 minutes and then serum blocked with 1% bovine serum albumin (BSA)/10% goat serum in PBS for at least 1 hour at room temperature followed by a quick rinse in distilled water. To block endogenous biotin, sections

were incubated with 10% (w/v) egg white (Sigma) mixture in water for 15 minutes at room temperature. Sections were rinsed with tap water to ensure remnants of egg whites are all removed. Sections were then treated with 5% (w/v) skim milk solution for 15 minutes at room temperature followed by quick rinse in distilled water. Sections were transferred to 0.1% PBS-Tween (PBS-T) for 5 minutes followed by a 30 minute incubation period in a humidity chamber with the primary antibody (1:100 dilution in PBS-T) at 37°C. Post-incubation, slides were washed 3 times in PBS-T following by a 20 minute incubation period at room temperature with 1:500 diluted streptavidin conjugated horse radish peroxidase (HRP; BD Pharmingen). After washing 3 times with PBS-T, 3,3'-Diaminobenzidine (DAB; Sigma) was applied to each slide for up to a maximum of 15 minutes. Exposure time was dependent on the primary antibody used. Slides were given a quick rinse in distilled water and dehydrated, cleared, and mounted. Mouse embryo at days post coitum (dpc) 15.5 was used as a positive control for PDGFRα and periosteum was used as a positive control for Sca-1.

2.2.2 Isolating murine synovial cells

Mice were euthanized using University of Calgary Animal Research Ethics accepted methods. The rear legs were removed, and the joint space was exposed. Using a dissecting microscope, pieces of synovial tissue were dissected out from the joint and placed in a petri dish containing PBS and 1% antibiotic-antimycotic (anti-anti; Gibco). Grooves/scratches were made in the bottom of a 12 well plate with a scalpel to improve tissue transfer efficiency and to promote tissue adherence. Tissue samples were transferred to empty 12 well plates and MSC expansion media, consisting of DMEM/F-12 (Biowhittaker), 10% lot-selected fetal bovine serum (Gibco), 1% non-essential amino acid (Gibco), 1% anti-anti (Gibco), and 0.2% beta-

mercaptoethanol (Gibco), was added to each well. Cells were then incubated at 37° C in 2% O_2 and 5% CO_2. Media was changed every 2-3 days until outgrowth was observed from the tissue, after which media changes were performed daily. When the cells localized around the tissue have reached confluency, the tissue piece was removed and the cells were passaged into a T25 flask. Subsequent media changes occured every 2-3 days, or as required.

2.2.3 In vitro detection of Sca-1 expressing cells

Cells were harvested from SMs of C57 mice as described above. Cells were plated in 12 well plates and incubated overnight at 37 °C, 2% O_2. Sca-1 biotin conjugated primary antibody was incubated with Biomag Streptavidin (BM568) beads (approximately 1.5 µm diameter and with a magnetite content (wt%) >90%) at 37 °C for 30 minutes. Cells were then incubated with either magnetic beads alone or the mixture containing antibody-bead (Ab-bd) complexes, for 30 minutes. Amount of beads and antibody added was based on the binding capacity of the beads (1 mg of beads will bind to 9 µg of biotin as described by manufacturer) with the endpoint of using 1 µg of antibody per well. After the 30 minutes incubation period, cells were washed with PBS three times and fixed with 4% paraformaldehyde (PFA; Sigma) for 15 minutes at room temperature. Cells were then stained with Prussian blue and counterstained with nuclear fast red as described above.

2.2.4 Sca-1 selection of cells

As soon as primary synovial cells at passage 1 reached 70%-80% confluency, Sca-1 positive selection was performed. Media was removed the T25 flask and cells were trypsinized with 0.25% trypsin-EDTA (Gibco) until cells were seen to lift from the plate after which media

was added to deactivate the trypsin. The cell suspension was then centrifuged for 5 minutes at 1000xg (Beckman, Model TJ-6). During this time, a working solution of BD IMAG buffer (BD Biosciences) was produced by mixing 1 mL of BD IMAG Buffer (10x) with 9 mL of sterile distilled water. The solution was kept on ice for the duration of the procedure. After centrifugation, the supernatant was discarded and the cell pellet was resuspended in 1 ml of diluted BD buffer. Five micro-litres of antibody was added to the cell suspension, then the solution was vortexed on minimum setting, and placed on ice for 15 minutes after which cells were centrifuge twice at 300xg for 10 minutes. After each spin, supernatant was removed and cell pellet was resuspended in 1m mL of diluted BD buffer. When the last resuspension has been completed, 5 µL of magnetic particles (Bangs Laboratories; BM568) was added. The suspension was vortexed on a low setting and allowed to sit on ice for 15 minutes after which the mix was transferred to a 5 ml vial and an additional 1 mL of buffer was added to the suspension. The cells were placed in the sorting magnet (BD) for 7 minutes after which the liquid phase was removed and remaining cells were plated in a T25 flask.

2.2.5 Tri-lineage (Adipo-, Osteo-, and Chondrogenic) Differentiation

For all three differentiation methods, a total of 10 000 cells/well/24well plate were used. For chondrogenic and osteogenic differentiation, cells were seeded into the wells of a 24 well plate using the hanging drop method. Briefly, cells were trypsinized and resuspended accordingly to obtain the cell concentration of 50 000 cells/ mL. Using a repeat pipettor, "drops" of cell suspension, each containing 20 µL (approximately 1000 cells), were plated onto the lid of a 100 cm^2 petri dish. When sufficient number of drops had been plated, the lids were placed back onto the dishes and incubated at 37 °C, 2% O_2 overnight to generate micro-masses. The next day,

1 ml of chondrogenic or osteogenic media was added to each well after which 10 drops of cell suspension that were plated the previous day were added. For adipogenic differentiation, 10 000 cells were plated per well in a 24 well plate.

Cells were cultured with either MSC expansion media or differentiation media at 37 ° C with 2% O_2 with media changes performed every 2-3 days (as needed) for 21 days.

Adipogenic Differentiation

Differentiation media consisted of MSC culture media with 0.5 mM isobutylmethylxanthine, 1 μM dexamethasone, 10 μM insulin, 200 μM indomethacin (all Sigma).

Osteogenic Differentiation

Differentiation media consisted of MSC culture media with 0.1 μM dexamethasone and 50 μM ascorbate-2-phosphate.

Chondrogenic Differentiation

Differentiation media consisted of sMPC culture media with 500 ng/mL BMP-2 (Peprotech, Rocky Hill, NJ), 10 ng/mL TGF-β3 (Peprotech), 10^{-8} M dexamethasone (Sigma, St. Louis, MO), 50 μg/mL ascorbic acid (Sigma), 40 μg/mL proline (Invitrogen), 100 μg/mL pyruvate (Sigma) and supplemented with insulin, transferrin, and selenium (Sigma).

2.3 RESULTS

2.3.1 PDGFRα is universally expressed while Sca-1 is localized to the synovium

In order to characterize the mouse synovium, we performed immunohistochemical analysis of mouse knee joints to determine the expression of markers PDGFRα and Sca-1. Sections containing mouse embryo at days post coitum (dpc) 15.5 were used as positive controls as the mesenchyme has been known to express PDGFRα [70] while periosteum was used as the

positive control for Sca-1. PDGFRα was found to be widely expressed in the joint environment (Figure 2.1). PDGFRα expressing cells were observed within the synovium, cartilage, fat pad, and meniscus. Sca-1 expression was observed to be more restricted within the joint. Sca-1 expression was localized to the synovium (Figure 2.2). Due to the broad expression of PDGFRα within the joint, the marker was excluded from future experiments, as it would not meet our criteria for being a marker for stem cell tracking. The remainder of the thesis will focus on Sca-1 positive cells only.

2.3.2 Sca-1 expressing cells are found in mouse synovium

To confirm the presence of Sca-1 expressing cells in synovium, primary mouse synovial cells were harvested using the explant culture method. The cells were cultured in low O_2 and at the initial passages, were observed to be healthy i.e. did not display flattened, hypertrophic morphology, but retained a small cell body with a few cell processes that are long and thin (Figure 2.3A). Incubation of magnetic particles conjugated to anti-Sca-1 with the heterogeneous population of cells for 30 minutes resulted in positive Prussian blue staining (Figure 2.3D), indicating that iron was present on the cells. Incubation with magnetic particles alone for the same duration did result in some level of non-specific binding; however, the level of binding was noticeably lower than cells incubated with both antibody and magnetic particles.

2.3.3 Sca-1 purified synovial cells display tri-differentiation potential

To characterize the Sca-1 population of cells in the synovium, the heterogeneous population of cells were purified for Sca-1 via magnetic sorting. The purified cells underwent a tri-differentiation assay for 21 days. At the midpoint (1.5 weeks), cells were fixed and stained to

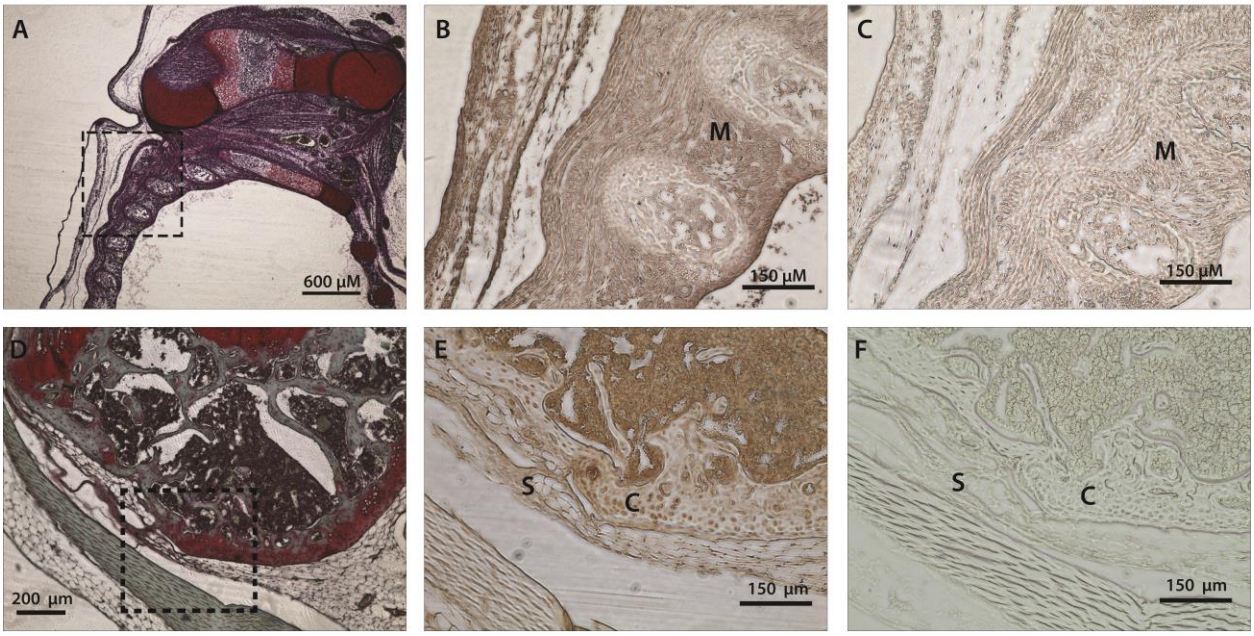

Figure 2-1 Histological assessment of PDGFRα. Mouse embryo at dpc 15 (A-C) was used as the positive control. Staining for PDGFRα was present in the mesenchyme (M) of the embryo (B) but was absent in the negative control (C). In the mouse knee joint (E), staining for PDGFRα was present in the synovium (S) as well as in the cartilage (C). Staining in the knee joint was absent in the negative control (F). A hematoxylin and eosin stained embryo (A) as well as a Safranin-O stained knee joint (D) are provided for reference.

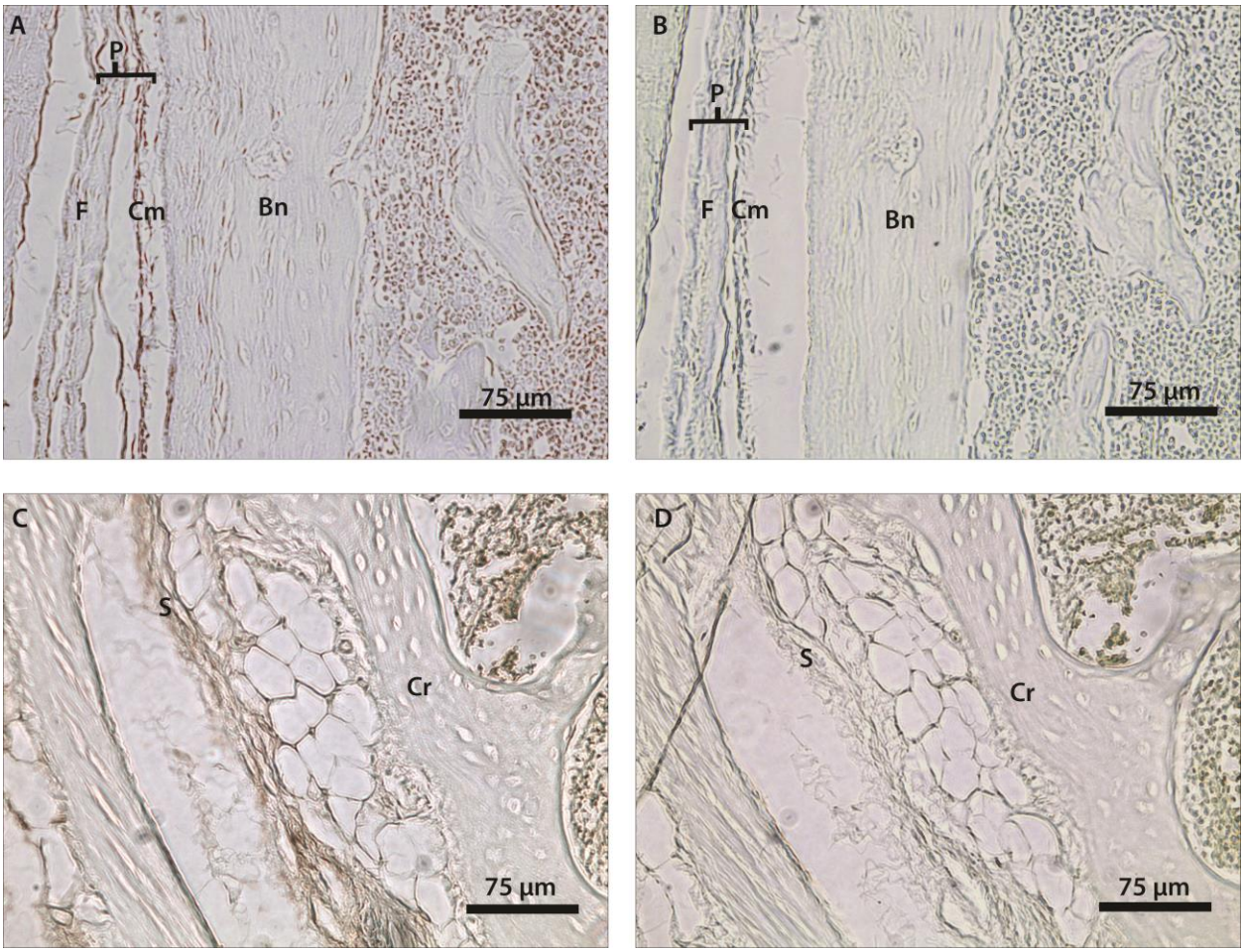

Figure 2-2 Histological assessment of Sca-1. Periosteum (A, B) was used as the positive control. Positive staining is seen only in the cambium (Cm) layer and not in the fibrous (F) layer of the periosteum. Staining is absent in the periosteum in the negative control (B). In the knee joint (C), positive staining was seen in the synovium (S) but was not seen cartilage (Cr). Staining was not seen in the knee joint of the negative control (D).

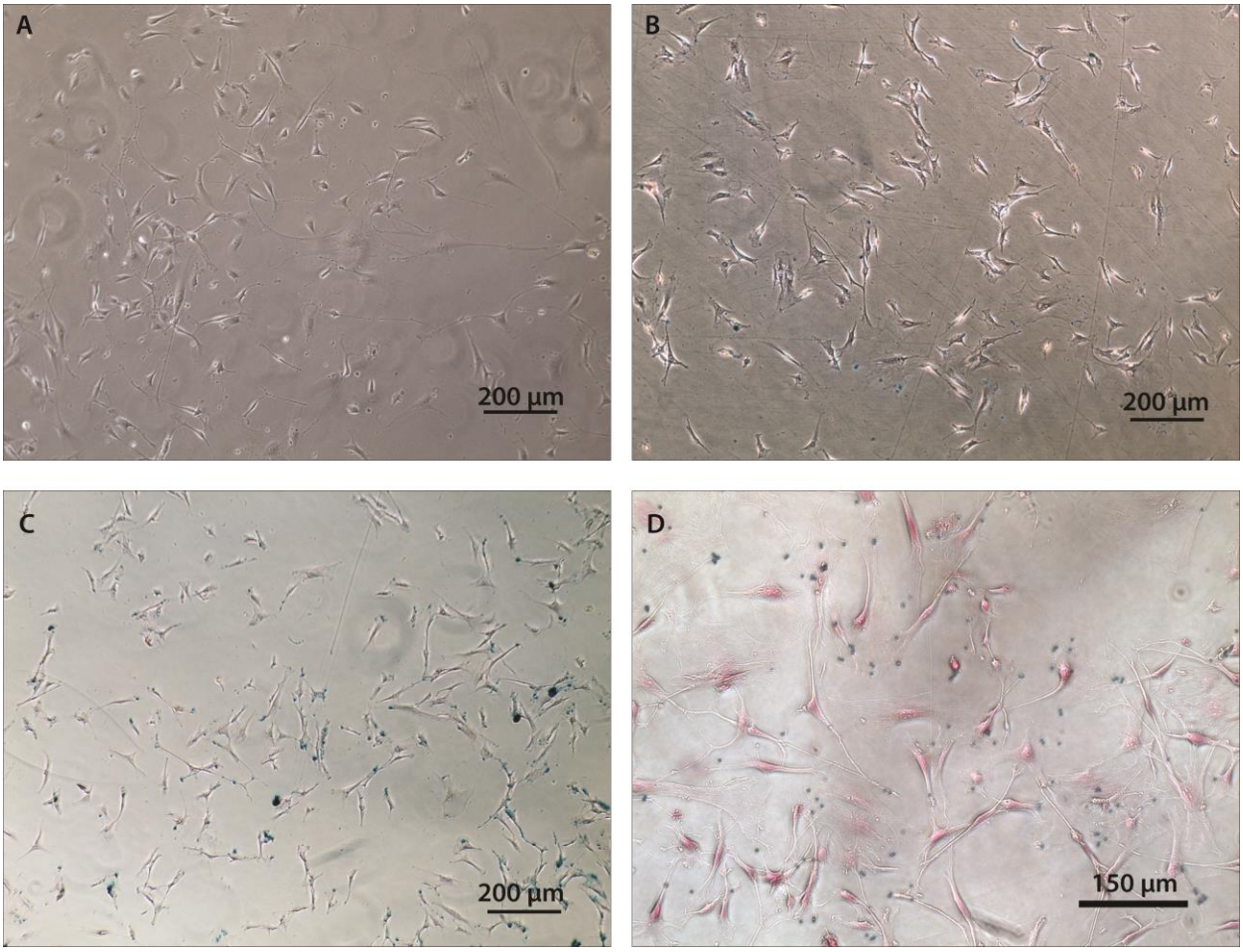

Figure 2-3 Sca-1 expressing cells exist in mouse synovium. Primary cells isolated from C57BL/6 mouse synovium (A) using the outgrowth method display healthy, rounded morphology. Incubation with magnetic particles alone for 30 minutes resulted in minimal unspecific labelling (B). Incubation with magnetically bound Sca-1 antibody for 30 minutes revealed Sca-1 expressing cells, as detected by Prussian Blue stain (B) and counterstained with nuclear fast red (C).

assess progress of differentiation. Adipogenisis was assessed using Oil Red O stain (Figure 2.4). Predictably, limited staining was observed at the midpoint (Figure 2.4C,D). Interestingly, at the end of differentiation, differences between control and cells cultured in adipogenic media were marginal (Figure 2.4E, F). Clusters of small red droplets were observed on the majority of cells in both control and adipogenic wells though large oil droplets were observed more frequently in the latter.

Cells undergoing osteogenic differentiation was assessed using alizarin red for calcification detection (Figure 2.5). Unexpectedly, wells stained at the midpoint were observed to contain higher number of mineralized nodules than wells stained at the end of differentiation.

Alcian blue was used to detect proteoglycan content in cells undergoing chondrogenesis. At the midpoint of differentiation, blue staining was observed to localize only in the cell bodies (Figure 2.6). Proteoglycan deposits were not observed in the extracellular matrix. Staining of the matrix was only observed at the end of differentiation in cells undergoing chondrogenesis. Contrary to the osteogenic and adipogenic wells, a clear difference was observed between chondrogenic and control wells, the latter displaying a lack of staining in both matrix and cell bodies.

2.4 DISCUSSION

Histological evaluation of PDGFRα and Sca-1 revealed that PDGFRα was widely expressed in the joint environment while Sca-1 expression was localized to the synovium and fat pad. As expression was not limited to stem/progenitor cell populations, PDGFRα could not be used for stem cell tracking purposes. The finding was surprising due to the recent use of

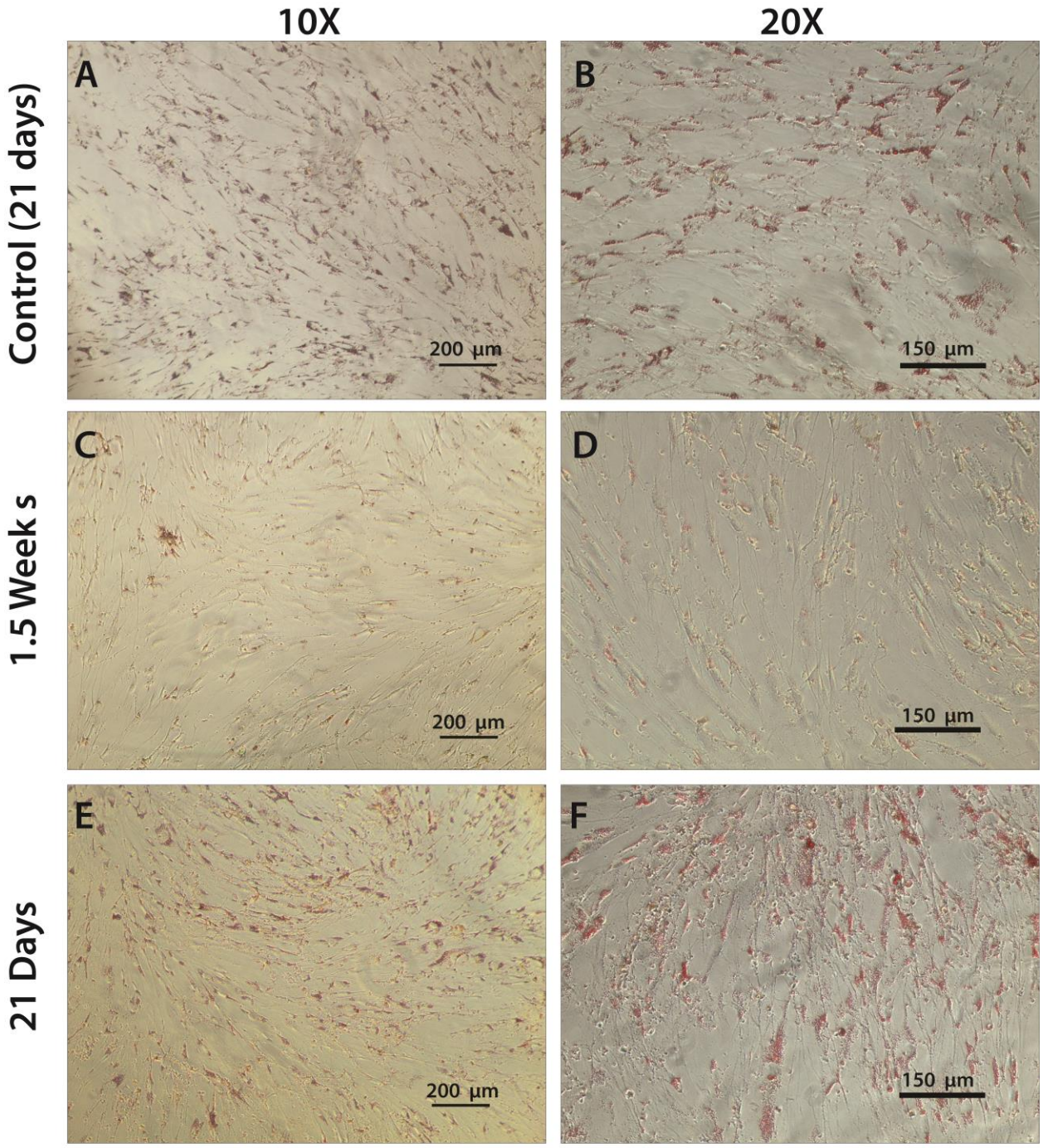

Figure 2-4 Adipogenic differentiation with C57BL/6 synovium derived Sca-1^{+} cells. At the end of 21 days, control wells (A, B) as well as experimental wells (E, F) contained oil droplets as detected by Oil Red O. Experimental wells fixed at the midpoint of 21 days contained fewer oil droplets (C, D).

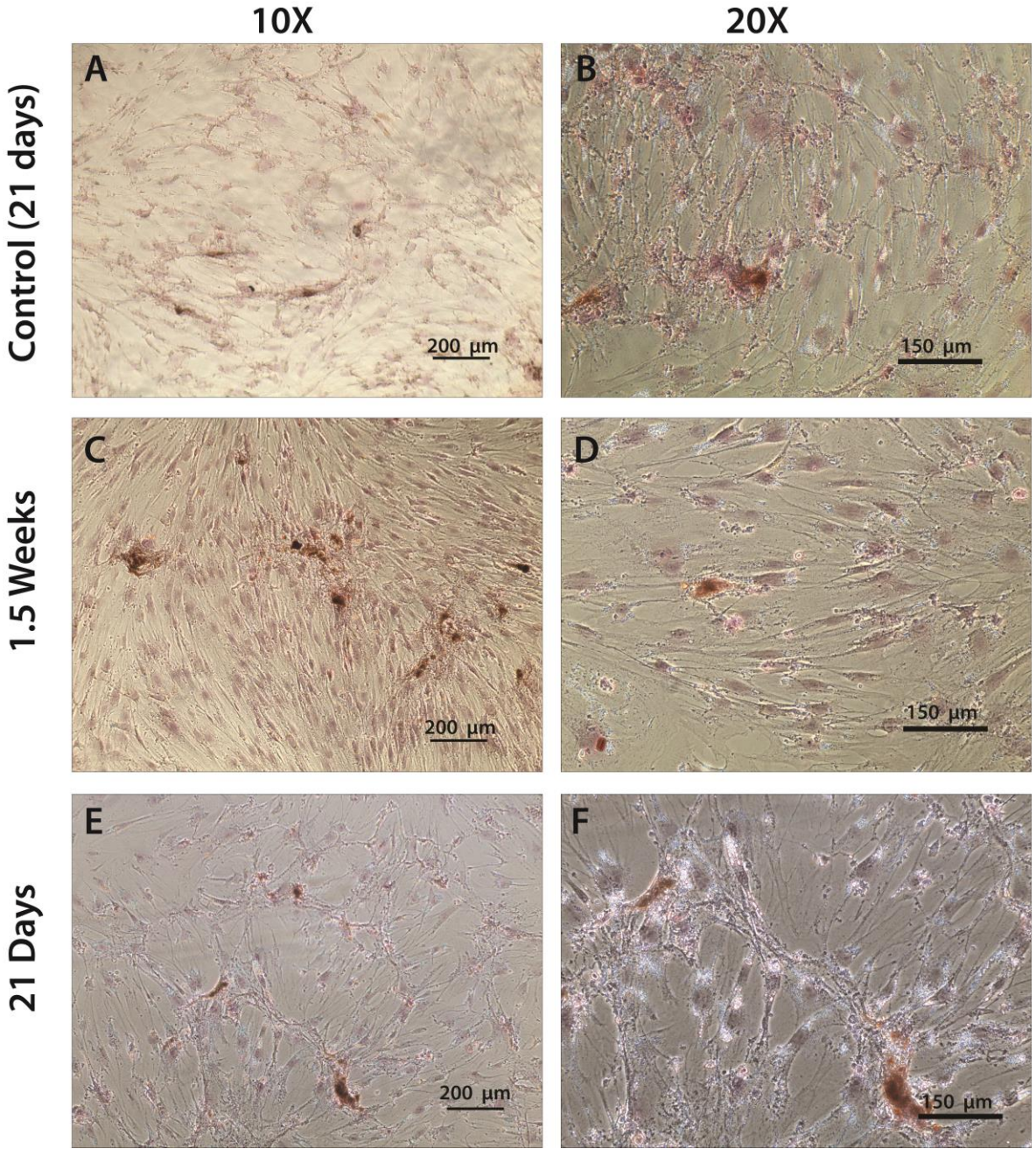

Figure 2-5 Osteogenic differentiation with C57BL/6 synovium derived Sca-1^{+} cells. At the end of 21 days, both control (A, B) and experimental wells (E, F) contained nodules that stained positive with Alizarin Red, indicative of calcium deposits. At the midpoint of 21 days (C, D), experimental wells seem to contain more nodules compared to wells at the end of 21 days but nodules were smaller.

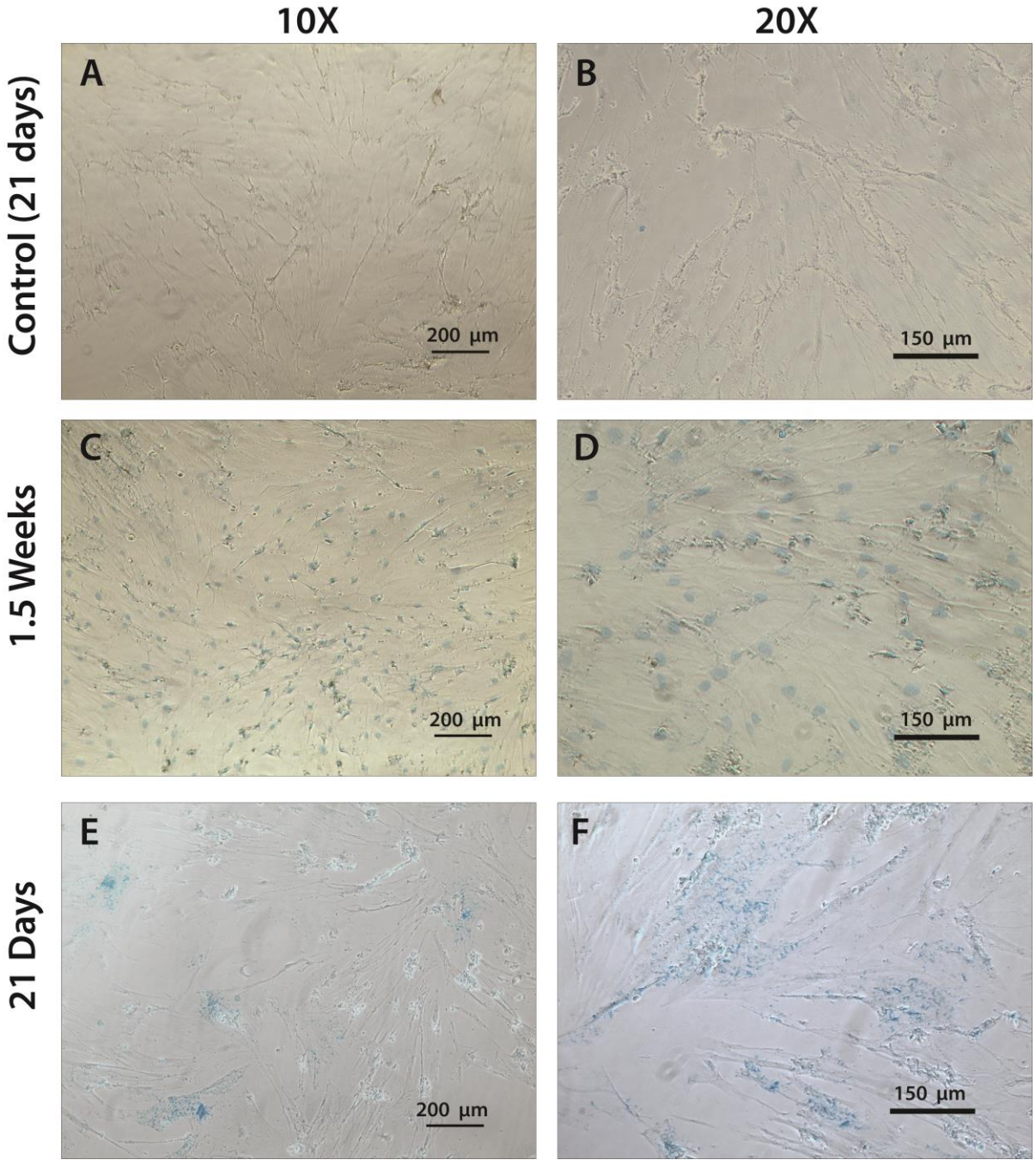

Figure 2-6 Chondrogenic differentiation with C57BL/6 synovium derived Sca-1^{+} cells. At the end of 21 days, control wells (A, B) did not stain blue with Alcian blue. At the midpoint of 21 days, cell bodies in the experimental wells (C, D) stained blue, indicative of proteoglycan production. At the end of 21 days (E, F), proteoglycan deposits could be detected although overall staining was low.

PDGFRα as one of the positive markers for mouse MSCs, however, these studies remove cells from the synovial tissue and then characterize the marker expression. Expression in the surrounding tissues was not examined and so it is possible that PDGFRα is expressed on the MSC population, but also on a wide range of other cell types present in the synovial joint. Earlier studies using human synovium have reported that PDGFRα was expressed only in inflamed synovium. Non-inflamed SM displayed little to no staining [71]. As the mice used for histological characterization were non-injured, it is still possible for the animals to have pre-existing conditions that would cause inflammation of the synovium; however, this is unlikely. Another possibility is that the antibody we have used is more specific to PDGFRα than previously published studies. The APA5 clone we are using is considered the state of the art in the field (developed in 1996) and is the gold standard for publishing on PDGFRα (~8000 publications). Nevertheless, our results suggest that PDGFRα alone cannot be used to identify a progenitor population, therefore, PDGFRα was excluded from subsequent experiments.

Since Sca-1 was localized to the synovium and not observed in the cartilage, we next decided to further characterize cells derived from the mouse synovium and investigate whether Sca-1 was present on SM-derived progenitors. Traditionally, synovial tissue from humans and animal such as dogs, rats, and rabbits have utilized various concentrations of collagenase to enzymatically digest the tissue [25,43,51,72,73]. Due to the limited quantity of tissue in any given mouse knee joint, we had decided to use explant culture instead to minimize cell damage and death. Furthermore, explant culturing would select for cells that adhere to plastic. In order to simulate physiological conditions, we decided to culture the cells in 2% O_2 [74]. In our experiments, primary cells were collected from explant outgrowth of mouse synovial tissue and cultured in hypoxic conditions, this resulted in rounded, fibroblast like cells.

To confirm Sca-1 expressing cells in synovium, primary cells were incubated with anti-Sca-1 bound to magnetic beads for 30 minutes. At this incubation period, non-specific binding was minimal. The presence of Prussian blue stain was detected on most, but not all cells, indicating, as expected that we had derived a heterogeneous population of synovial cells that contained a sub-population of Sca-1 positive cells.

As Sca-1 is a known stem cell marker, we positively selected the primary cells using anti-Sca-1 and tested the differentiation potential of the purified cells. Since one of the criteria for MSC includes tri-lineage differentiation, we induced chondrogensis, adipogenesis, and osteogeneis in our purified cells for 21 days. Alcian blue, oil red O, and alizarin red were used to detect proteoglycan in chondrogenic wells, oil droplets in adipogenic wells, and calcium deposits in osteogenic wells, respectively. At the end of 21 days, there were no observable differences between control and adipogenic wells, which can be explained by our histological data suggesting Sca-1 positive cells can reside within the fat pad and therefore, may have a bias towards adipogenesis. For cells treated with osteogenic media, cells stained at 1.5 weeks seem to display more mineralized nodules than those stained at 3 weeks. Despite displaying fewer nodules, those found at the end of 3 weeks were larger than those at 1.5 weeks. This result may be an effect of cell survival during differentiation. It was anecdotally observed that mouse Sca-1 progenitors were difficult to expand in culture and had to be kept at 2% O_2 to achieve sufficient numbers for differentiation. It has also been published that osteogenic differentiation of progenitors can lead to cell death [75]. The combination of difficult to culture cells with the addition of stress (osteogenesis), may have lead to a net loss of cells undergoing osteogenesis resulting in the decreased number of positive nodules. For cells treated with chondrogenic media, cells stained at 1.5 weeks displayed localized staining in the cell body while cells stained at 3

weeks displayed proteoglycan deposits not only at the cell body but in the matrix surrounding the cells. Overall, our Sca-1 purified cells displayed weak differentiation potential suggesting that not all Sca-1 expressing cells are progenitor cells. Positive staining, though weak, indicate that though cell population is heterogeneous, a proportion of the cells are progenitors capable of undergoing differentiation.

It is important to note that control wells had displayed spontaneous adipogenesis and osteogenesis but no chondrogensis as assessed by histological staining. As control cells were cultured in MSC growth media for the full 21 days without passaging, aging and spontaneous differentiation can occur in the progenitor cells [76]. Furthermore, culturing MSCs in hypoxia has been shown to increase proliferation [77], conserve stem cell state [78], and increases in adipogenic and osteogenic differentiation capacity [79].

In summary, we have shown here that within the uninjured mouse knee joint, PDGFRα is widely expressed and therefore is not suitable for use as a marker for progenitor cells. Sca-1, on the other hand, is found to localize in the synovium and fat pad but absent in the cartilage. We have shown that within the synovium, there is a subset of Sca-1 expressing cells. Sca-1 purified cells, as a whole, display weak tri-lineage potential. Positive staining, however, for chondrogenesis, adipogenesis, and osteogenesis was present, indicating that the Sca-1 purified cell population is heterogeneous in nature but do contain progenitor cells that can undergo adipogenic, osteogenic, and more importantly for our purposes, chondrogenic differentiation.

Chapter Three: **Characterizing Endogenous Response to Cartilage Injury**

3.1 BACKGROUND

In humans, endogenous cartilage repair is an ineffective process. If the defect is deep enough to reach the marrow cavity, repair is minimal, with the repair tissue consisting of fibrocartilage. Overall, fibrocartilage is inferior to hyaline cartilage with respect to robustness since it is composed mainly of collagen type 1 instead of collagen type 2 [80] and is not able to withstand the same mechanical loading as the original hyaline cartilage surface. However, the presence of stem cells in the joint environment (synovial membrane and fluid) that are able to differentiate into chondrocytes suggests that an intrinsic repair mechanism may exist.

To study the natural mechanism of repair, the mouse strain MRL/MpJ (MRL) is of particular interest due its ability to repair cartilage. In one study, intra-articular fracture was induced in C57BL/6 mice (C57) and MRL mice and evaluated for post-traumatic arthritis [81]. At 4 and 8 weeks, MRL mice appear to be protected from the morphological changes that occur in the C57 mice in response to traumatic injury. Like patients afflicted with osteoarthritis, reduced bone density and thickening of the subchondral bone was seen only in C57 mice. Furthermore, the authors observed significant differences in cartilage degeneration in C57 mice when compared to the contralateral limb, while degeneration was not statistically different in the experimental limb of MRL mice compared to contralateral control limb. In a separate study, the authors induced full thickness and partial thickness lesions in C57 and MRL mice and evaluated injury sites at 6 and 12 weeks [50]. The authors observed that partial thickness lesions did not result in repair in either strain. On the other hand, full thickness lesions resulted in significant repair in MRL mice at both 6 and 12 week time points. Morphologically, the repair tissue contained chondrocytes and

was comprised of proteoglycans and collagen. It is important to note that in both the Ward et al. study and Fitzgerald study, only morphological changes were observed and no attempt was made to elucidate the repair response at a cellular level.

The first attempt to investigate the cell types involved in the response was published in 2011. The authors induced joint surface injury in C57 animals and evaluated cellular response at 4, 8, and 12 days post injury [40]. Using DNA label retention, the authors observed increased proliferation, at 4 and 8 days, of slow-cycling cells in the synovium that stained negative for hematopoietic markers but positive for MSC markers. At 12 days post injury, the authors observed double-labelled cells that also expressed chondrogenic markers. However, the presence of chondrogenic markers may indicate chondrogenic potential of these cells but whether these cells would be able to terminally differentiate into chondrocytes is unclear. Due to the heterogeneous population of cells that were labelled, the authors also cannot be certain whether the double-labelled cells are all stem and/or progenitor cells of mesenchymal origin. Furthermore, the study utilized C57 animals, which have previously been documented to have poor repair capacity. To date, there has not been a study that characterized cellular response of repair in MRL animals.

In our experiments, we set out to characterize early cellular response following an acute injury using the markers Sca-1, c-kit, and F4/80. Stem cell antigen-1 (Sca-1) is a mouse specific surface protein belonging to the *Ly6* gene family and is expressed in HSCs as well as stem and progenitor cells in a number of tissues and organs [82]. In this study, Sca-1 will be used to identify all undifferentiated progenitor cells while c-Kit will be used to selectively determine progenitors of hematopoietic origin. The latter marker, a transmembrane receptor tyrosine kinase, is the receptor for stem cell factor (SCF) also known as mast cell growth factor. Upon ligand binding,

subsequent signal transduction leads to proliferation and differentiation of c-Kit expressing cells, which includes hemtapoietic progenitors, mast cells, eosinophils and basophils, as well as structural cells such as epithelial cells and umbilical endothelial cells [83,84].

In addition to the above markers, macrophage marker F4/80 will also be used in our histological analysis. Recent studies and reviews suggest that inflammation plays an important role in degenerative joint diseases such as osteoarthritis [85,86]. In fact, it has been shown that monocyte chemotactic protein-1, a chemokine that recruits progenitor cells to the site of injury as well as inflammatory cells such as monocytes, can inhibit the chondrogenic capability of synovial progenitor cells [87]. Although our focus is on the ability of progenitor cells to repair cartilage defects as oppose to the progressive deterioration in response to injury, inflammation is an integral part of the wound healing process. In our study, we will be analyzing F4/80 at various time points after injury to characterize the interaction between macrophages and progenitor cells.

With regards to assessing cartilage integrity and joint anatomy in response to injury, the use of magnetic resonance imaging (MRI) for cartilage evaluation has been and continues to be intensely researched. Compared to X-ray, MRI is ideal due to its ability to visualize not only cartilage but also the surrounding tissues in the joint. The use of MRI in rodent cartilage repair studies, however, remains limited. Preclinical studies involving focal cartilage repair often utilize large animal models such as rabbits, sheeps, dogs, pigs, etc. Murine models are underutilized due to the gross size of the joint, and also the cartilage thickness. Rodent cartilage is only a few cells thick and thus correlating mechanisms of degeneration and/or repair in rodents to that of humans is difficult [47].

Despite these potential biological limitations/differences, the wide spectrum of genetic tools that are available in mice makes the use of this animal model ideal to study complex

systems. In recent years, the use of mouse models has led to the development of various murine cartilage injury models [81,88]. Along with these new animal models, new cartilage grading systems have also been developed. Of interest to this project is the ability to grade cartilage repair in mice. In our experiments, we used a previously published scoring system to histologically evaluate the level of repair [50]. Briefly, the grading scheme involves evaluating the joint based on various weighted categories and the combined score for each section is used to assess the level of repair. While there are other mouse cartilage scoring systems available, the grading scheme used in this study was the only previously published grading scheme that focused on repair of cartilage injury as oppose to the level of joint deterioration in mouse models of OA.

While longitudinal studies regarding cartilage repair have been undertaken on patients and in larger animal models, a method has yet to be developed that will allow for mouse cartilage to be repeatedly and non-invasively evaluated over time. In this study, we sought to first develop an MRI protocol that will allow non-invasive, morphological evaluation of cartilage repair. Furthermore, adapting a previously published protocol for mouse model of focal cartilage defect [88], we set out to characterize early cellular response of cartilage repair in MRL and C57 mice.

3.2 MATERIALS AND METHODS

All animal experiments were done in accordance to the standards of the research ethics committee at the University of Calgary.

3.2.1 Creating surgical apparatus- stopped needle

A custom made stopped needle was used to induce the cartilage defect. Similar to the needle described by Eltawil et al. (2009), a stopper in the form of a bead was made from Apoxie

Sculpt® and placed on a 26 gauge (26G) needle such that approximately 1.45 mm of the tip was exposed (Figure 2). The bead was cured by drying overnight at room temperature after which the bead was secured to the needle with Krazy glue®. Excess glue was used such that when placing the needle in an upright position, the extra liquid will collect at the bottom of the bead. When this buildup of liquid dries, it functioned as a secondary stopper for the bead itself. It should be noted that from preliminary experiments (data not shown), that the size of the stopper bead does not influence the ability of the tool to induce a cartilage defect.

3.2.2 Inducing cartilage defect

Mice were anaesthetized with isoflurane (2.5L/min) for the duration of the surgery. The hair around the knee joint was clipped followed by swabbing of the surgical area with betadine. A small skin incision on the medial side of the left knee was made to expose the patella and the associated tendon. Keeping the knee extended, the tip of a custom-made 26G stopped needle was inserted under the patella tendon from the medial side and aimed towards the femur. Pressure was applied with a twisting motion until the tissue was at the hilt of the stopper. The resistance upon withdrawing the needle and the sight of bleeding indicated that the needle had successfully penetrated into the subchondral bone. Sterile gauze was used to blot excessive bleeding and the incision was closed using wound clips. The surgical area was then swabbed with gentamycin to prevent infection. Animals received buprenorphine (0.05 mg/kg) at the conclusion of the surgery as well as the day after for pain management.

3.2.3 Experimental outline

Focal cartilage defects were induced in the left knee of 4-6 week old mice (n=3 per timepoint, per strain) using a 26 gauge stopped needle, a technique previously described and validated [89]. Injuries were induced in the first group of animals, which were allocated for t=0 timepoint (euthanized immediately after injury), while remaining animals were euthanized 2 and 4 weeks post-injury. Both legs were dissected out and fixed with 10% neutralized buffer formalin.

3.2.4 Magnetic Resonance Imaging (MRI)

Wooden splints were attached to dissected and fixed leg samples using silk sutures and the splinted sample was placed inside a 15 ml falcon tube [APPENDIX FIG]. Additional wooden supports were strategically placed in the tube such that the sample was fixed, centred and knee was as close to the inner surface of the tube as possible without being compressed. The tube was then filled with Fluorinert (3M) and care was taken to minimize air bubbles. Samples were imaged *ex vivo* using a 9.4 T magnet and a surface cryocoil. A proton density weighted, four-segment Rapid Acquisition with Relaxation Enhancement (RARE) sequence was used with the following parameters: RARE factor = 4, Repetition time = 2000 ms, echo time = 9.346 ms, FOV = 1.92 cm, slice thickness = 0.25 mm, matrix = 256 x 256. Once imaged, samples were processed, embedded into paraffin wax, and sectioned at 7 µm thickness. Sections were stained with Safranin-O and graded using a scoring matrix previously described [50].

3.2.5 Characterizing defect size by image analysis

Tip to bead distance on the surgical apparatus was measured using calipers. To measure defect size in an MRI scan, pixel size was calculated to be 75 µm x 75 µm with a slice thickness of 250 µm. MRI scan section was saved as a DICOM (.dcm extension) file and subsequently opened with ImageJ. Under image → properties, unit of length was set to µm, pixel width and depth were set to 75 µm, and voxel depth was set to 250 µm. The defect was measured using the straight line tool, where the length of the drawn line was given. To measure the defect size in the corresponding histological image, the .TIF file containing a scale bar was opened with ImageJ. Using the straight line tool, a line is drawn to the length of the scale bar. Under analyze → set scale, length of scale bar and the unit of length was inputted into known distance and the box next to 'global selection' was selected. The defect was measured using the straight line tool where length of the line drawn was now presented in the unit of measurement (length) inputted.

3.2.6 Histological Analysis

3.2.6.1 Decalcification

Legs were fixed for 3 days in 10% neutral buffered formalin (NBF; Sigma) after which tissue samples were washed with water. For the first week of decalcification, legs were submerged in 10% EDTA (in double distilled water, pH 7.4; Sigma) and solution was changed every day. After the first week, solution was changed once per week for the second and third week. After decalcification was completed, samples are washed with water and underwent tissue processing and embedding. Paraffin-embedded tissue blocks were sectioned at 7 µm.

3.2.6.2 Safranin-O/Fast-green

Slides were deparaffinized and rehydrated with a 100% ethanol to 100% distilled water series of wash steps. Slides were placed in Gill's hematoxylin (Fisher) for 20 minutes followed by 15 minutes in running tap water. Slides were transferred to fast green (Fisher) for 10 minutes followed by 1 minute in 1% acetic acid. Slides were then quickly rinsed with distilled water and stained with Safranin-O (Fisher) for 2 minutes. With quick dips, slides were dehydrated with a progressive ethanol series to 100% ethanol after which they were cleared and mounted.

3.2.6.3 Immunohistochemistry

The following primary antibodies were used: biotin-conjugated anti-mouse CD140a (also known as PDGFRα; eBioscience), biotin-conjugated anti-F4/80 (eBioscience) and biotin-conjugated anti-mouse Ly-6A/E (also known as Sca-1; eBioscience).

Slides were deparaffinized and rehydrated with a decreasing ethanol series to distilled water. Slides were then incubated with 20 µg/mL of proteinase K (Invitrogen) in distilled water at 37 ° C for 15 minutes followed by 2 washes in distilled water, 2 minutes each. Endogenous peroxidase was quenched by incubating cells with 0.3% hydrogen peroxide in methanol for 30 minutes at room temperature. Slides were then rinsed with PBS for 5 minutes and then blocked with 1% bovine serum albumin (BSA)/10% goat serum in PBS for at least 1 hour at room temperature followed by a quick rinse in distilled water. To block endogenous biotin, sections were incubated with 10% (w/v) egg white (Sigma) mixture in water for 15 minutes at room temperature. Sections were rinsed with tap water to ensure remnants of egg whites were removed, then treated with 5% (w/v) skim milk solution for 15 minutes at room temperature followed by a quick rinse in distilled water. Sections were transferred to 0.1% PBS-Tween (PBS-

T) for 5 minutes followed by a 30 minute incubation period in a humidity chamber with the primary antibody (1:100 dilution in PBS-T) at 37°C. Post-incubation, slides were washed 3 times in PBS-T following by a 20 minute incubation period at room temperature with 1:500 diluted streptavidin conjugated horse radish peroxidase (HRP; BD Pharmingen). After washing 3 times with PBS-T, 3,3'-Diaminobenzidine (DAB; Sigma) was applied to each slide for up to a maximum of 15 minutes. Exposure time was dependent on the primary antibody used. Slides were given a quick rinse in distilled water then dehydrated, cleared, and mounted.

3.2.7 Cartilage grading

Cartilage repair was histologically graded in blinded evaluations using a previously published scoring system [50]. The five weighted categories each section was assessed include the following: cell morphology (0-4), matrix staining (0-3), surface regularity (0-3), thickness of cartilage (0-2), and integration with native cartilage (0-2). For each sample, only the lowest score was considered to ensure we evaluated repair at the centre of the defect as oppose to the edges of the injury.

3.3 RESULTS

3.3.1 Characterization of defect with MRI and histology.

Defects induced using 26G needles were characterized using MRI and histology and compared with the measurements of the surgical device itself. The external diameter of the needle, as provided by the manufacturer BD biosciences, is 0.45 mm (450 µm). The length from the tip of the needle to the edge of stopper is approximately 1.45 mm (1450 µm) as measured using calipers. Analysis using imaging software, ImageJ, the diameter of defect seen in a

disarticulated injured femur (Figure 3.1) was measured to be approximately 0.516 mm x 0.5844 mm. The MRI scan of an injured defect 2 weeks post injury revealed a defect that was approximately 375 µm in diameter and 1125 µm in length. ImageJ analysis with the stained section of the same animal that was MRI imaged, revealed a defect opening of approximately 441.7 µm. Overall, measurements from the disarticulated joint, MRI scan, and histology suggests that the defects can be visualized by MRI.

3.3.2 Defects can be visualized with MRI up to 4 weeks post-injury in both strains

At endpoints 0, 2, and 4 weeks post-injury, animals were euthanized, legs were imaged *ex vivo* using MRI, and processed for histology. Side by side comparisons show that the focal injury can be visualized up to 4 weeks in both C57 (Figure 3.2) and MRL mice (Figure 3.3). MRI scans for both strains at timepoint 0 display hyperintense signaling which appears to decrease with time. Furthermore, hypointense signaling increases in the patella and striations can be observed in localized areas. At the two week time points, proteoglycan staining was not present in the defect area, as assessed by Safranin-O (Figure 3.2 & 3.3). Furthermore, the defect area displayed hyperintense signal while areas with proteoglycan staining were hypointense as assessed by MRI (Figure 3.4). However, it appears that proteoglycan content does not directly correlate with signal intensity. In one of the MRL animals, hypotintense signaling was not present in the corresponding MRI scan in areas where proteoglycan staining in the patellar tendon was present.

3.3.3 MRL/MpJ mice display superior repair compared to C57BL/6 mice

Histological analysis of the joints using Safranin-O reveal cartilage defects in MRL mice display superior repair compared to C57 mice (Figure 3.5). At four weeks, total joint

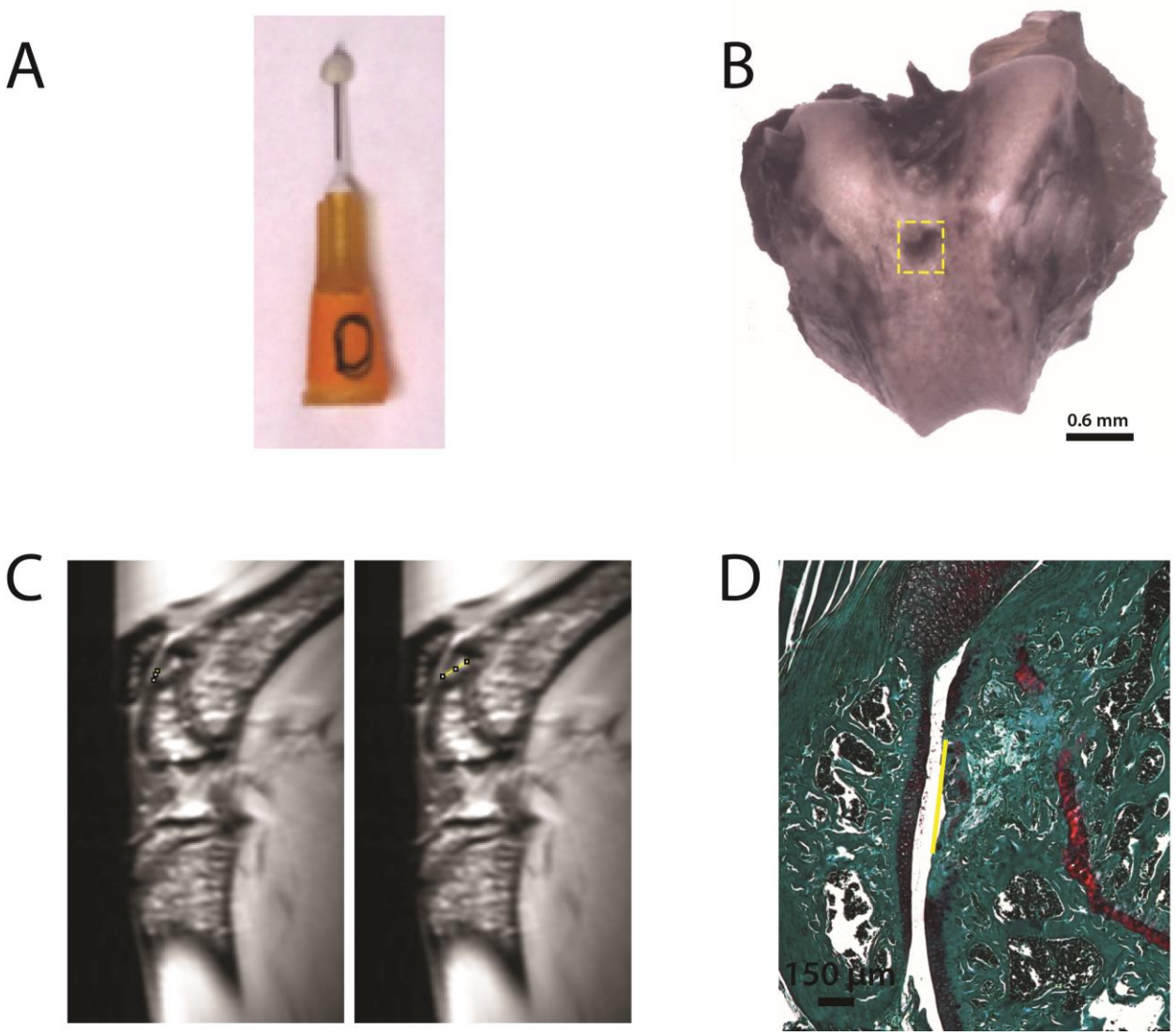

Figure 3-1 Characterization of defect. A 26G stopped needle (A) was created to induce focal defects in mice. The surgical apparatus as a diameter of 45 µm and a bead-to-needle tip distance of approximately 1450 µm. To confirm injury, the injured leg was disarticulated and india ink was used to increase contrast for visualization of defect (B), which is seen in the yellow box. When defect size was measured from the MRI scans (C), the defect measurements were 375 µm in diameter and 1125 µm in length. The yellow lines on the MRI scan indicate the dimentions in which the measurements were taken. Sample scanned in the MRI was also analyzed histologically (D) and the defect opening, as indicated by the yellow line, was measured to be 441.7 µm.

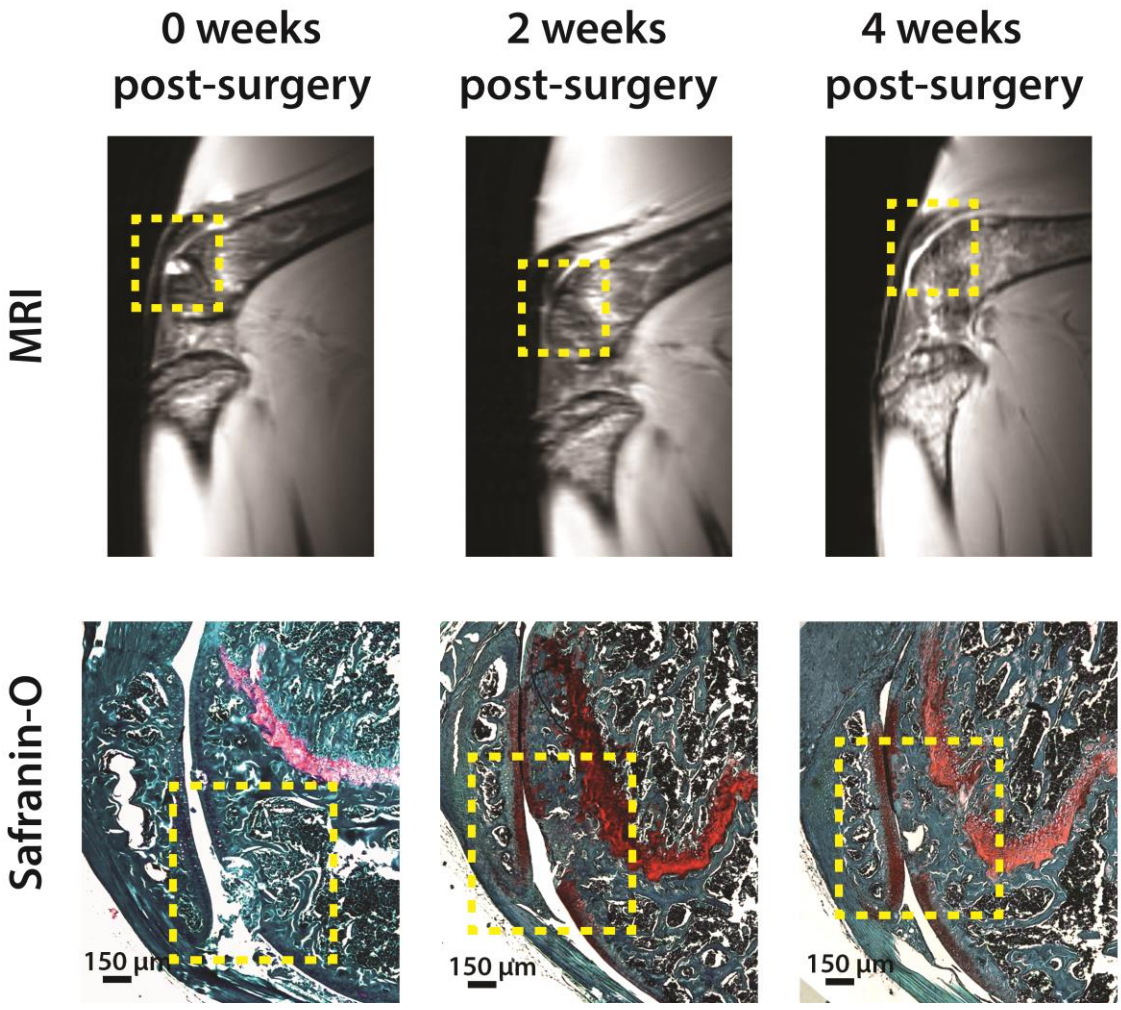

Figure 3-2 MRI evaluation of cartilage defect in C57BL/6 mice at 0, 2, and 4 weeks post-injury. Evidence of a defect, as indicated in the yellow box, can be seen at each time point in the MRI as well as in the corresponding Safranin-O stained sections.

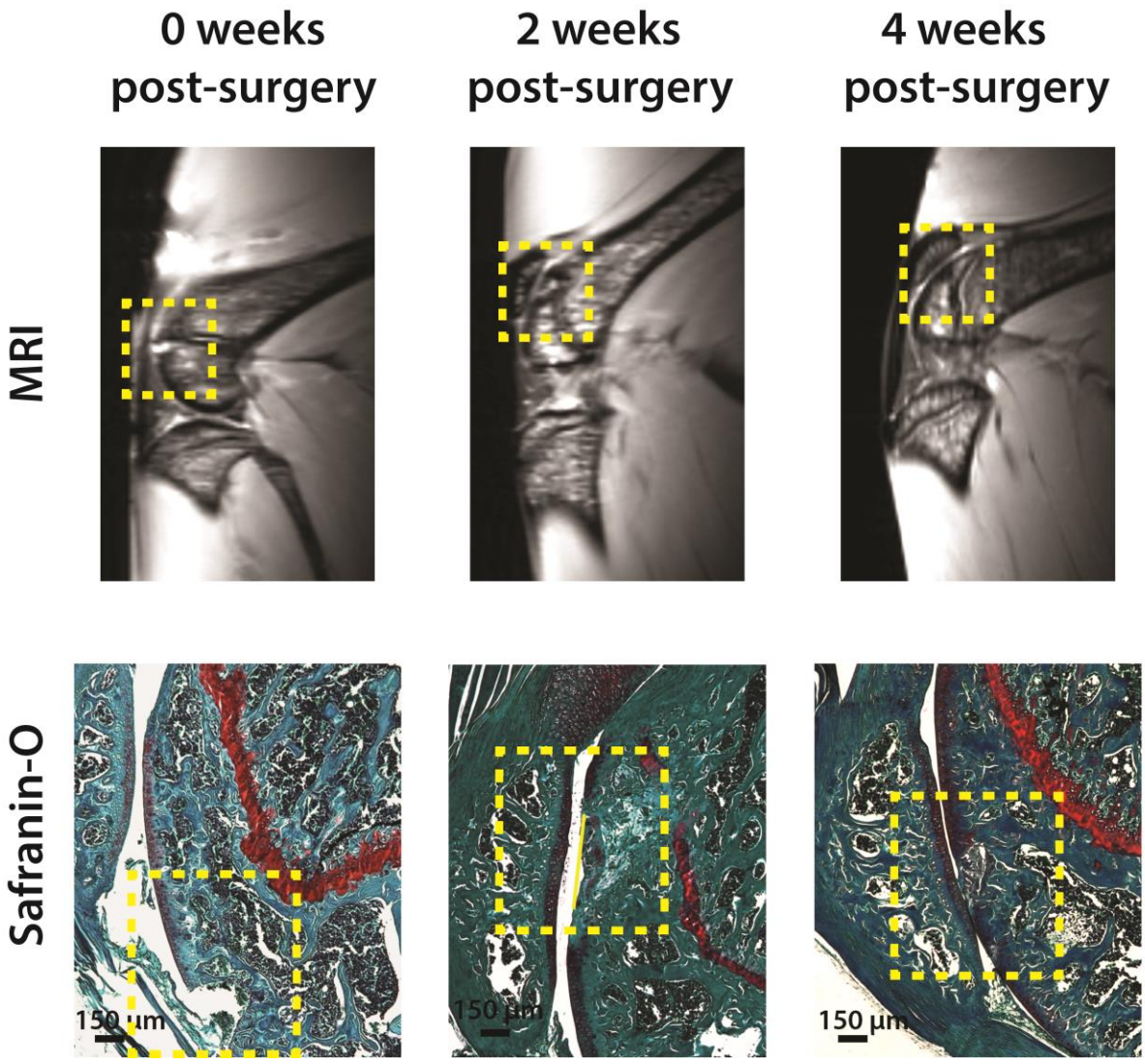

Figure 3-3 MRI evaluation of cartilage defect in MRL/MpJ mice at 0, 2, and 4 weeks post-injury. Evidence of a defect, as indicated in the yellow box, can be seen at each time point in the MRI as well as in the corresponding Safranin-O stained sections.

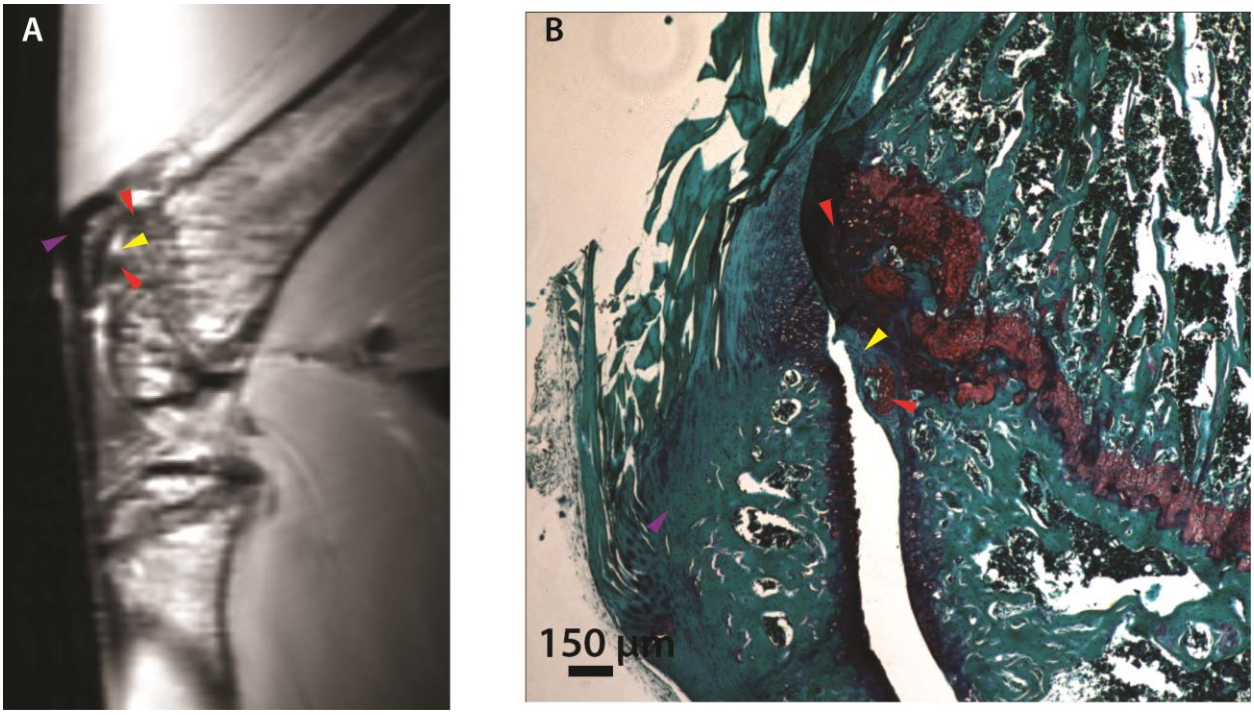

Figure 3-4 Correlation of signal intensity with histology. In both strains, repair tissue is observed to be hypointense when proteoglycan production has begun (red arrows). Areas with lack of proteoglycans are observed to display higher signal intensity (yellow arrows), which can be due to the magic angle effect or due to increased fluid content. Areas of low signal intensity do not always correlate with proteoglycan content. Low signal intensity can be seen in a region of the patella (purple arrow) where proteoglycan content, as assessed by Safranin-O, is low.

morphology seem to be better preserved in MRL mice compared to C57 animals. Blinded cartilage grading was done according to according to a previously published scoring protocol show that at four weeks post-injury, there was a significant difference between MRL and C57 (Figure 3.6) repair [50]. With healthy joints scoring a maximum score of 14, mean histological score 4 weeks post injury for C57 were of 4.818 (SD= 1.537, SE=0.4635) and 7 (SD=1.323, SE=0.4410) for MRL. Un-paired student's t-test revealed a p value of 0.0035 where significance was defined as $p < 0.05$.

3.3.4 C57 mice display extensive infiltration by various cell types into injury site

To assess the presence of various cell types, immunohistochemistry was performed using antibody against Sca-1 (mesenchymal and hematopoietic stem cell marker), F4/80 (macrophage marker), and c-kit (hematopoietic stem cell marker). Sca-1 staining was observed to localize at the articular surface as well the defect at 2 and 4 weeks post injury (Figure 3.7). Sca-1 staining was also seen in the patella adjacent to the defect at two weeks but is absent at four weeks. F4/80 staining was weakly localized at the defect at 0 weeks (Figure 3.8). At 2 and 4 weeks post injury, F4/80 staining was observed in the defect as well as patellar

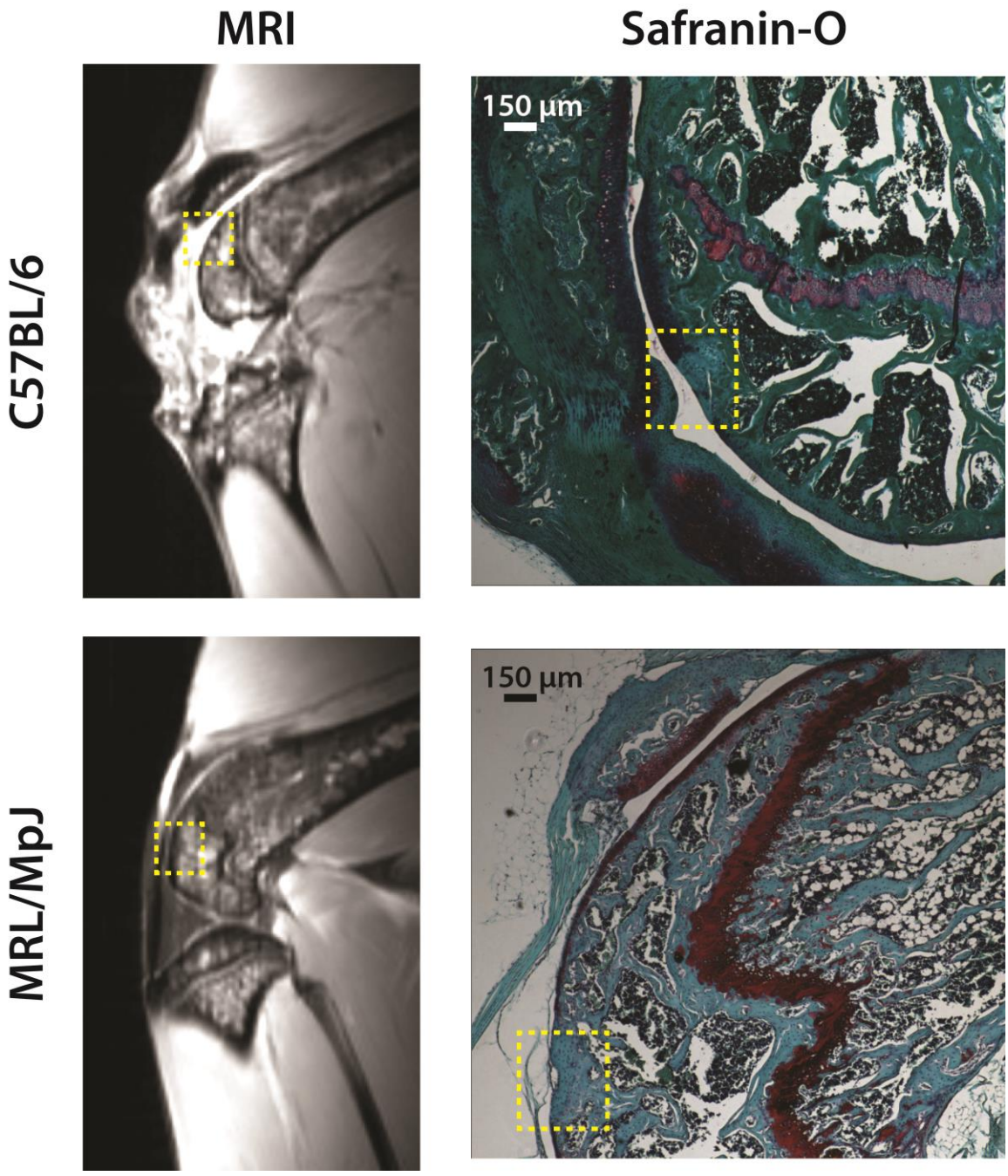

Figure 3-5 Comparison of total joint morphology in the poorest healers at 4 weeks post injury. Level of repair was assessed by blinded cartilage grading. In both MRI and histology, the C57 sample displayed extensive changes in tissue morphology, especially at the patella tendon. A diminished growth plate as well as the loss of proteoglycan content in the surrounding articular cartilage are also seen in the C57 sample. In contrast, the MRL sample display a robust growth plate and no gross changes in patella tendon morphology. Proteoglycan content in the cartilage surrounding the defect is also diminished in the MRL sample.

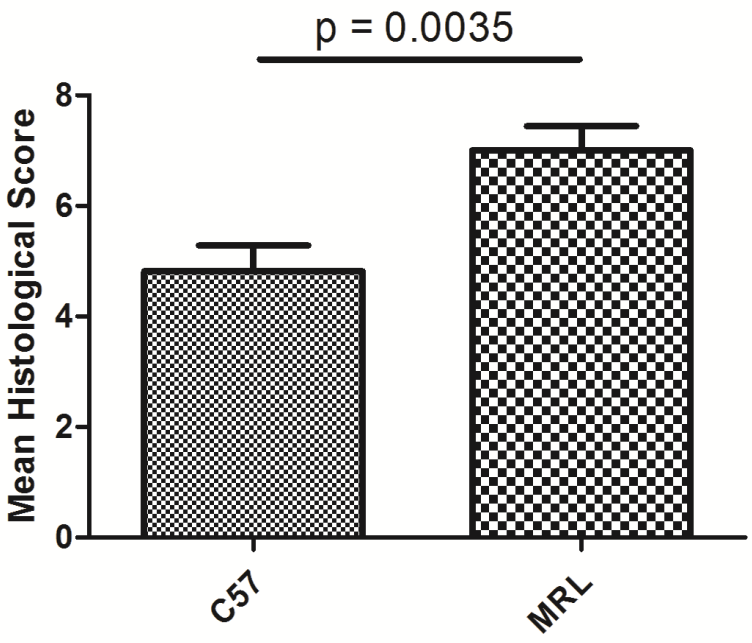

Figure 3-6 Statistical analysis of cartilage gradings at 4 weeks post injury in both C57 and MRL mice. MRL mice display significantly superior repair compared to C57 animals.

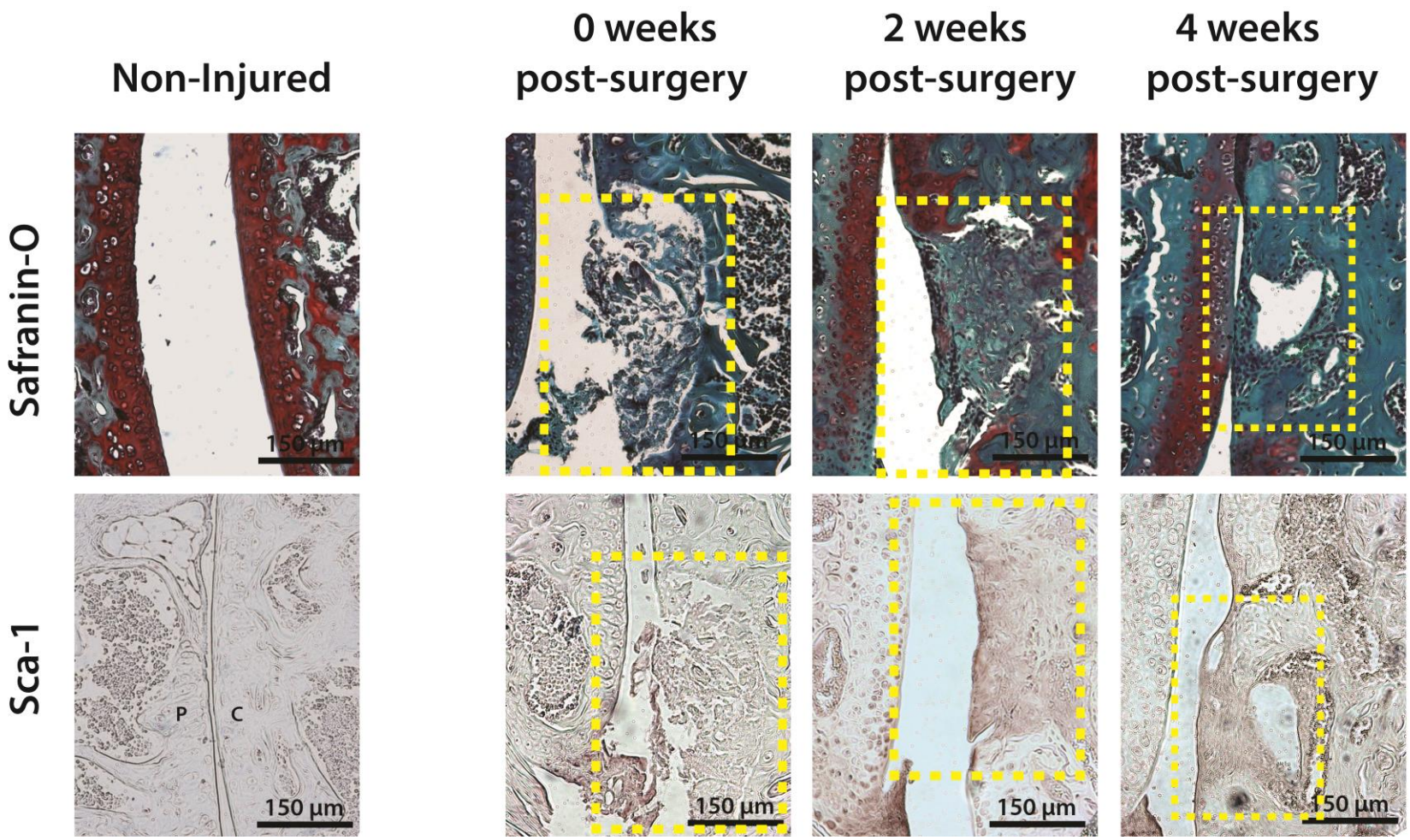

Figure 3-7 Sca-1 analysis during early cartilage repair in C57BL/6 mice at 0, 2 and 4 weeks post surgery. Defects are indicated in the yellow boxes. Sca-1, a marker for undifferentiated cells, is strongly localized in the defects at both 2 and 4 weeks. P- patella; C- cartilage. See appendix for positive and negative controls for Sca-1 staining.

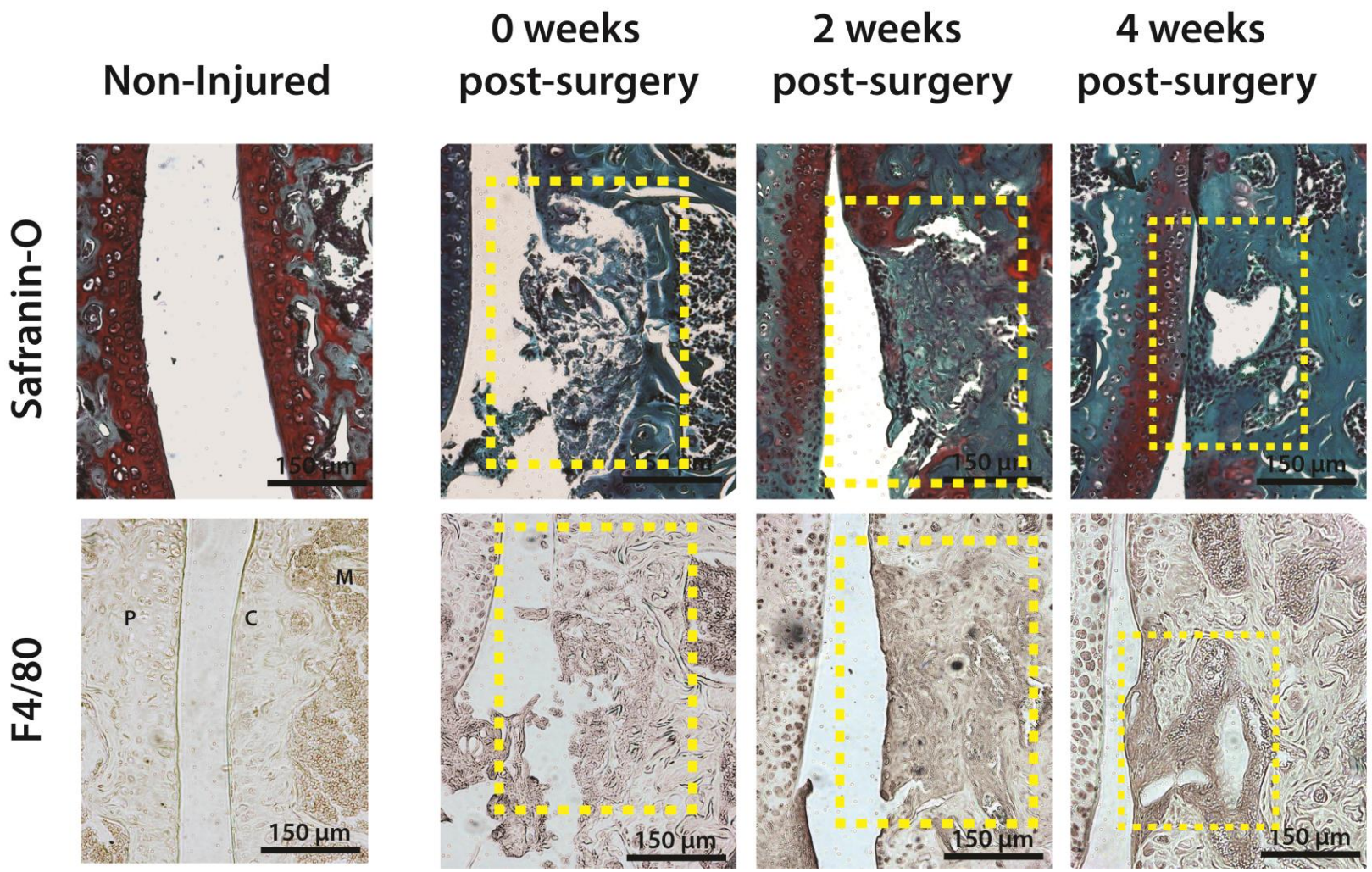

Figure 3-8 F4/80 analysis during early cartilage repair in C57BL/6 mice at 0, 2 and 4 weeks post surgery. Defects are indicated in the yellow boxes. F4/80, a macrophage marker can be seen at 0 weeks but is strongly localized in the defects at both 2 and 4 weeks. P- patella; C- cartilage; M-marrow. See appendix for positive and negative controls for F4/80 staining.

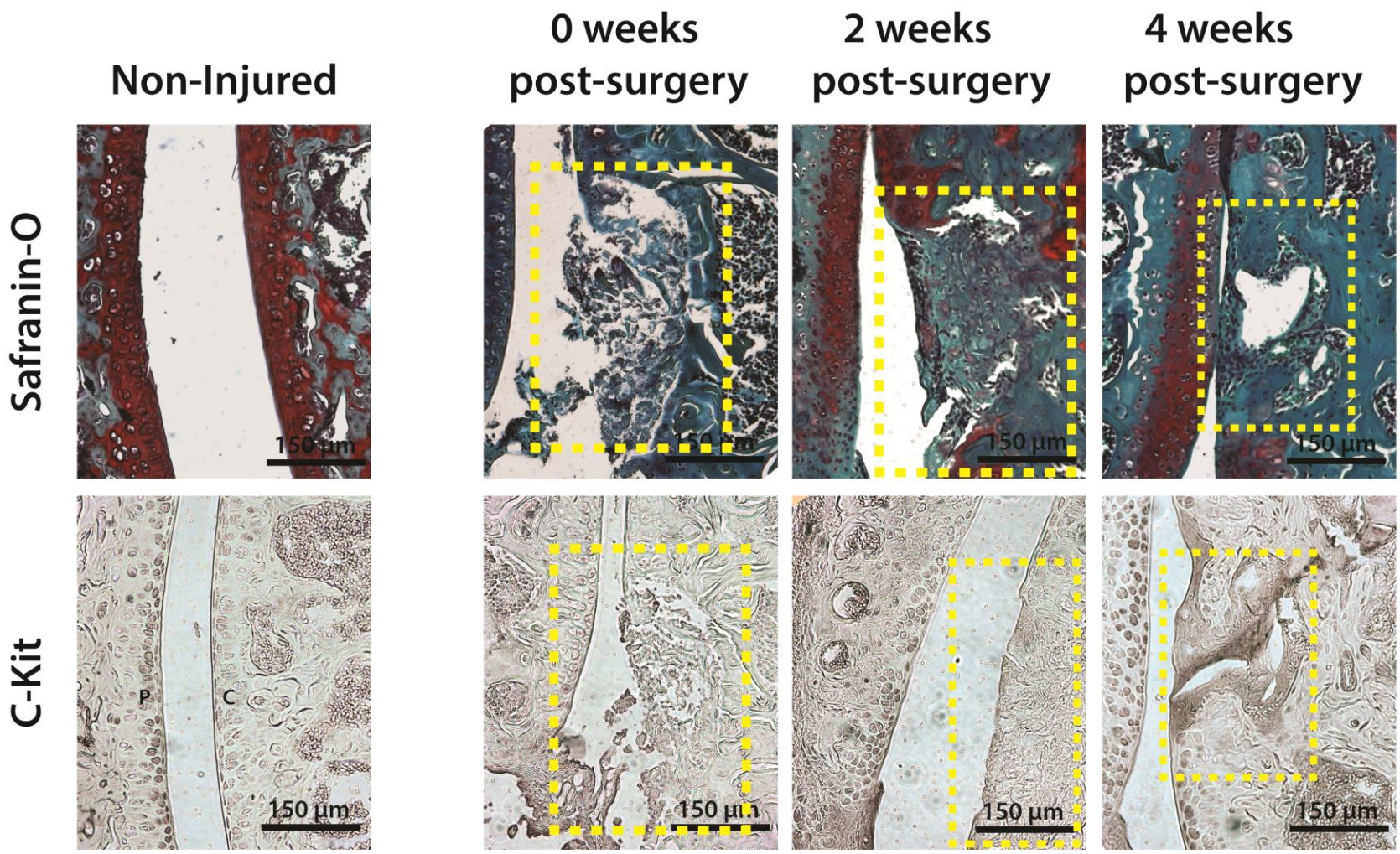

Figure 3-9 C-Kit analysis during early cartilage repair in C57BL/6 mice at 0, 2 and 4 weeks post surgery. Defects are indicated in the yellow boxes. C-kit, a marker for cells of hematopoietic origin, can be seen to localize to the defect only at 4 weeks. P- patella; C- cartilage. See appendix for positive and negative controls for c-Kit staining.

surface adjacent to the injury. Unlike the other two markers, c-kit was found in the defect and adjacent patellar surface only at 4 weeks post-injury (Figure 3.9).

3.3.5 MRL mice display minimal cell infiltration into defect site

Unlike C57 mice, immunohistochemical assessment revealed an absence of Sca-1 (Figure 3.10) and c-Kit staining (Figure 3.12) in the defect at both 2 and 4 weeks post injury. F4/80 staining, on the other hand, were detected in the repair tissue and in the adjacent patellar surface at 2 weeks post injury (Figure 3.11). At four weeks, F4/80 staining was absent in the defect but was still present in cells at the patellar surface.

3.4 DISCUSSION

Here, we show MRI can be used to visualize our joint injury model. The scan parameters used in the experiments were chosen to optimize for clear visualization of the mouse knee joint. While the injury was clearly visible, defect size as measured on the MRI was smaller compared to the measurements of the needle as well as the measurements generated from the histological sections. Taken together, we concluded that the injury model utilized in our study could be monitored *ex vivo* with MRI for gross changes in anatomy though assessing incremental changes would be difficult due to the resolution limit.

Having established and validated an injury model, we set out to characterize the healing process following a focal cartilage injury in both C57 and MRL mice. It was evident that defects could still be visualized for up to 4 weeks post injury. In defects generated in both strains, proteoglycans were observed in the repair tissue as assessed by Safranin-O. Furthermore, the

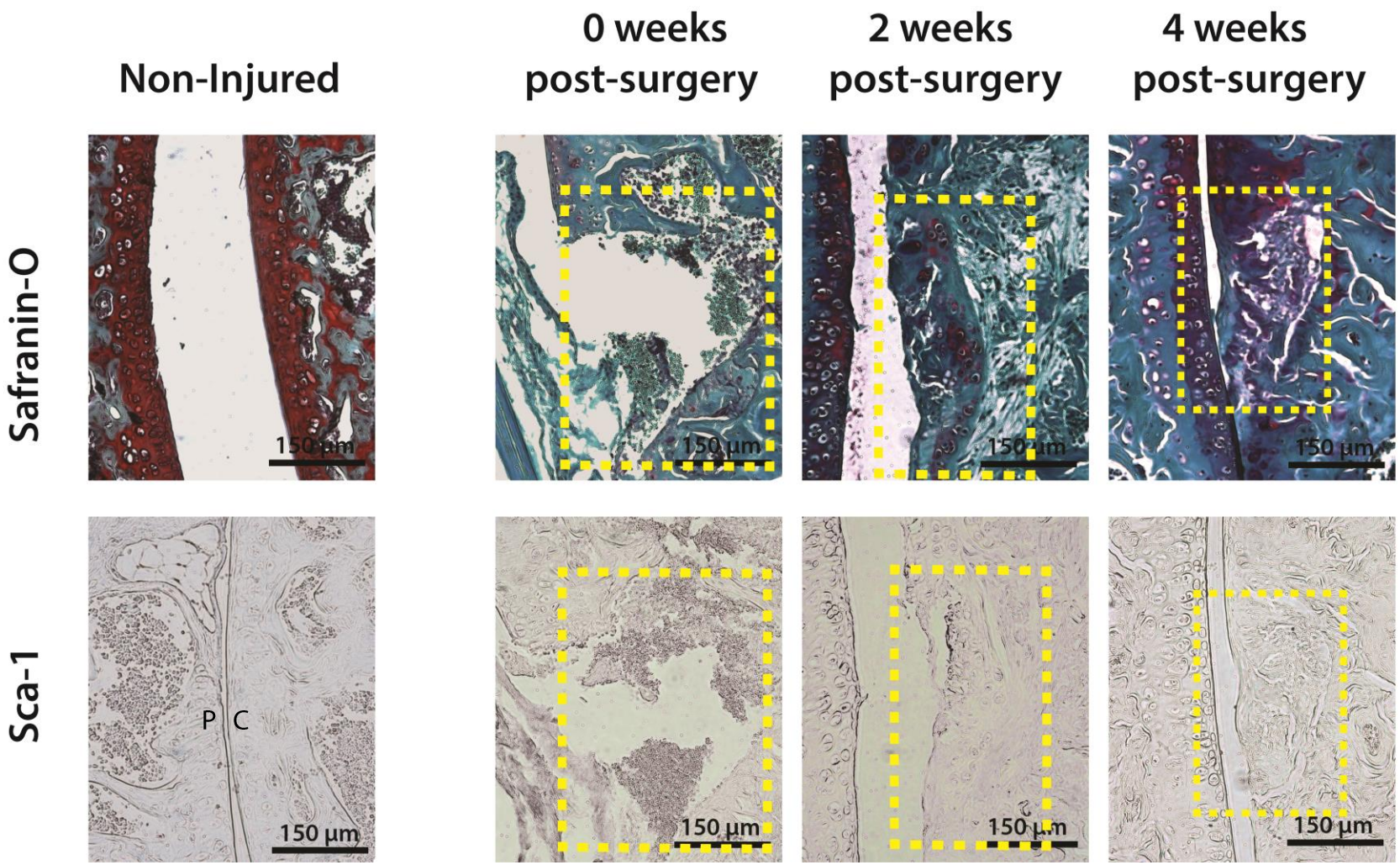

Figure 3-10 Sca-1 analysis during early cartilage repair in MRL/MpJ mice at 0, 2 and 4 weeks post surgery. Defects are indicated in the yellow boxes. Sca-1, a marker for undifferentiated cells, is absent all time points. P- patella; C- cartilage. See appendix for positive and negative controls for Sca-1 staining.

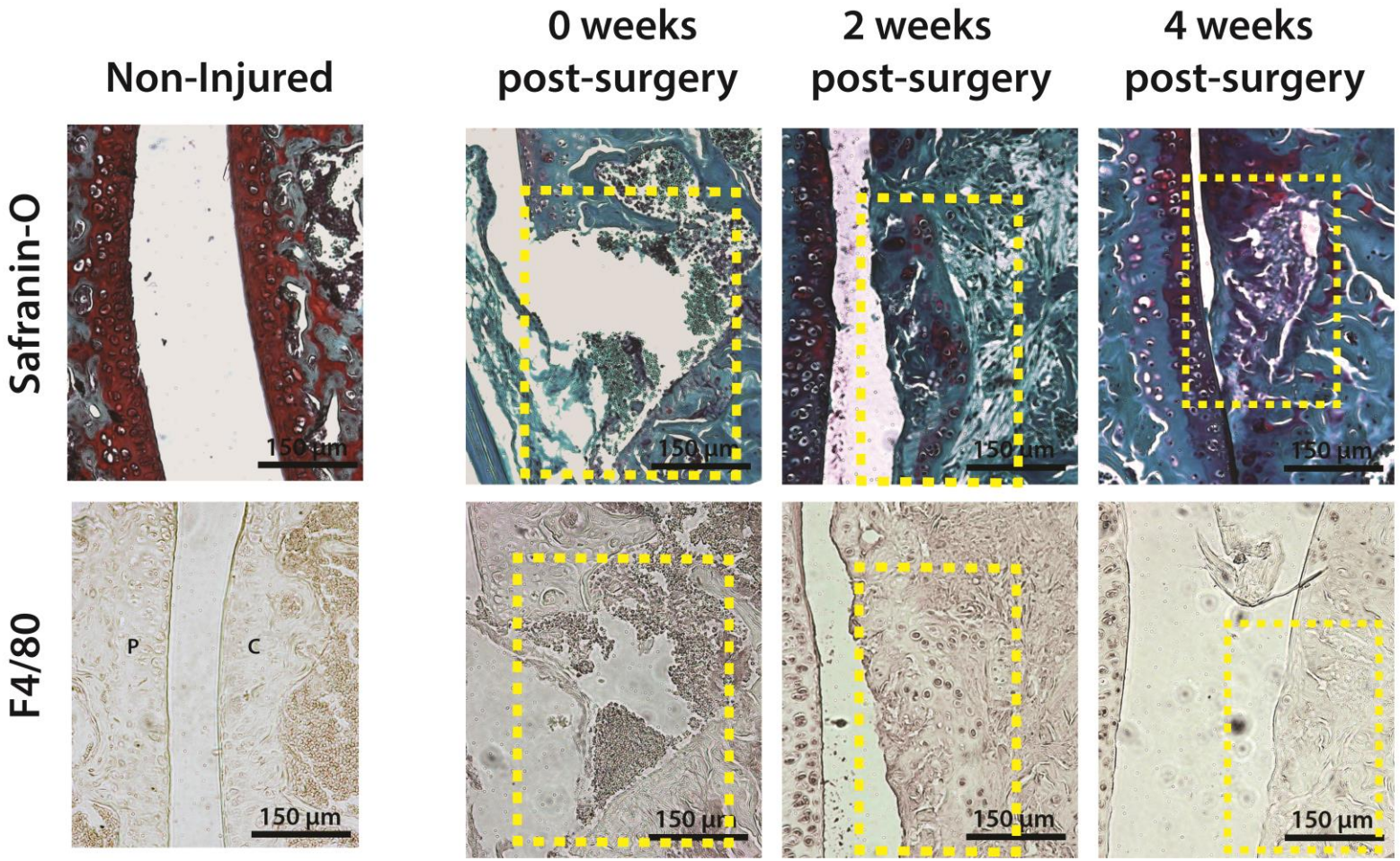

Figure 3-11 F4/80 analysis during early cartilage repair in MRL/MpJ mice at 0, 2 and 4 weeks post surgery. Defects are indicated in the yellow boxes. F4/80, a macrophage marker, is present at only 2 weeks. P- patella; C- cartilage. See appendix for positive and negative controls for F4/80 staining.

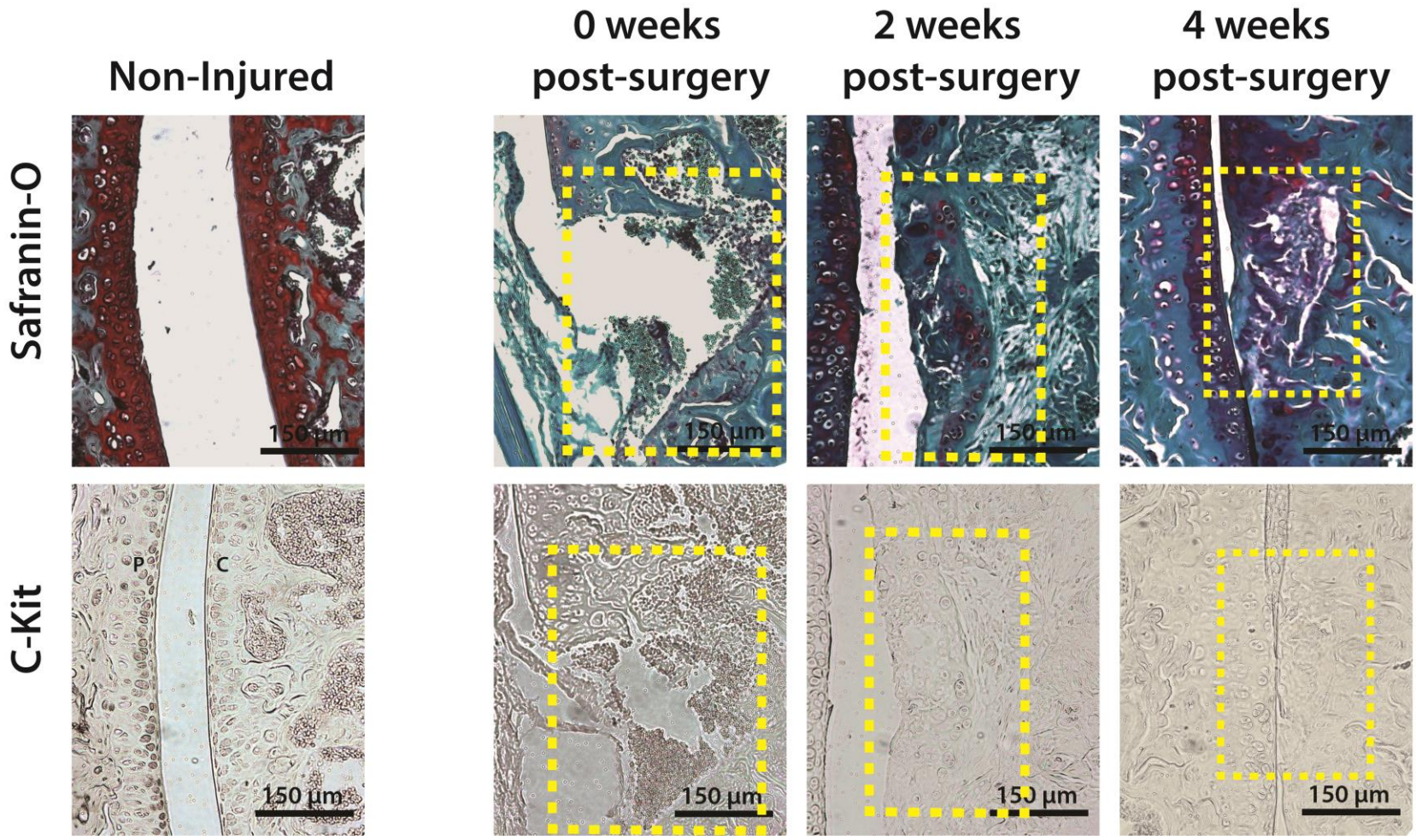

Figure 3-12 C-Kit analysis during early cartilage repair in MRL/MpJ mice at 0, 2 and 4 weeks post surgery. Defects are indicated in the yellow boxes. C-Kit, a marker for cells of hemtopoeitc origin, is absent all time points. P- patella; C- cartilage. See appendix for positive and negative controls for c-Kit staining.

repair area displays hypotense signalling while adjacent areas without proteoglycan appear hyperintense. Defects that appear to be undergoing some level of repair, yet did not produce proteoglycans, displayed increased signal intensity compared to adjacent areas that contained proteoglycans content. One possible explanation for the increase in signal intensity can be due to a phenomenon, called the "magic angle effect" that mostly affects structures containing parallel collagen fibres when using imaging sequences with short TE [90,91]. Ligamentous tissue usually appear with low signal intensity but when collagen fibers are at the magic angle of 55° to the magnetic field of the magnet, T2 relaxation times, i.e. the time it takes to reach phase incoherence and therefore loss of signal, is extended and signal intensity increases. The magic angle effect can be eliminated when imaging with a longer TE. For future experiments, an additional scan with a longer TE should be included to ensure increase in signal intensity is due to a structural feature of the tissue as oppose to an artefact [92].

The cause due to increase in signal intensity seen in Figure 3.5, however, is unclear. It has been documented that though the magic angle effect most often affects structures with parallel collagen fibers, disorganized fibers could still induce the effect [91]. An alternative hypothesis could be that as the MR images are proton-density weighted, increase in signal intensity is associated with increases in the number of hydrogen atoms. A localized increase in fluid content may also induce increase in signal intensity. Though the exact cause of the hyperintense signal is unclear, it is apparent that the MR images provide insight on the structural/architectural integrity of the tissue, e.g. collagen fiber orientation or fluid content, that is not apparent in histology.

In both strains, we observed hypointense signaling in the patella and its associated tendon while striations were seen in load bearing areas. These findings have been documented before in

humans and have been associated with areas of high collagen and high proteoglycan content [5]. In contrast to the findings of Foster et al., we have observed that signal intensity does not always correlate with high proteoglycan content. Comparing the histology with the corresponding MRI scan, we have also observed that hypointense signaling in the patella and tendon occurs despite low levels of Safranin-O staining. Nevertheless, our data suggests that *ex vivo* MRI can reveal structural and morphological changes in the joint in response to injury that is not evident in histology.

In addition to Safranin-O staining, we performed immunohistological analysis to determine the various cell types recruited to the defect in response to injury. In C57 animals, the stem cell marker, Sca-1, could be detected in the defects at both 2 and 4 weeks but hematopoietic stem/progenitor cells marker, c-kit, could only be detected at 4 weeks, suggesting that the initial infiltration of progenitor cells are not of hematopoietic origin. Detection of macrophages at both time points suggests an early and chronic involvement of the immune system. In MRL animals, however, both Sca-1 and c-kit were not detectable at 2 and 4 week time points while F480 was only detected at 2 weeks post-injury. A possible explanation could be that the presence of c-kit expressing cells are dependent on the presence of the initial progenitor (mesenchymal) cell population, Sca-1^{+}/c-kit^{-} cells. Noticeably, lack of macrophage detection at 4 weeks suggests that the immune reaction in response to injury is transient in MRL mice but potentially chronic in C57 mice. This is potentially interesting, since similar results have be demonstrated in OA joints [93].

In hematopoietic stem cells (HSCs), expression of Sca-1 is downregulated as HSCs differentiate into blood/immune system progenitor cells [82]. The poor cartilage repair observed within C57 mice may also be a result of early and prolonged recruitment of progenitor cells to

the defect, coupled with a joint micro environment that does not permit these cells to differentiate and repair the injury. A possible explanation for the lack of stem/progenitor markers in MRL is that recruitment of progenitor cells occur earlier than the 2 week time point. Previous studies have also documented the transient expression of Sca-1 in response to injury. In one study involving skin wound repair, the authors found that Sca-1^{+} cells increased from 2.7% in unwounded skin to 11% seven days post injury but decreased to 4.8% at fourteen days post injury [94].

Our histological data also supports the findings by Kurth et al. (2011) in that Sca-1 staining can be seen in C57 defects at 2 weeks post-surgery, indicative of migration of progenitor cells to the injury site. Absence of c-Kit staining at 2 weeks suggests progenitors in the defect are not of hematopoietic origin. Our analysis, however, also challenges the authors' conclusion that MSCs differentiate in the injury site. The authors found the engrafted cells expressed Sox9 and type 2 collagen, but our results suggests that C57 mice display prolonged Sca-1 expression up to 4 weeks post-surgery, indicative that the cells localized at the defect are still progenitors and have not differentiated. While it is possible that a subset of these cells may express chondrogenic markers, there is no direct evidence that terminal differentiation into chondrocytes has occurred based on morphological & histological assessment. Further supporting this notion is that at 4 weeks post-surgery, C57 animals display significantly less cartilage repair than MRL mice despite extensive and intense Sca-1 staining in the defect. Further studies will be required to determine the mechanism behind MRL animals' superior ability to repair cartilage injury.

Chapter Four: **Evaluating the role of exogenous synovial progenitor cells in a cartilage injury model system**

4.1 BACKGROUND

The discovery of MSCs in the synovium lead to widespread characterization of MSCs from different tissue sources. Studies have shown that MSCs isolated from varying tissues have distinctly different cellular phenotypes. Synovium derived MSCs have been widely documented to display superior chondrogenic potential compared to either adipose derived MSCs or bone marrow derived MSCs. With regards to cell based cartilage repair, however, bone marrow and adipose derived MSCs have been the most common cell types used, with the bone marrow derived MSCs being approved for human cartilage repair clinical trials [95].

MSCs have been shown to secrete soluble factors that regulate apoptosis, angiogenesis, and cell homing, among other cellular processes [96]. This cell type also has been demonstrated to have the ability to migrate to sites of injury [97]. Previous studies on MSC transplantation have observed that while injection of bone marrow derived MSCs seems to attenuate the progression of joint destruction, cellular engraftment was seen at both the cartilage surface and interior zones of the new repair tissue, suggesting that MSCs may contribute to repair via engraftment and differentiation into the cell types required to replace the missing/damaged tissue. During separate engraftment experiments, however, injected cells localized and integrated into the various joint tissues e.g. fat pad, synovial lining [45], suggesting that widespread integration in an injured joint implies engraftment can be non-specific.

With respect to cartilage repair, numerous studies have investigated the effect of intra-articular injection of MSCs on various animal models [45,46,98]. While a protective effect has been

observed, the mechanism underlying the effect is still unclear. Furthermore, the majority of the studies investigating the MSC repair of cartilage utilize bone marrow or adipose derived MSCs as the cell source. The role of exogenous synovium derived MSCs in repairing cartilage in a murine mouse model has not been previously studied.

In one particular study, the authors were investigating whether bone marrow derived MSCs from MRL mice were superior in slowing down post traumatic arthritis compared to bone marrow derived MSCs from C57 mice. The authors had observed a protective effect but there was no difference between which mouse strain the MSCs where derived from. The authors also observed engraftment of a small subset of cells into the injury site [63]. Due to the increased ability of the MRL mice to repair cartilage, the lack of difference observed between MRL and C57 MSC repair capacity *in vivo* is surprising. It may be possible, however, that synovial cells from MRL mice may demonstrate increase cartilage repair capacity compared to C57 cells, since synovial stem/progenitor cells have increased *in vitro* chondrogenic capacity when compared to bone marrow stem/progenitors. Therefore, the objective of this study is to determine if exogenous synovial progenitors migrate to the site of focal cartilage injury similar to bone marrow derived MSCs and furthermore, if synovial progenitors isolated from MRL mice are superior to those isolated from C57 mice in contributing to cartilage repair.

4.2 MATERIALS AND METHODS

4.2.1 Isolating murine synovial cells

Eight male mice were euthanized, legs were removed, and the joint space was opened. Using a dissecting microscope, synovial tissue was dissected out from the joint and placed in a

petri dish containing PBS and 1% anti-anti (Gibco). Grooves were made along the bottom of a 12 well plate with a scalpel to improve tissue transfer efficiency and to promote tissue adherence. Tissue samples were transferred to the empty 12 well plate and MSC expansion media, consisting of DMEM/F-12 (Biowhittaker), 10% lot-selected fetal bovine serum (Gibco), 1% non-essential amino acid (Gibco), 1% anti-anti (Gibco), and 0.2% beta-mercaptoethanol (Gibco), was added to each well. Cells were then incubated at 37° C in 2% O_2 and 5% CO_2. Media was changed every 2-3 days until outgrowth was observed after which, media was changed daily. When cells localized around the tissue had reached confluency, the tissue piece was removed and the cells were passaged and transferred to a T25 flask. Subsequent media changes occured every 2-3 days.

4.2.2 Sca-1 Selection of cells

Media was removed and cells were trypsinized with 0.25% trypsin-EDTA (Gibco) until cells were seen to lift from the plate after which media was added to deactivate the trypsin. Cell suspension was then centrifuged for 5 minutes (Beckman, Model TJ-6). During this time, a working solution of BD IMAG buffer (BD Biosciences) was produced by mixing 1 mL of BD IMAG Buffer (100x) with 9 mL of sterile distilled water. Diluted BD buffer solution was kept on ice for the duration of the procedure. After centrifugation, supernatant was discarded and the cell pellet was resuspended in 1 ml of diluted BD buffer. 5 µL of antibody was added to the cell suspension, vortexed on minimum setting, and placed on ice for 15 minutes after which cells were centrifuge twice at 300 G for 10 minutes. After each spin, supernatant was removed and cell pellet was resuspended in 1m mL of diluted BD buffer. When the last resuspension has been completed, 5 µL of magnetic particles (Bangs Laboratories; BM568) was added. Cell suspension

was vortexed on low setting and allowed to sit on ice for 15 minutes after which the mix was transferred to a 5 ml vial and an additional 1 mL of buffer was added to the suspension. Cells were placed in the sorting magnet for 7 minutes after which liquid was removed and cells were plated in a T25 flask.

4.2.3 GFP Lentiviral Transduction

GFP lentivirus was generously given by Dr. Jeff Biernaskie and Eko Raharjo. At passage 2, Sca-1 purified synovial cells are incubated with the following mix overnight (~12hrs) at 37 °C at 2% O_2: 5 mL MSC expansion media, 5 µL GFP lentivirus, and 2 µL of Polybrene (8 µg/mL, Sigma). Media was changed the following day.

To assess transduction efficiency, one confluent T25 flask of purified Sca-1 synovial derived cells were split into two T25 flasks. Once adherent, cells in one of the flasks underwent GFP lentiviral transduction while cells in the second flask remained unlabelled. Cells in both flasks were expanded until passage 4 where GFP expression would be visually detected under a microscope. Proper consideration was taken to ensure both flasks contained approximately the same number of cells. When flasks were confluent at passage 4, cells were trypsinized and subsequently centrifuged for 5 minutes. Cell pellets were resuspended in 4% PFA at room temperature for 15 minutes after which cells were centrifuged for 5 minutes at 300 G. Supernatant containing the PFA was removed and the cells were resuspended in sterile PBS. Centrifugation at 300 G for 5 minutes was repeated two more times where each time, pellets were resuspended in PBS. After the final wash, cell suspensions were stored at 4 °C until they were to be counted using a flow cytometer. A total of 10 000 events were counted.

4.2.4 Toxicity Assay

Approximately 2000 C57 Sca-1^+-GFP^+ synovial cells at passage 4 were plated for each well of a 96 well up to a total of 6 wells. Cells were incubated overnight at 37 °C with 2% O_2 to ensure adherence. Media was removed the next from each well and cold media was added to each well. Cells either received a treatment of 10% dimethyl sulfoxide (DMSO), media, or underwent Sca-1 selection. For the selection, cells were incubated with 3 µl of biotin-conjugated anti-mouse Ly-6A/E (also known as Sca-1; eBioscience) for 15 minutes on ice after which 3 µl of BioMag Streptavidin beads (BM568, Bangs Laboratories) was added for 15 minutes on ice. For positive control, cells were incubated with 10% DMSO for 30 minutes on ice. After the incubation period, wells were washed 3 times with sterile PBS and new media was added. Cell death was assessed at 0 and 48 hours using ethidium homodimer-1 (EthD-1;Molecular Probe). Fluorescence was analyzed using the InCell 2000 (GE).

4.2.5 Receptor Internalization

Sca-1^+ synovial cells from C57 mice (passage = 4) and BioMag Streptavidin beads were used in the following experiment. The experiment was run in quadruplicate.

Cells were inactivated with mitomycin C for 1-1.5 hours at 37 °C and 2% O_2 to inhibit proliferation. Cells were then trypsinized, spun down, and resuspended in expansion media. Initial cell count was taken using Trypan blue and cell concentration was adjusted such that a density 20 000- 50 000 cells per well in a 12 well plate could plated. Cells were then incubated overnight at 37 °C and 2% O_2. In the following day, antibody and bead incubated together for 30 minutes after which the antibody-bead (Ab-Bd) complex was magnetically pulled/sorted out. A

master mix of 0.5 µg of biotin-conjugated anti-mouse Ly-6A/E and 55.56 µg of streptavidin-bound beads were used. The Ab-Bd complexes were then washed with PBS x 3 times and resuspended in 200 µL of media. Ab-Bd was added to appropriate wells and incubated for 30 minutes. At the end of 30 minutes, media from the wells were removed and cells were washed 5 times with PBS. Additional 2 ml of expansion media was added to each well. At 30 min, 3, 6, and 9 hour, cells were trysinized for 5 minutes. Cells were centrifuged and resuspended in media. Cell mixture was then magnetically sorted for 5 minutes after which the media was removed and sorted cells were resuspended with 100 µL PBS. Cells were then counted using a Multisizer 3 Coulter Counter (Beckman Coulter).

4.2.6 Animal experimental outline

All animal experiments were done in accordance to the standards of the research ethics committee at the University of Calgary.

Intra-articular injections of either Sca-1^+-GFP^+ C57 synovial cells, Sca-1^+-GFP^+ MRL synovial cells, or sterile PBS were performed on male C57 mice, aged 4-6 weeks. For controls, intra-articular injections of Sca-1^+-GFP^+ C57 synovial cells were performed on 2 male C57 animals. *In vivo* MRI scanning was done on one mouse immediately post-injection while the other mouse was imaged 24 hours post-injection. After imaging was done, both animals were euthanized and legs were dissected out, fixed in 10% neutral buffered formalin, underwent decalcification by RDO [Sigma], and processed for histological analysis.

In experimental animals, focal cartilage defects were induced in the left knee 24 hours post-injection using a 26G stopped needle. Each treatment consisted of 5 animals, n=2 for the 2

week time point and n=3 for the 4 week time point. In the latter group, 2 out of 3 mice were assessed by MRI. Animals underwent *in vivo* imaging at 1 hour post intra-articular injection, 1 hour post surgical induction of focal cartilage injury, 2 weeks post injury, and at 4 weeks post injury after which they were euthanized. For animals that were not imaged, they were euthanized by cervical dislocation at the end of either 2 or 4 weeks post-injury. Legs were then dissected out and processed for histological analysis.

4.2.7 Injection Apparatus

The injection apparatus (APPENDIX FIG) used for knee joints was developed by Dr. Paul Salo and has been previously described for use in rat knee joints (Salo et al., 1997a, b). The apparatus consisted of a custom-made knee holder that stabilized the joint during the surgeries and ensured consistency between different animals. Silicone tubing was used to connect a 30G needle to a 50 µL Hamilton microliter syringe (model # 705). A 1 µL dispensing Hamilton repeating dispenser (PB-600) was also used in conjunction with the syringe to ensure accurate volumetric injections into the joint space. A three axis micromanipulator was used to adjust the entry angle of the needle

4.2.8 Intra-articular injection

Mice were anaesthetized with isoflurane (2.5L/min) and remain under anaesthesia for the duration of the surgery. Surgery was performed under a dissecting scope (M300; Leica Microsystems) using the intra-articular injection surgical setup described above.
Hair around the knee joint is shaved and surgical area was wiped with betadine. With the mouse on the platform in supine position, the knee was placed into the holder such that the screws were

aligned just above the patella tendon. The screws were tightened superior to the lateral and medial epicondyles of the femur. When done correctly, the knee joint was completely immobile. A small skin incision was made to expose the patella and the tendon. Using the micromanipulator, the 30G needle was inserted through the tendon and into the space between the patella and the femur. Entry into the joint space was considered successful when the patella can be seen lifting upwards as the needle slides underneath. Total volume of injection used was 2 µL with each injection containing approximately 10 000 cells. For animals undergoing MRI scans, incisions were closed using 5-0 Ethilon nylon suture. For all other animals, incisions were closed using wound clips.

4.2.9 Inducing cartilage defect

Mice were anaesthetized with isoflurane (2.5L/min) and continued to be under for the duration of the surgery. Wound clips or sutures were removed and surgical area was swabbed with betadine. Keeping the knee extended, the tip of a custom-made 26G stopped needle was inserted under the patella tendon from the medial side and aimed towards the femur. Pressure was applied with a twisting motion until the tissue was at the hilt of the stopper. The resistance upon withdrawing the needle and the sight of bleeding indicated that the needle had successfully penetrated into the subchondral bone. Sterile gauze was used to blot excessive bleeding and the incisions were closed using 5-0 Ethilon nylon sutures for animals undergoing *in vivo* imaging. When imaging was completed, closure of wounds were reinforced with wound clips. For all other animals, incisions were closed using wound clips. The surgical area was then swabbed with gentamycin to prevent infection. Animals received buprenorphine (0.05 mg/kg) at the conclusion of the surgery as well as the day after for pain management.

4.2.10 Magnetic Resonance Imaging

Mice were anaesthetized with isoflurane (2.5L/min) and continued to be under for the duration of the scan. The animal was placed in a supine position on the animal bed with the knee of interest resting on a triangular, closed cell polyethylene foam block. The block, with a height of approximately 2 cm, base length of 5 cm, and base width of 1 cm, was used to elevate the knee such that the joint could be as close to the surface coil as possible without compression. Angle of flexion was determined to be 110° (see appendix). Animals were monitored using small animal monitoring systems MRI compatible physiological monitoring system. A thermal probe (physitemp) was used to monitor body temperature which was maintained at 32 °C using a water loop. A Graseby Respiration Sensor was placed over the chest cavity to monitor respiration such that anaesthesia level could be controlled. Respiration rate was maintained at around 100 beats per minute.

Animals in the MRI group were imaged *in vivo* using a 9.4 T magnet and a surface cryocoil. A proton density weighted, four-segment Rapid Acquisition with Relaxation Enhancement (RARE) sequence was used with the following parameters: RARE factor = 4, Repetition time = 2000 ms, echo time = 9.346 ms, FOV = 1.92 cm, slice thickness = 0.25 mm, matrix = 256 x 256. Animals in the MRI group were imaged at 0, 2 and 4 weeks after injury and transplantation. After the final time point, animals were euthanized and legs were processed for histological analysis.

4.2.11 Histological Analysis

4.2.11.1 Decalcification

Legs were fixed using a rapid decalcifying agent, RDO (Sigma). Legs were fixed in 10% NBF overnight at 4°C. Excess tissue was removed and samples were washed 3 times, 10 minutes each in water and immersed in RDO for 1-1.5 hours at 4°C. Samples were then washed 3 times, 10 minutes each in water and placed back into 10% NBF for 2 days. When fixation was complete, samples were washed with water and underwent tissue processing and embedding. Parraffin-embedded tissue blocks were sectioned at 7 µm.

4.2.11.2 Safranin-O/ Fast-green

Slides were deparaffinized and rehydrated with an ethanol to distilled water series. Slides were placed in Gill's hematoxylin (Fisher) for 20 minutes followed by 15 minutes in running tap water. Slides were transferred to fast green (Fisher) for 10 minutes followed by 1 minute in 1% acetic acid. Slides were then quickly rinsed with distilled water and then stained with Safranin-O (Fisher) for 2 minutes. With quick dips, slides were dehydrated with a progressive ethanol series to 100% ethanol after which they were cleared and mounted.

4.2.11.3 Immunohistochemistry

The following primary antibodies were used: anti-GFP (goat) antibody biotin conjugated (Rockland Antibodies and Assay) Slides were deparaffinized and rehydrated with an ethanol to distilled water series. Slides were placed in Gill's hematoxylin (Fisher) for 20 minutes followed by 15 minutes in running tap water. Slides were transferred to fast green (Fisher) for 10 minutes followed by 1 minute in 1% acetic acid. Slides were then quickly rinsed with distilled water and

then stained with Safranin-O (Fisher) for 2 minutes. With quick dips, slides were dehydrated with a progressive ethanol series to 100% ethanol after which they were cleared and mounted.

Slides were deparaffinized and rehydrated with a decreasing ethanol series to distilled water. Slides were then incubated with 20 ug/mL of proteinase K (Invitrogen) in distilled water at 37 ° C for 15 minutes followed by 2 washes in distilled water, 2 minutes each. Endogenous peroxidase was quenched by incubating cells with 0.3% hydrogen peroxide in methanol for 30 minutes at room temperature. Slides were then rinsed with PBS for 5 minutes and then blocked with 1% bovine serum albumin (BSA)/10% goat serum in PBS for at least 1 hour at room temperature followed by a quick rinse in distilled water. To block endogenous biotin, sections were incubated with 10% (w/v) egg white (Sigma) mixture in water for 15 minutes at room temperature. Sections were rinsed with tap water to ensure remnants of egg whites are all removed, then treated with 5% (w/v) skim milk solution for 15 minutes at room temperature followed by quick rinse in distilled water. Sections were transferred to 0.1% PBS-Tween (PBS-T) for 5 minutes followed by a 30 minute incubation period in a humidity chamber with the primary antibody (1:100 dilution in PBS-T) at 37°C. Post-incubation, slides were washed 3 times in PBS-T following by a 20 minute incubation period at room temperature with 1:500 diluted streptavidin conjugated horse radish peroxidase (HRP; BD Pharmingen). After washing 3 times with PBS-T, 3,3'-Diaminobenzidine (DAB; Sigma) was applied to each slide for up to a maximum of 15 minutes. Exposure time was dependent on the primary antibody used. Slides were given a quick rinse in distilled water then dehydrated, cleared, and mounted.

4.2.11.4 Prussian Blue

For staining of paraffin-embedded sections, slides were deparaffinized and rehydrated with a decreasing ethanol series to distilled water. The working solution (1:1 ratio of 20% hydrochloric acid and 10% potassium ferrocyanide) was added to the slides and left to rest for 20 minutes. Working solution was then removed and the slides were rinsed three times with distilled water. Sections were then counterstained with nuclear fast red for 5 minutes and washed twice in distilled water. Slides were then dehydrated, cleared with xylene, and mounted using Flo-Texx.

4.2.12 Scratch-wound assay

Cells used for the following experiment were Sca-1^+-GFP^+ synovial cells from C57BL/6 mice. At the start of the experiment, cells were at passage 4. Approximately 9000 cells were seeded into each well up to a total of 24 wells in a 48 well plate. Cells were cultured overnight or at least until 90-100% confluence at 37°C at 2% O_2. When confluence was reached, 12 wells were incubated with biotin-conjugated anti-mouse Ly-6A/E (also known as Sca-1; eBioscience) for 15 minutes at room temperature. The antibody mastermix consisted of 7 µL of antibody mixed with 12 mL of MSC expansion media. The mix was vortexed briefly and 500 µl of the mix was added to each well. After the incubation period, each well was washed 2-3 times with PBS. Cells were then incubated with BioMag streptavidin beads for 15 minutes at room temperature. The mastermix used consisted of 7 µL of beads into 12 mL of expansion media. After the incubation period, wells were washed 3 times with PBS. A p200 pipette tip was used to scratch the bottom of the wells, leaving a strip in each well that is devoid of cells. Wells were washed with PBS to remove debris and fresh media was added. At 0, 6 hr, 12 hr, 24 hr, and 48

hrs, pictures were taken of the wells and a subset of wells were fixed so that a Prussian blue stain could be done to confirm migrated cells were carrying a magnetic bead.

4.3 RESULTS

4.3.1 Sca-1 cell population is heterogenous and GFP lentiviral transduction was not efficient

GFP lentiviral transduction efficiency was assessed using flow cytometry. In the scatter plots, forward scatter (FSC) which measures cell size, is plotted against side scatter (SSC) which measures cell granularity. Absence of clustering in the scatter plots of the Sca-1^+-GFP^- cell samples indicate heterogeneity in Sca-1 expressing cell population (Figure 4.1A). Analysis of Sca-1^+-GFP^+ cells resulted in a two-peak histogram, indicating that the T25 flask subjected to lentiviral transduction contained two population of cells: GFP^+ and GFP^- cells (Figure 4.1B). Setting individual histogram gates revealed that within the Sca-1^+-GFP^+ cell sample, only 18% of the cells express GFP.

4.3.2 Labelling of primary C57BL/6 synovial cells with BioMag Streptavidin beads were not toxic.

Magnetic labelling induced toxicity was assessed using EthD-1 and cell treated with DMSO were used as positive control (Figure 4.2). A slight increase in staining can be seen in the labelled cells at 48 hours though an increase is seen also in the negative control. At 48 hours post labelling, we did not observe any differences in fluorescence between labelled and the negative

A

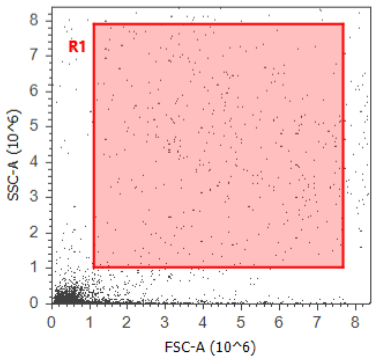

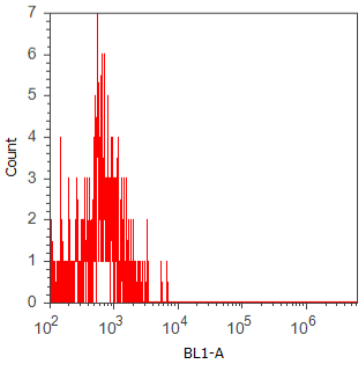

Parameters: **BL1-A vs Count**
Gate: **R1**
Experiment Name: **11-08-2013 10 39 AM(2)**
Specimen Name: **GFP study**
Sample Name: **GFP negative**
Showing **10,000** of **10,000** events.

Name	Event Count	% Parent	% Total
All Events	10,000	100.000%	100.000%
R1	394	3.940%	3.940%

B

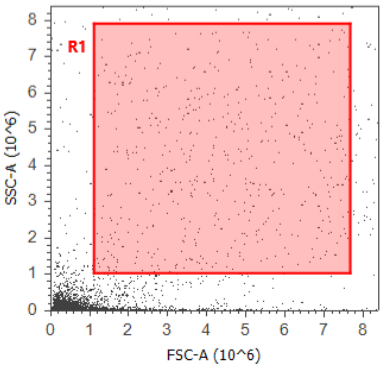

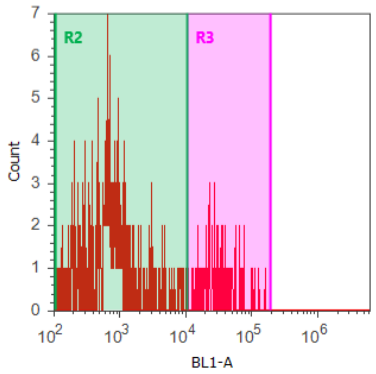

Parameters: **BL1-A vs Count**
Gate: **R1**
Experiment Name: **11-08-2013 10 39 AM(2)**
Specimen Name: **GFP study**
Sample Name: **GFP positive**
Showing **10,000** of **10,000** events.

Name	Event Count	% Parent	% Total
All Events	10,000	100.000%	100.000%
R1	518	5.180%	5.180%
R2	365	70.463%	3.650%
R3	97	18.726%	0.970%

Figure 4-1 Evaluation of GFP lentiviral transduction efficiency with flow cytometry. Absence of clusters with Sca-1^{+}-GFP^{-} cells (A) indicate heterogeneity in the cells purified for Sca-1. Analysis of Sca-1^{+}-GFP^{+} cells (B) resulted in a two-peak histogram. R2 peak represents GFP^{-} cells and is similar to the peak shown in (A). R3 peak represents GFP^{+} cells. Gating the individual peaks revealed that of the live cells counted, only approximately 18% of the cells counted expressed GFP.

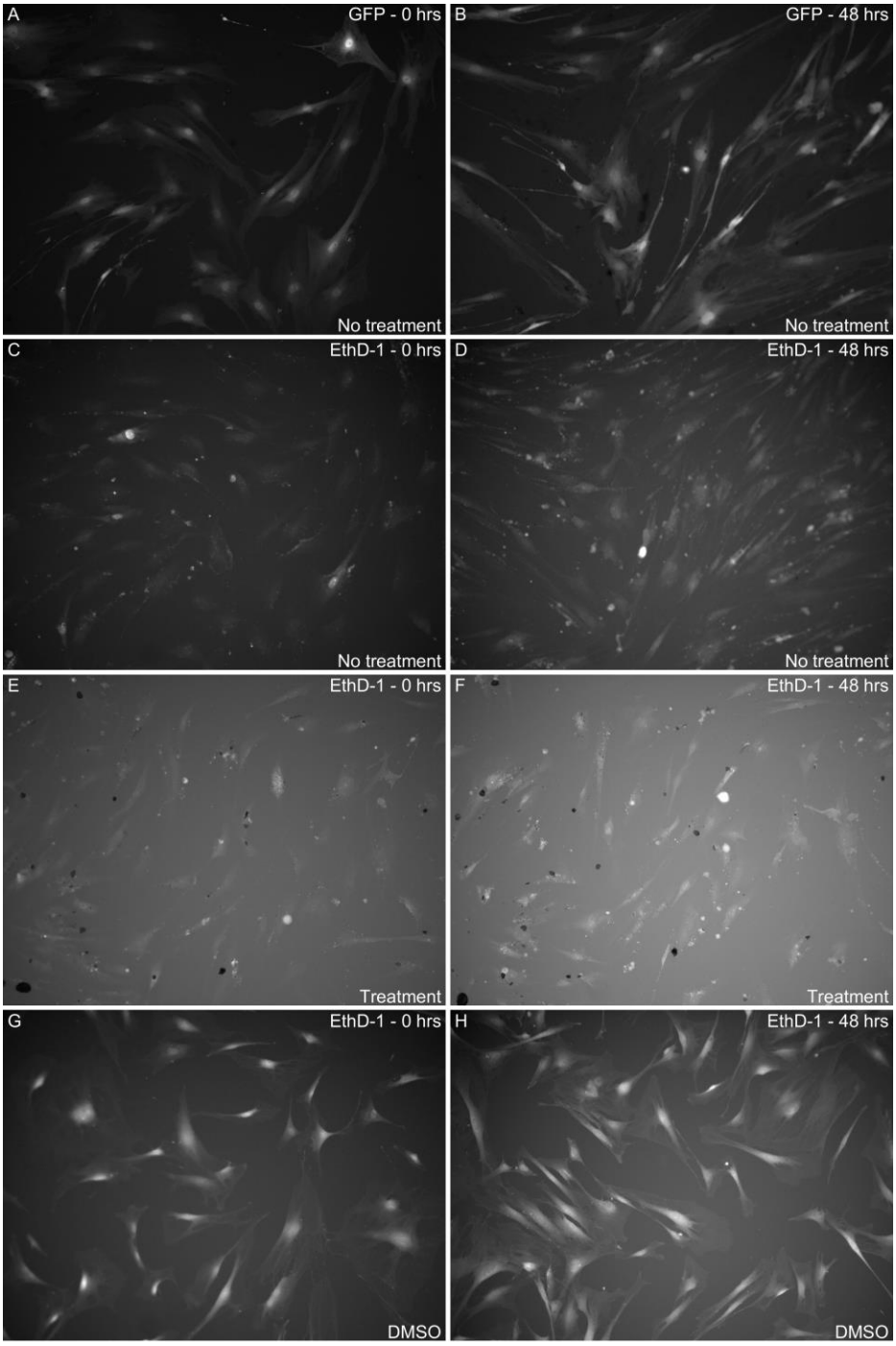

Figure 4-2 Determining the toxicity of magnetic particles using Sca-1^{+}-GFP^{+} cells derived from C57BL/6 synovium. At time = 0, cells labelled with magnetic beads (E) displayed similar levels of cell death compared to the controls (C). A slight increase in EthD-1 staining was observed in treated cells 48 hours later (F) though levels were comparable to negative controls (D). Cells treated with DMSO displayed the most cell death at both time points (G,H).

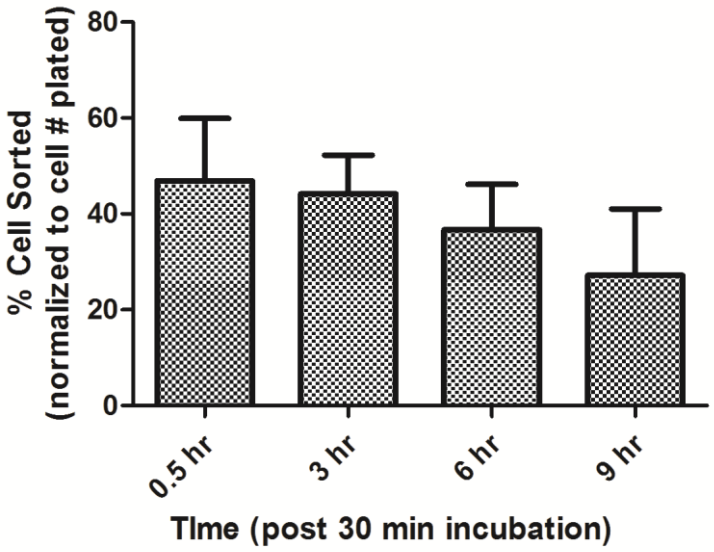

Figure 4-3 Assessing the rate of internalization and the level of retention of magnetically bound Sca-1 receptor. Maximum internalization was reached at 30 minutes after incubation of biotinylated anti-Sca-1 and BioMag streptavidin beads. Although the number of sorted cells appear to decrease at 9 hours, there was no significant difference in % cell sorted between each of the time points.

control. An increase in cell death can be seen, however, in cells treated with DMSO compared to the magnetically labelled cells as well as the negative control.

4.3.3 Maximum internalization of magnetically bound Sca-1 receptor is reached in 30 minutes

As we were interested in using magnetic beads to track labelled cells, the rate of internalization of the magnetic particles was assessed to determine the time it took for cells to internalize the beads. By performing magnetic sorting at regular timed intervals and counting the number of cells sorted, we observed maximal internalization at 30 minutes post incubation (Figure 4.3). At 30 minutes post-incubation, the mean % cell sorted was 46.9% (SD = 26.03; SE = 13.01) and by 9 hours post-incubation, the mean % cell sorted was 27.16% (SD = 27.73; SE = 13.87). Despite the downward trend, there was no significant difference between the number of cells sorted out at each time point, indicating that cells reach maximum internalization at 30 minutes post-labelling and retain magnetic particles up to at least 9 hours.

4.3.4 Intra-articular injection of magnetically labelled cells results in localized hypointense signaling

We next decided to assess whether intra-articular injection of 10 000 labelled cells could be visualized with MRI. Injection of PBS alone resulted in hyperintense signaling localized under the patella (Figure 4.4A) while imaging *in vivo* immediately after injection resulted in hypointense signaling underneath the patella (Figure 4.4B). Signaling appears to localize to the synovium (red arrow) with a diffuse line of signal that appears to trail off towards the patellar tendon (yellow arrow). When *in vivo* imaging was performed 24 hours post injection, hypointense signaling is further localized to the synovium (Figure 4.4C). When a focal cartilage

defect was induced 24 hours post injection, we see hypointense signaling localized to the synovium and fat pad (red arrows; Figure 4.4D) but defect is also seen as a circular hypointense disruption at cartilage surface (yellow region of interest).

4.3.5 Minimal difference between MRL and C57 derived Sca-1$^+$ cell treatment of focal cartilage injury as assessed by MRI

Using MRI, we evaluated whether intra-articular injection of MRL Sca-1$^+$-GFP$^+$ synovial cells would result in superior repair of focal cartilage defect compared to an injection of C57 Sca-1$^+$-GFP$^+$ synovial cells (Figure 4.5). In both groups, we can see an area of hyperintense signaling underneath the patella at week 2 as well as at week 4. In the C57 cell treated group, the hyperintense signaling appears to decline from week 2 to week 4 whereas the reverse appears to be the case in MRL cell treated animals. Joints at week 4, regardless of treatment type, appear to display a more even layer of hypointense signaling along the cartilage surface compared to joints at week 2. Safranin-O assessment of joints at week 4 reveal minimal differences between MRL and C57 treated joints. Both groups display retention of proteoglycan at the cartilage surface adjacent to the injury site compared to the PBS controls. However, repair of defect in both groups remains incomplete. Safranin-O analysis of shams and controls (Figure 4.6) showed that our surgical model did not induce joint deterioration.

4.3.6 No observable difference in cartilage grading between C57 and MRL Sca-1$^+$ cell treated joints

Blinded cartilage grading reveal that joints at week 4 after treatment display better healing compared to samples at week 2 after treatment (Figure 4.7). However, at both time points, we did not observe any significant differences between the two treatment groups

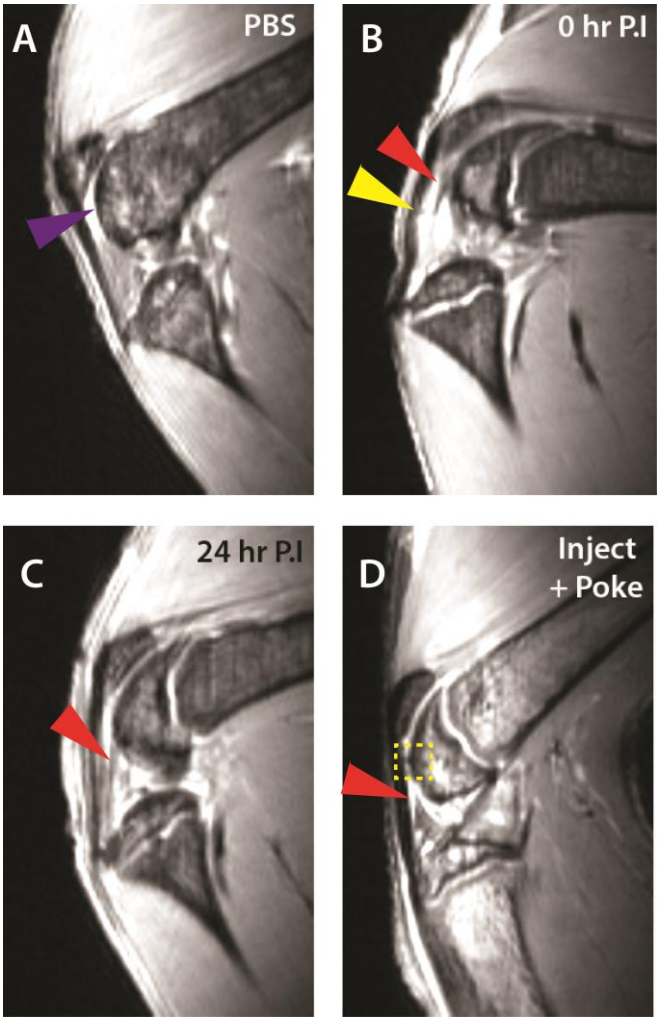

Figure 4-4 MRI visualization of 10 000 magnetically labelled cells. Intra-articular injection of sterile PBS (A) resulted in an increase in signal intensity between the patella and the articular surface (purple arrow). Imaging 0 hours post-injection (P.I) of labelled cells (B) resulted in hypointense signal appearing below the patella (red arrow) and appears to trail off at the needle entry point (yellow arrow). Imaging 24 hours after injection (C) showed hypointense signaling along the synovium (red arrow). Imaging 24 hours after injection and an injury (defect in yellow box) revealed hypointense signaling below the femur (red arrow). Hypointense band appears to be thicker compared to (B) and (C), and appears to be in the fat pad.

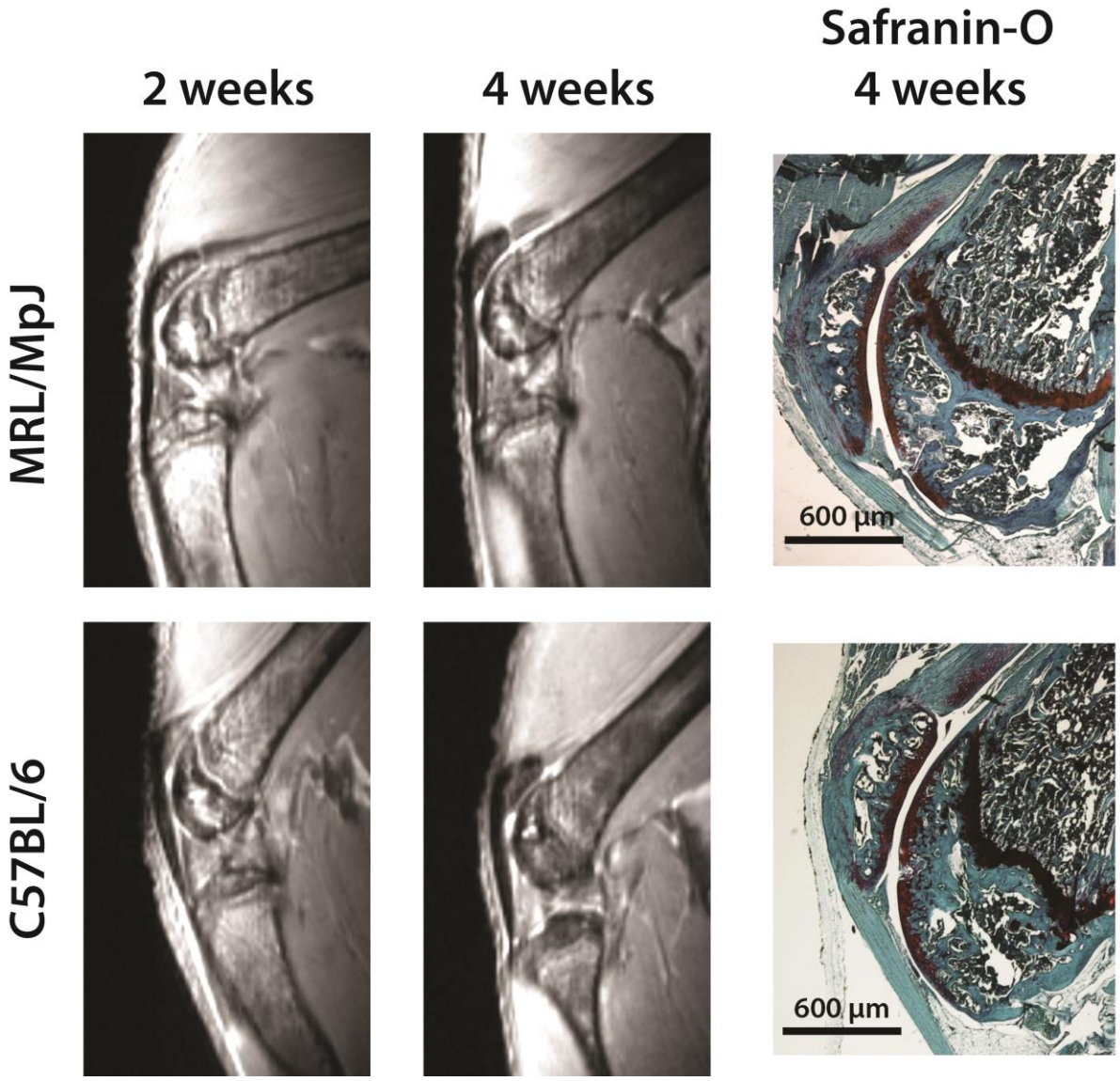

Figure 4-5 MRI evaluation of intra-articular injection of either C57BL/6 or MRL/MpJ derived synovial progenitor cells. Corresponding Safranin-O stain of the same sample is shown.

(MRL vs. C57 Sca-1^+ cells).

4.3.7 Cells remain viable following intra-articular injection

Animals that were treated with C57 Sca-1^+-GFP^+ synovial cells and euthanized at 0 and 24 hours post injection, then were histologically analyzed. Cellular debris within the joint space could be detected at both time points (Figure 4.8 A, B respectively) but Safranin-O staining surrounding transplanted cells was observed only at 24 hours post injection. Staining was also widespread within the joint (Figure 4.9 A, D). Since the injected cells had been transfected with GFP, detection of GFP by IHC revealed positive staining demonstrating that injected cells were still present (Figure 4.9B). GFP was not detected in the negative control (Figure 4.9C). It should be noted that GFP cell were not able to be found in all injected joints.

Since injected cells were also labelled with magnetic particles, sections from the 24 hour time point were also verified with Prussian blue. Iron particles could be detected (Figure 4.9E) and when serial sections were analyzed for GFP, we were not able to see GFP detection in the same location where iron was detected. Positive GFP staining, however, could be observed nearby (Figure 4.9F), indicating that not all GFP positive cells were labelled with magnetic particles and not all cells labelled with the beads were GFP positive cells. It should be noted that compared to GFP, detection of iron particles was significantly lower; therefore, detection of injected cells in treatment groups was accomplished using IHC with anti-GFP.

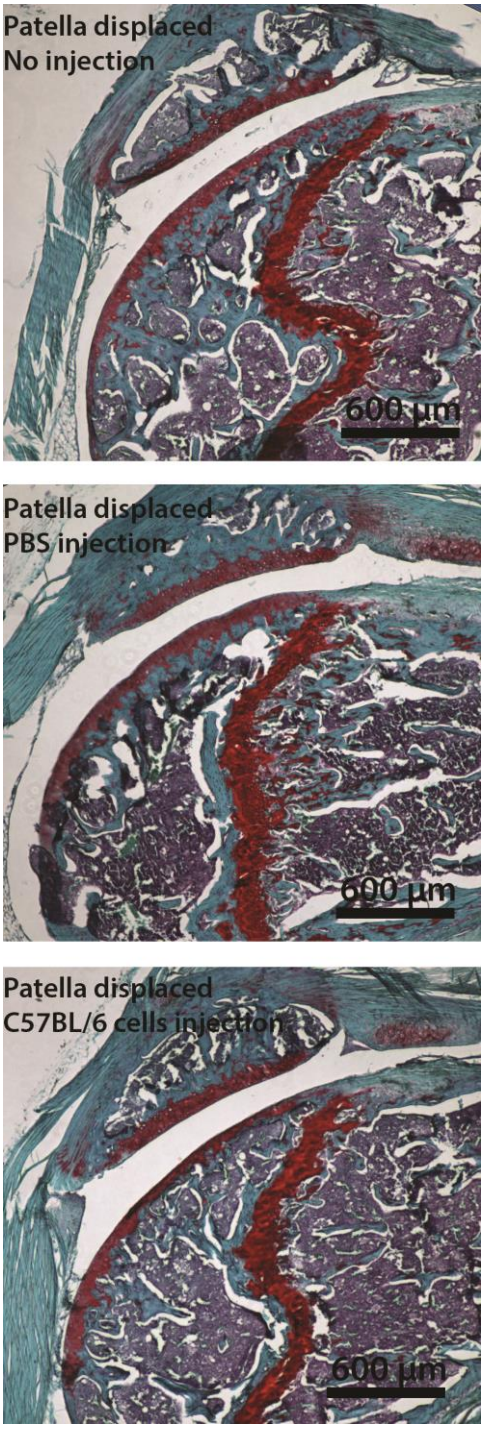

Figure 4-6 Safranin-O stains of the surgical shams and controls after 4 weeks. Proteoglycan content was preserved in samples that either had patella displaced and no injection, patella displaced with PBS injection, and patella displaced with C57BL/6 cells injection. Some of the samples that received PBS injection displayed surface irregularity despite the preservation of proteoglycan content.

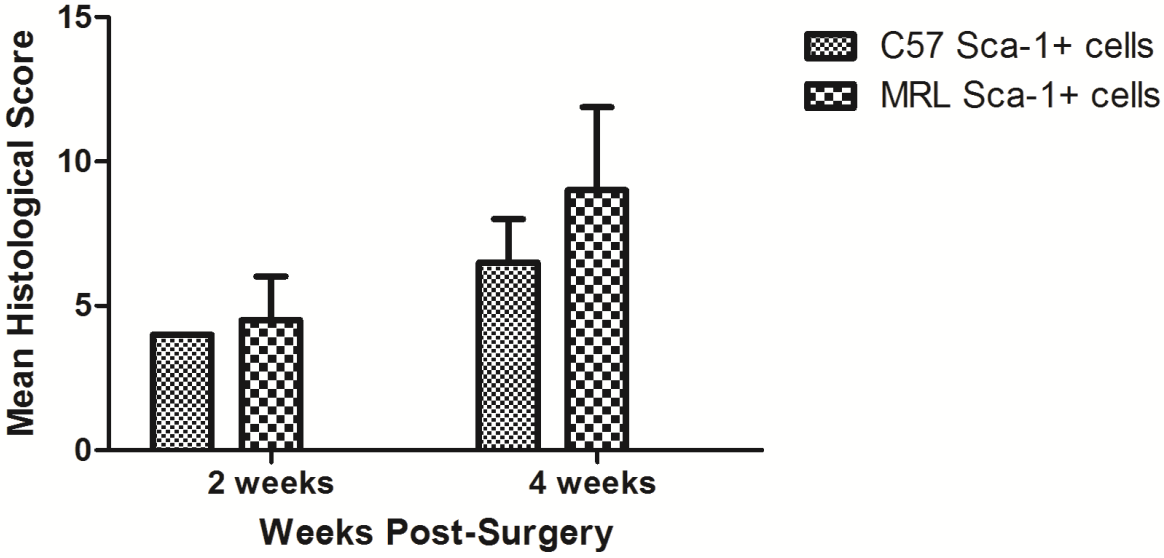

Figure 4-7 Mean histological score for cartilage repair at 2 and 4 weeks. The grading scheme used was previously published by Fitzgerald et al. where a score of 14 represented complete repair and 0 represented no repair.

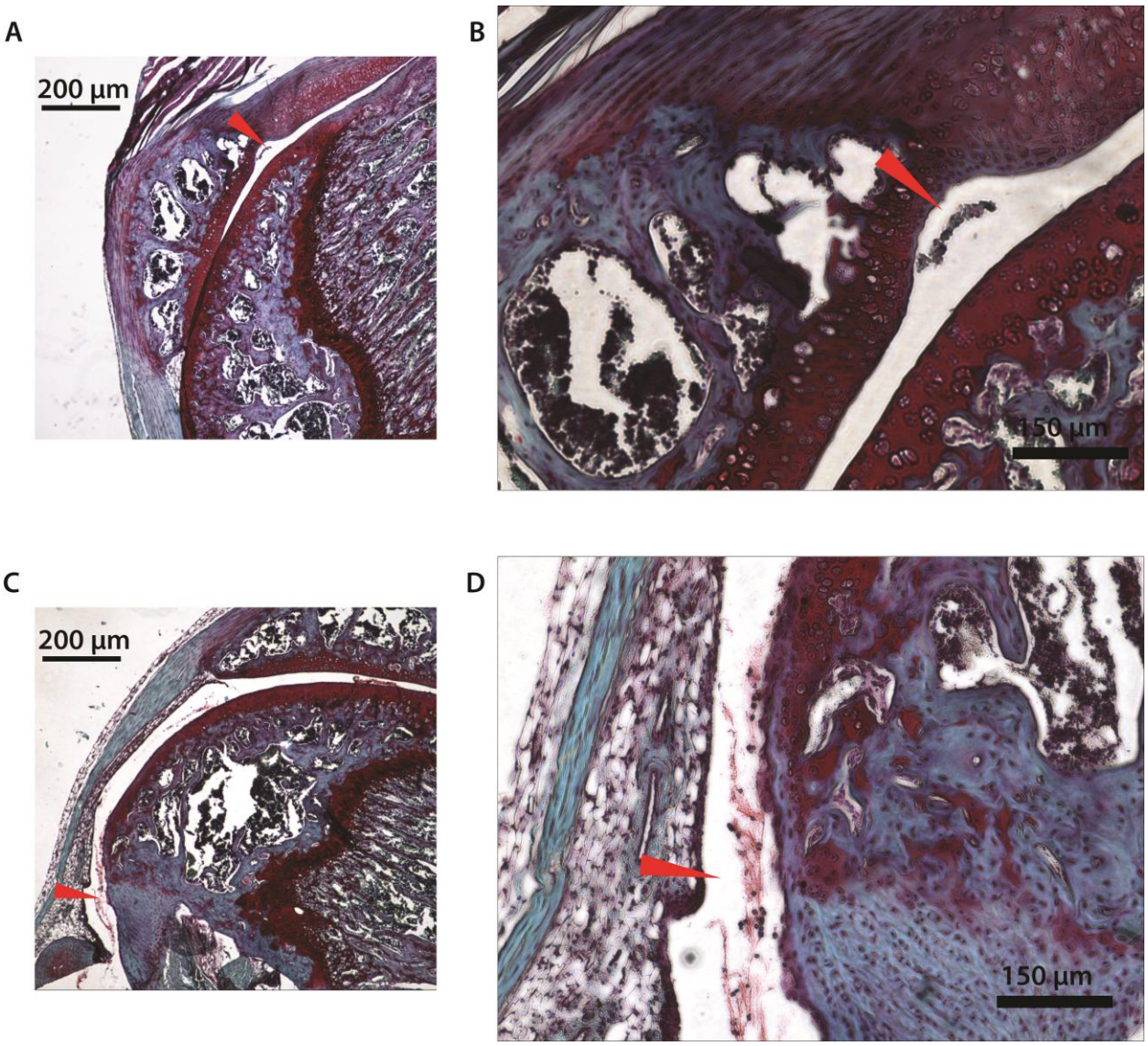

Figure 4-8 Presence of cellular debris in the joint space after intra-articular injection of C57BL/6 derived Sca-1^{+}-GFP^{+} cells. Cellular debris was detected in the joint space at 0 hours after injection (A, B) as indicated by the red arrows. At 24 hours after injection (C, D), debris was also detected in the joint space (red arrows). Positive Safranin-O staining was also detected surrounding the debris.

4.3.8 Injected Sca-1^{+}-GFP^{+} synovial cells, irrespective of mouse strain and time point, are absent in the defect

Presence of GFP expressing cells in defect sites was evaluated using IHC and anti-GFP antibody. We observed that irrespective of whether animals were treated with cells from MRL or C57 mice, GFP staining was absent in the defect site at both week 2 and week 4 time points after injury (Figure 4.10). However, positive staining was inconsistently observed outside the defect (Figure 4.10D).

4.3.9 Sca-1^{+}-GFP^{+} synovial cells do not participate in active migration

As we did not observe engraftment of the exogenous cells in the injury site, we decided to assess the migration ability of the cells and whether labelling the cells would influence the rate of migration. An *in vitro* wound healing assay was performed and in both labelled and unlabelled cells, the wound (gap) was not closed by migrating cells (Figure 4.11 A, B). Furthermore, early attempts at fixing cells at various time points proved to be difficult as cells were washing off the plate (Figure 4.11 C, D). While migration did not occur, we observed progressive changes in morphology in response to the wound (Figure 4.12). At the start of the experiment (0 hours), cells displayed a flattened morphology. As time passed, cells started to appear more rounded and were starting to reduce in size until finally at 48 hours, cells appeared as detached, rounded cells. Media was not changed at any point in time and cellular debris was not observed. To assess whether cells were still alive, Calcein AM and EthD-1 was added to the wells at 48 hours to assess viability and after the incubation period, we observed that the majority of the cells were alive despite the change in morphology (Figure 4.13).

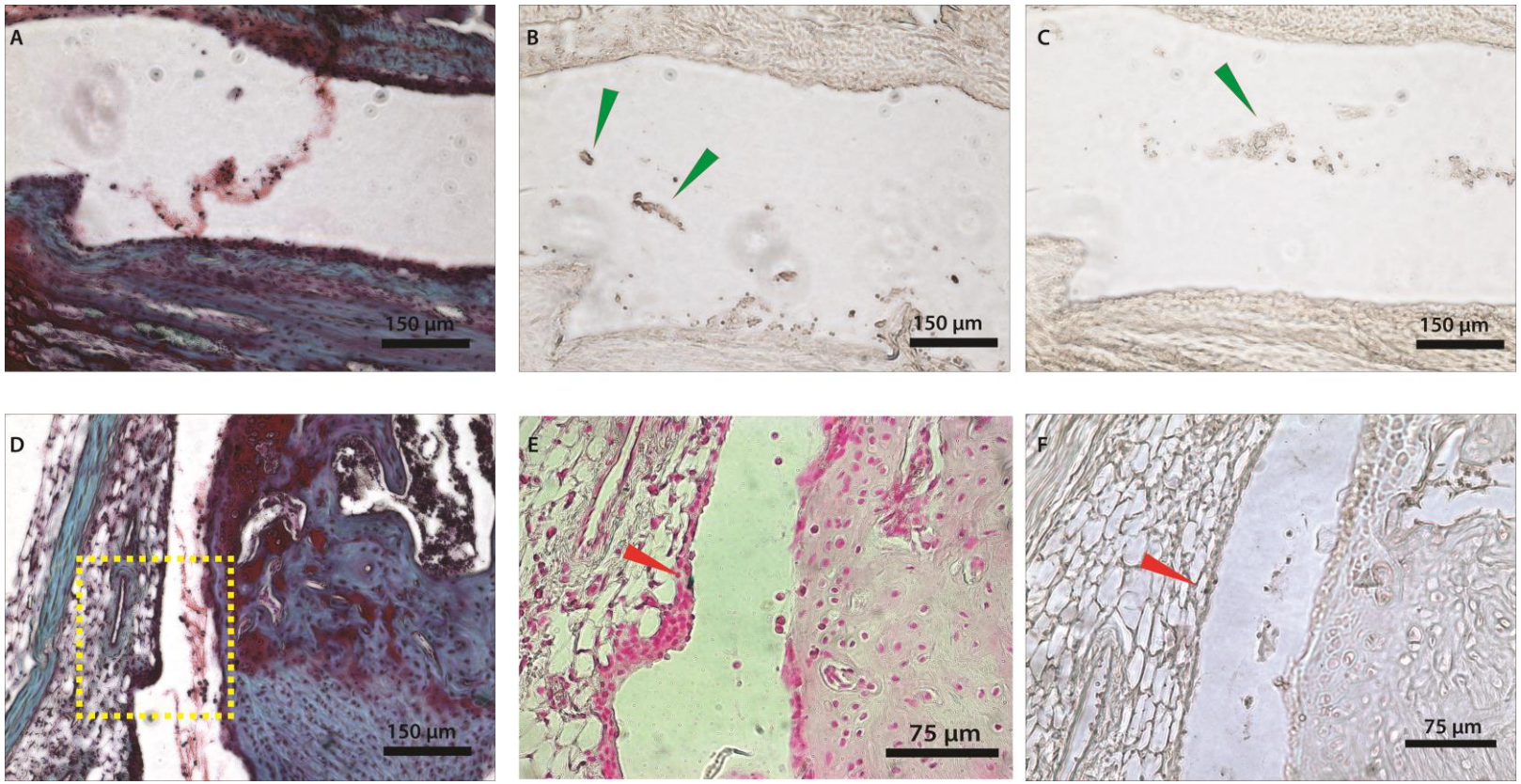

Figure 4-9 Characterization of magnetically labelled C57BL/6 derived Sca-1^{+}-GFP^{+} cells 24 hours after intra-articular injection. Cellular debris was detected throughout the joint (A, D) 24 hours after injection. Detection of GFP using immunohistochemistry on serial sections revealed positive staining on the debris (B) as indicated with the green arrows. The debris seen in the negative control (C), however, did no stain positive, as indicated by the green arrow. Magnetic particles could be detected by Prussian Blue (E) as indicated by the red arrows. Iron detection, however, was low and did not overlap with GFP staining (F; cell staining positive for GFP is indicated by the red arrow).

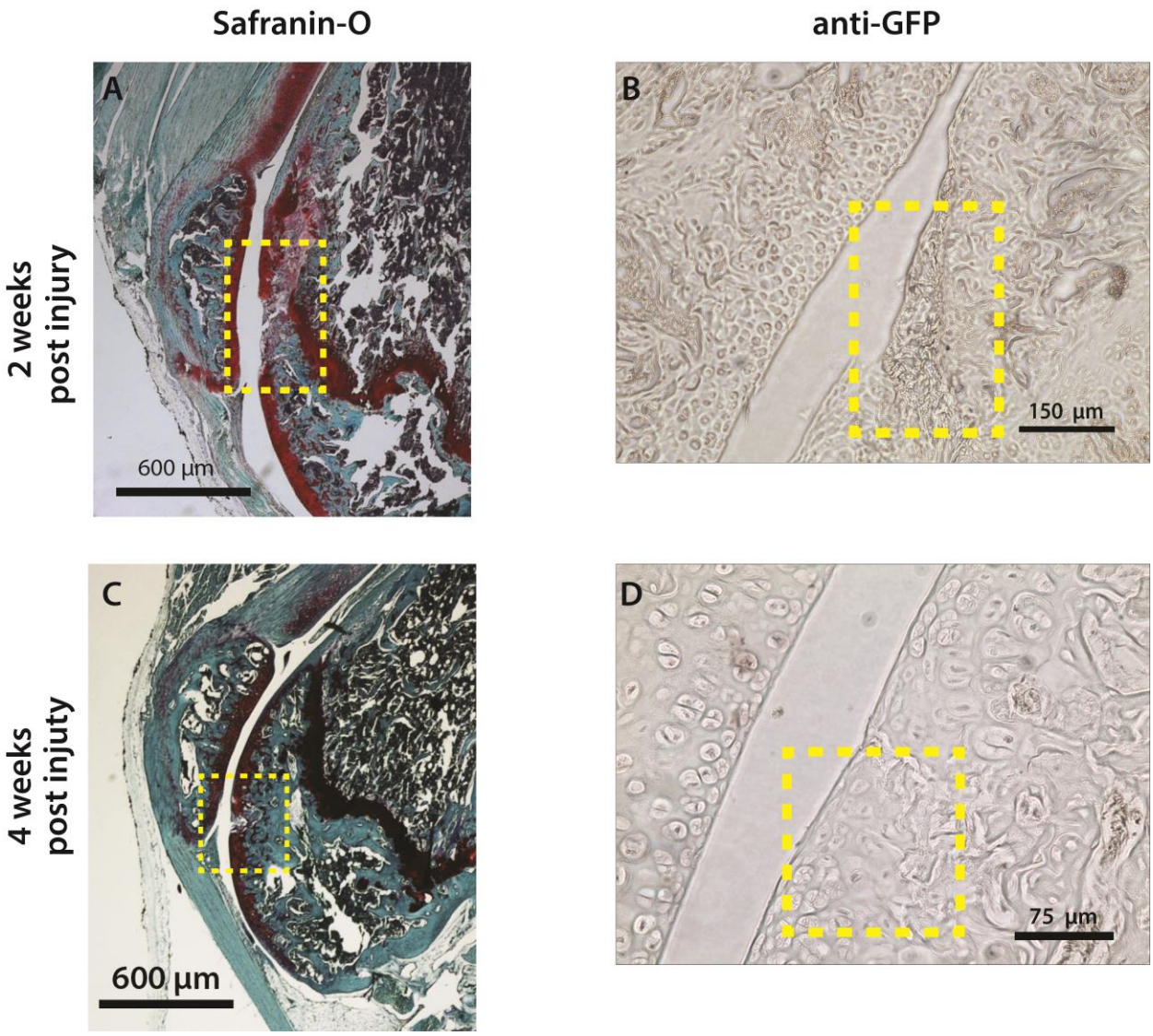

Figure 4-10 GFP detection at 2 and 4 weeks post injury (representative figures). GFP staining was absent at both time points, irrespective of whether the progenitor cells were isolated from MRL/MpJ or C57BL/6 mice (B, D). Cartilage defects are indicated in the yellow boxes.

4.4 DISCUSSION

In this experiment, we sought to determine whether MRL synovium derived progenitors demonstrated an enhanced capacity for repairing focal cartilage defects compared to C57 synovium derived progenitors. A number of previous studies involving intra-articular injection of exogenous cells have observed varying levels of repair coupled with low levels of engraftment of cells at the injury cite (Diekman et al., 2012; Lee, Hui, Song, Ardany, & Lee, 2007; Murphy, Fink, Hunziker, & Barry, 2003). To determine whether our cells would engraft or not, we employed two methods of cell tracking: magnetic labelling as well as GFP transduction. Characterization of the effect of the labelling on the purified synovial cells was important, because to date, only a few studies have used magnetic particles in a similar manner to you proposed approach. Traditionally the particles are used for cell sorting, with one study using them for MRI cell tracking (Artemov, Mori, Okollie, & Bhujwalla, 2003), but no studies have utilized this approach with synovial progenitors. Our results indicate that the beads were not toxic to the cells, and that significant internalization of the beads occurred in as little as 30 minutes after exposure to the cells. The beads used were also retained for at least 9 hours with no significant decreases in internalization. In the future, a longer *in vitro* experiment should be conducted to better understand the kinetics of the Sca-1^{+} receptor recycling and the intercellular localization of the beads after internalization.

Analysis with flow cytometry revealed that the efficiency of the GFP lentiviral transduction was only about 18%. Furthermore, lack of clustering of the GFP^{-} cells in the scatter plots indicate that purifying primary synovial cells with Sca-1 does not yield a homogenous population. The lack of homogeneity and the low transduction efficiency are limitations that

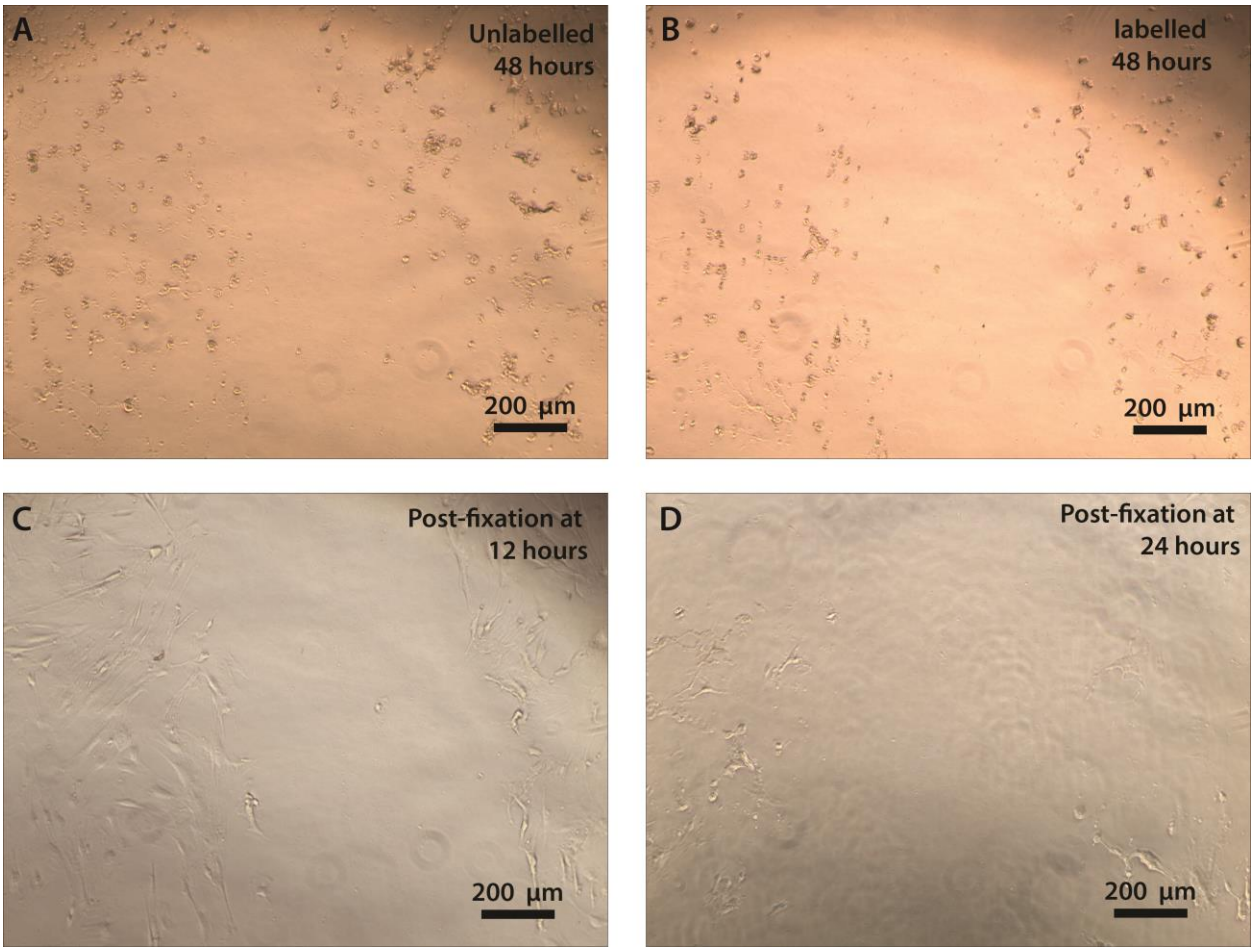

Figure 4-11 A lack of migration was seen in both magnetically labelled (A) and labelled (B) cells at 48 hours post-scratch. Attempts at fixation at 12 hours (C) and 24 hours (D) was not successful due to cellular detachment.

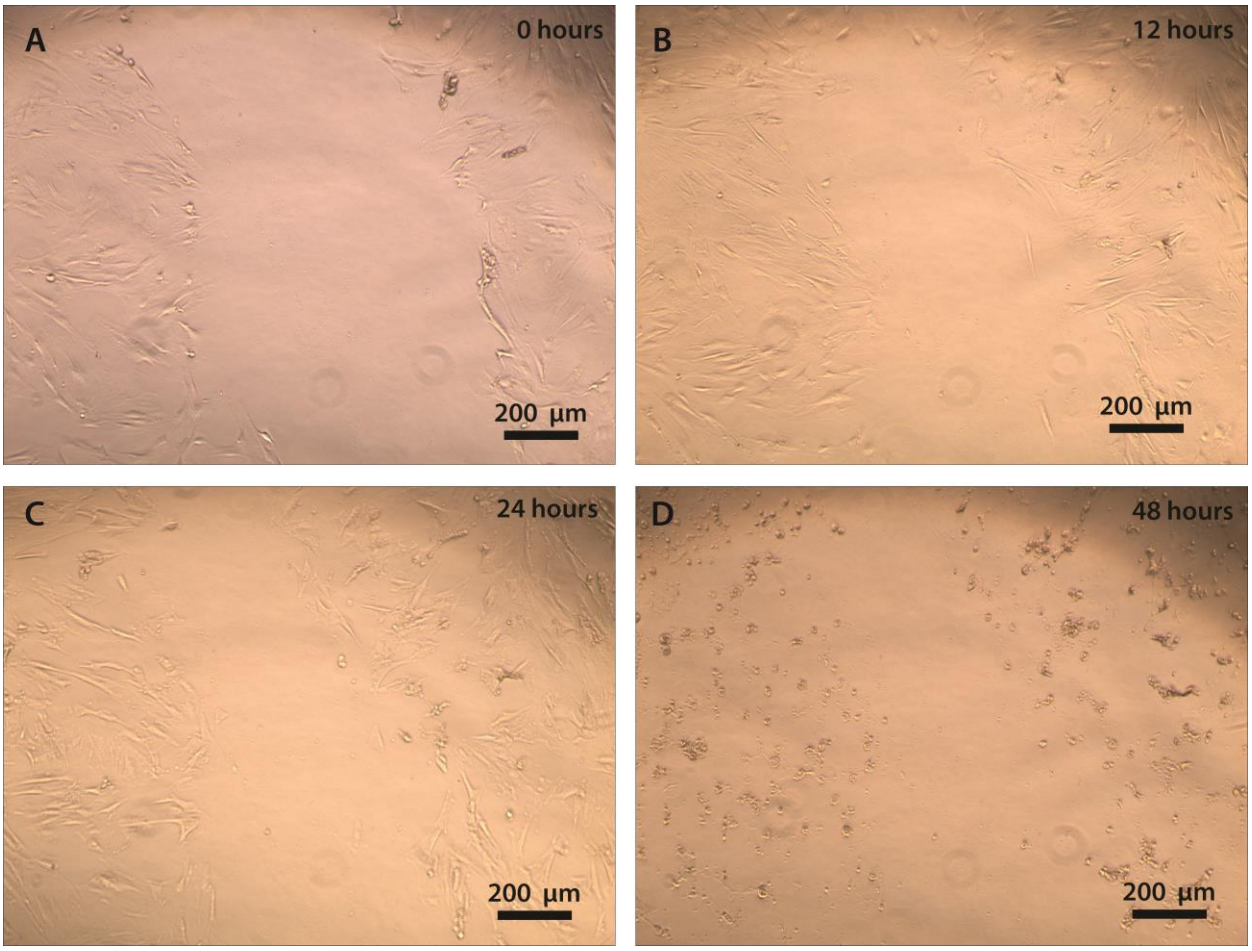

Figure 4-12 Progressive changes in morphology observed at 0, 12, 24, and 48 hours post-scratch. At 0 hours (A), cells display a flatten, fibroblast-like morphology. At 48 hours (D), cells display a detached, spherical morphology.

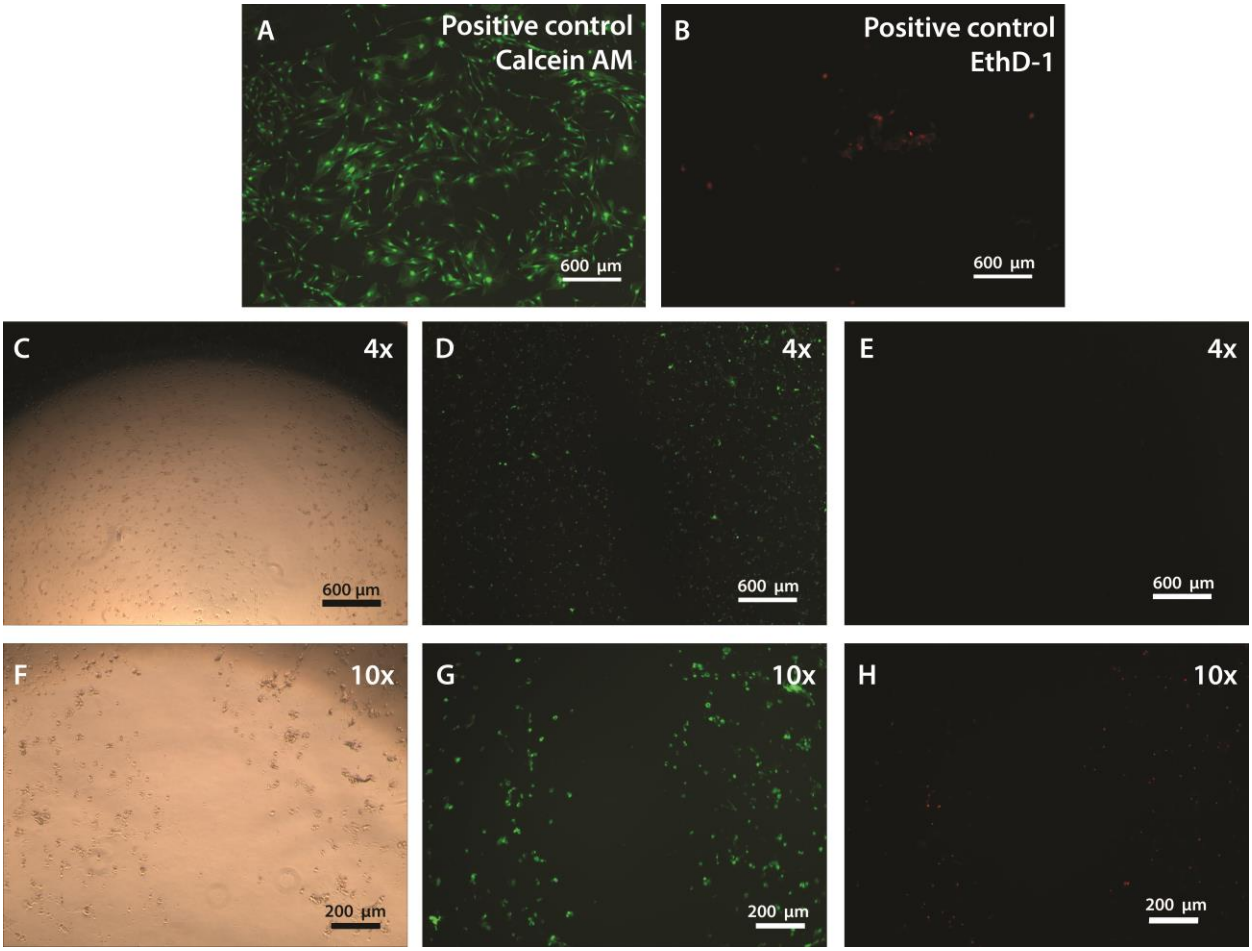

Figure 4-13 Live/dead assay performed at 48 hours post-scratch using Calcein AM and Ethidium homodimer-1. Majority of the cells were alive (D, G) despite changes in morphology. Dead cells could be detected (G, H) though to a lesser degree compared to live cells.

have been taken into consideration in the following discussion as well as the final discussion in the following chapter.

Before we could start our transplantation experiments, we had to ensure that the labelled cells were visible in the MRI. When the animal was imaged immediately after injection, we observed a streak of hypointense signaling in the joint. When imaged 24 hours after injection, the hypointense signal appears to be localized to the synovium. We had initially thought that the signal was the result of the magnetic particles bound to the cells but when the samples were analyzed histologically, few iron particles were detected in samples at both time points. A possible explanation could be that the hypointense signaling could result from bleeding, leading to the formation of a trapped pool of blood. An alternative explanation could also be the magic angle effect as discussed in the previous chapter. Further analysis will be required to determine the source of the hypointense signaling.

When we assessed the ability of either MRL or C57 synovium derived progenitor cells to repair focal cartilage defects, we observed that there were little difference between the two treatment groups. Defects in both treatment groups were not fully repaired though we do see extensive preservation of proteoglycan surfaces adjacent and surrounding the defect. Interestingly, histological analysis of samples 24 hour post injection revealed extensive safranin-o staining surrounding the injected GFP^+ cells but not in the 0 hour time point. As Safranin-O stains for glycosaminoglycan (GAG) content, our data might suggest that the exogenous cells are being surrounded by GAGs, or that the cells are producing GAGs, however our experimental design cannot distinguish between this possibilities. As mentioned, it is possible that the presence of GAGs around the exogenous cells could be a result of the recruitment of pre-existing GAGs in the joints to the cells, however, we believe that the exclusivity of the staining to the 24

hour time point suggests secretion as the more likely mechanism. It is possible that the animal examined 24 hours after injection would have had time to load the joint and mechanically stimulate the injected cells, however, this requires additional testing to verify. Previous studies have outlined that mechanical stimulation of MSCs can increase proteoglycan production (Huang, Hagar, Frost, Sun, & Cheung, 2004; Kisiday, Frisbie, McIlwraith, & Grodzinsky, 2009). As our purified cell population is still heterogeneous, it is unclear if it is the MSCs in the population that secretes the proteoglycan which then diffuses out or if the other cell types within the mix population can secrete GAGs in response to mechanical stimulation as well. Positive detection of GFP confirms that the cells inside the joint are indeed the cells we had injected.

When presence of GFP in defects were analyzed for animals treated with either C57 or MRL synovium derived progenitors at 2 and 4 weeks post injury, we observed a lack of GFP at the defect in all animals at all-time points though sporadic detection did occur at locations outside of the defect. Detection suggests that exogenous cells are still alive though they do not seem to engraft into the defect like other studies have observed (Diekman et al., 2012; Horie et al., 2009; Lee et al., 2007; Murphy et al., 2003). Furthermore, GFP detection was not assessed for the entire defect. Rather, sections with the lowest cartilage grading were used for GFP detection. It is possible that sections with closer to the edge of the defect may display some level of engraftment.

Another possibility could also be that the magnetic labelling of the cells could hamper the cells' ability to migrate and engraft into the defect. Therefore, we used a wound healing assay to assess migration capacity of cells labelled with magnetic particles and non-labelled cells. For both groups, we did not observe 'healing' of the wounded area by 48 hours which was surprising since previous papers involving human MSCs show migration into the area by 6 hours and near

complete repopulation by 10 hours (Schmidt et al., 2006; Yuan, Sakamoto, Song, & Sato, 2012) while human chondrogenic progenitor cells have been show to migrate by 48 hours (Joos, Wildner, Hogrefe, Reichel, & Brenner, 2013). In mouse cells, dermal fibroblasts have been shown to migrate by 48 hours in the presence of MSCs (Smith et al., 2010). In our study, however, cells in both groups have changed from a flattened fibroblast-like morphology to a detached and spherical shape. As media did not contain cellular debris, we questioned whether the cells were alive or dead. Analysis using live/dead assay revealed that the majority of cells were alive. Given the lack of migration in the cells, we concluded that the exogenous cells we injected may not participate in active migration. Rather, sporadic engraftment can most likely be attributed to the convective forces of the synovial fluid that occur each time the joint is loaded could potentially carry the free floating cells passively and indiscriminately to various areas of the joint.

To summarize, the objective of this study was to determine whether MRL synovium derived progenitors were superior to C57 synovium derived progenitors in regards to focal cartilage defect repair. In our study, we did not observe any significant differences in the treatment effects between MRL and C57 derived cells. Both groups displayed preservation of proteoglycan levels of the articular cartilage though repair of defect remains incomplete. The mechanism behind the retention of proteoglycan levels could be due in part to the secretion of GAGs by the exogenous cells due to mechanical stimulation by joint loading. Increase in GAGs lead to better joint lubrication and water uptake of the cartilage and may ultimately attenuate further deterioration of the joint. We have also shown that the synovial progenitors are not migratory *in vitro*, and despite the protective effect demonstrated through exogenous cell

treatment, we observed a lack of engraftment. Therefore, it is likely that intra-articular injection of synovial progenitor cells protects joint degeneration by indirect mechanisms.

Chapter Five: **Discussion**

The overall hypothesis of the thesis is that mesenchymal stem/progenitor cells in the synovial membrane will demonstrate the ability to differentiate into chondrocytes (*in vitro*) and contribute to cartilage repair by migrating to the site of injury when exogenously injected into a cartilage injury model system. The experiments presented in this thesis suggests, however, injection of exogenous synovial progenitor cells does not appear to migrate to the site of injury but rather, protected the joint from further degradation by trophic effects. These observations will be discussed in the following sections:

5.1 Large quantities of purified MSCs may not be required for joint protection

Before our findings are discussed further, it is important to discuss the results of a paper that was published at the time we were completing the experiments presented in this thesis due to the similarities involved. In a 2012 paper, Diekman et al. conducted a study in which the authors hypothesized that injection of MSCs could prevent post-traumatic arthritis (PTA) in mice. The authors also hypothesized that MSCs derived from MRL mice would be superior to C57 derived MSCs due to the heightened ability to repair cartilage in MRL mice. Bone marrow, but not synovium derived MSCs were isolated using the markers $CD45^-/TERR119^-/PDGFR\alpha^+/Sca\text{-}1^+$. The cells were cultured at 2% O_2 which the authors found enhanced the differentiation potential of the cells. The authors also observed that a single injection of 10 000 cells, irrespective of which animal the cells were isolated from (MRL vs. C57), was able to prevent PTA up to 8 weeks. Furthermore, a small portion of the cells were observed to engraft.

The findings from our studies largely mirrors what Diekman et al. observed but a key distinction is that the authors used 10 000 highly purified cells to prevent PTA. In our studies,

primary synovial cells were purified based on only one marker (Sca-1) and our differentiation assay as well as our flow cytometry data confirms that Sca-1 purified synovial cells are still heterogenous in nature. Therefore, despite the use of 10 000 cells in the injections, the actual number of MSCs in our cell population would be significantly less. Despite the lower levels of MSCs, intra-articular injection of 10 000 Sca-1 purified cells resulted in the preservation of proteoglycan in the cartilage at 2 and 4 weeks, indicating that a highly purified population of MSCs is not required for protection against trauma induced joint degradation. It should be noted that while proteoglycan levels were preserved at 2 and 4 weeks post injury, repair of defects remained incomplete.

5.2 Intra-articular injection of exogenous synovial progenitors leads to the production of GAGs

There is a growing number of reviews and studies that suggests that MSCs modulate the environment by secreting cytokines and growth factors [99,100]. In our experiments, we found that at 24 hours post injection, Safranin-O staining can be seen to surround the cells free floating in the joint cavity. The significance of this observation may lie in the fact that the animal injected would have had been mobile for 24 hours, inducing mechanical stimulation to the exogenously injected cells *in vivo*. While there have been previous studies that investigated joint loading on tissue constructs, to our knowledge, there has yet to be a published paper on the effect of joint loading on a single dose, intra-articular injection of synovial progenitors. It should be noted that while the cells used for intra-articular injections were not homogenous, evidence of chondrogenic potential, although weak, indicated that a small subpopulation consists of chondro-progenitors.

5.3 In response to *in vitro* injury, cells change morphology and detach

Perhaps the most surprising result, was the change in morphology that occurred in response to an *in vitro* "wound". The intent was to assess how labelling with magnetic beads would hinder the migration capability of the cells. Interestingly, and contrary to the outcome of this assay with cells from different tissue origins, the synovial cells became spherical by 48 hours and could be easily detached from the plate. When combined with the observation that by 48 hours, no migration occurred to repopulate the scratched area, suggests that in response to injury, endogenous synovial progenitor cells may dissociate themselves from the substrate and end up in the supernatant by yet unknown mechanisms. If we extrapolate this result to an *in vivo* system, them sporadic injury engraftment might be a result through the action of convective forces of the synovial fluid on the cells which could potentially transport the free floating cells to the joint surface or any other joint tissue. In our studies, GFP detection was absent at the injury site at both 2 and 4 weeks but as GFP expression level after transduction was not always robust it is possible that engraftment has occurred but was not detectable using our IHC methodology.

Despite our findings, numerous studies in the past have observed cellular engraftment [63,79,101]. One potential explanation for the discrepancies is the number of cells that are injected. In one study, the authors were interested in assessing the bioavailablility and toxicity of human adipose derived MSCs repairing chemically induced joint degeneration [102]. The authors had injected a million cells in 7 µL and like others, have observed engraftment to take place up to 6 months. With oversaturation of the joint with cells, however, it is hard to conclusively demonstrate that engraftment is due to active migration by the injected cells.

The change in morphology occurred within the span of 48 hours after 'wounding' and as our time points for both the injury and transplant studies include 2 and 4 weeks, we cannot confirm whether this change in morphology and cellular detachment occurs *in vivo*. Upon closer inspection of our injury experiment, however, we can see cellular debris in an MRL sample 2 weeks post-injury (Figure3.8, 10x). A slight Safranin-O staining can be seen to surround the debris, which leads us to believe that detachment of synovial cells in response to injury may occur *in vivo* as well and that a possible reason for the detachment is to preserve existing proteoglycan levels or stimulate proteoglycan production. However, rigorously defined and conducted experiments would be required to undertake testing of this hypothesis.

While our results suggest that engraftment is minimal and homing to the injury site of exogenous cells in not robust, one question that now arises is why we observe such intense Sca-1 staining in C57 animals after injury? Further studies will be required to understand the how Sca-1 expression became localized to the defect

5.4 No observable difference between animals treated with C57 and MRL cells – C57 synovial cells are not overtly deficient in repair

Our results show, along with the findings from a previous paper by Diekman et al., no observable differences in the ability to produce a protective effect against joint degradation by C57 and MRL derived cells. If in a C57 injury model, exogenously injected C57 derived cells function just as well as MRL derived cells and both treatments lead to a better outcome, then the question that arises is why do we not see a maintenance effect in the C57 animals in the injury study? Since the cells used in our intra-articular injections are heterogenous, they should, in

theory, reflect a more accurate portrayal of the global cell types that reside in the mouse synovial membrane compared to if we had injected 10 000 highly purified MSCs. The C57 joint environment post injury should also be the same in both the injury and transplant study. Therefore, if the environment is the same, why is a protective effect only observed after we inject cells from arguably the same synovium back into the injured joint? The answer could be that the injected cells are already detached and free floating (Figure4.6) and therefore can be mechanically stimulated to secrete proteoglycan. Further supporting this notion is a brief analysis of the MRL sample 2 weeks post-injury (Figure3.8, 10x) where there appears to be cellular debris within the joint space that is stained with Safranin-O. Alternatively, it could also be that the injured joint environment differentially affects the endogenous cells vs. the exogenous cells. It has also been suggested that the inflammatory molecules present in injured/diseased synovial fluid may negatively regulate the chondrogenic capacity of the progenitor cells.

5.5 Summary

Taken altogether, the experiments presented in the thesis have shown that progenitor cells are present in the mouse synovium and can be expanded *in vitro*. While purification of primary mouse synovial cells with Sca-1 yields a sub-population of cell that have the capacity for chondrogenic differentiation, the cell population as a whole remains heterogenous. Intra-articular injection of Sca-1^{+} synovial cells leads to protection against joint deterioration that would normally result after a surgically induced focal cartilage defect although we did not see a difference between MRL derived cells and C57 derived cells. The mechanism of protection may be related to observed proteoglycan into the joint space after exogenous cell injection rather than active migration and differentiation in the defect itself.

5.6 Limitations

A major experimental limitation was the small sample size used for the studies. An n=3 was generally used to keep animal costs low due to the numerous treatment groups and time points that were included in the study. However, in the event that a sample is lost due to human error, analysis of the data and ensuring the data is representative becomes much more difficult. However, this issue is partially offset with the ability to perform repeated non-invasive imaging on all the animals within a group, allowing us to tract the individual healing process in each animal, which helps describe the natural heterogeneity within a given population.

The scale used for cartilage grading also had several limitations. As the grading scheme involved weighted categories individual analysis of the scores from each category would have provided a deeper insight as to the differences in repair process between mouse strains. However, when combined with the low sample size, breaking down the separate categories for analysis would not have produced reliable and significant results. Therefore, we decided to analyze the level of repair using the cumulative score, which provided us only with a general idea of which strain had better repair potential.

Another limitation was the stopped needle apparatus used to induce focal cartilage defects. The presence of the stopper limits how deep the needle can penetrate into the tissue, but does not give us control on how shallow the defect is. Variations in defect size and depth are still evident between samples and can bias cartilage grading scores. Furthermore, though cartilage grading was done in a blinded fashions, grading were done by only one person, since only one other person in the lab had significant expertise using the grading system other than myself.

The heterogeneous nature of the Sca-1 purified cells are also a limitation. Because the cell population is mixed, proper characterization was not possible. Comparing our results with previous studies are also difficult since other groups typically study a highly purified cell population based on multiple cell surface markers. Because of the mixed population, we do not know which cell type produced the protective effects observed after intra-articular injections. Furthermore, *in vitro* expansion of Sca-1 purified cells to passage 4 was necessary to generate enough cells to inject into the joint. Due to possible culture-induced changes to the cells, the exogenous cells cannot be directly compared to the endogenous cell population within the joint.

With regards to MR imaging, we had not taken into account the magic angle effect at the time of scanning and thus, we cannot confirm whether changes in signal intensities are caused by an artefact or by structural changes in the tissue. In the future, an additional scan with a longer TE will be required to differentiate the two.

Appendices

Appendix A: QPCR analysis of Tri-lineage Differentiation

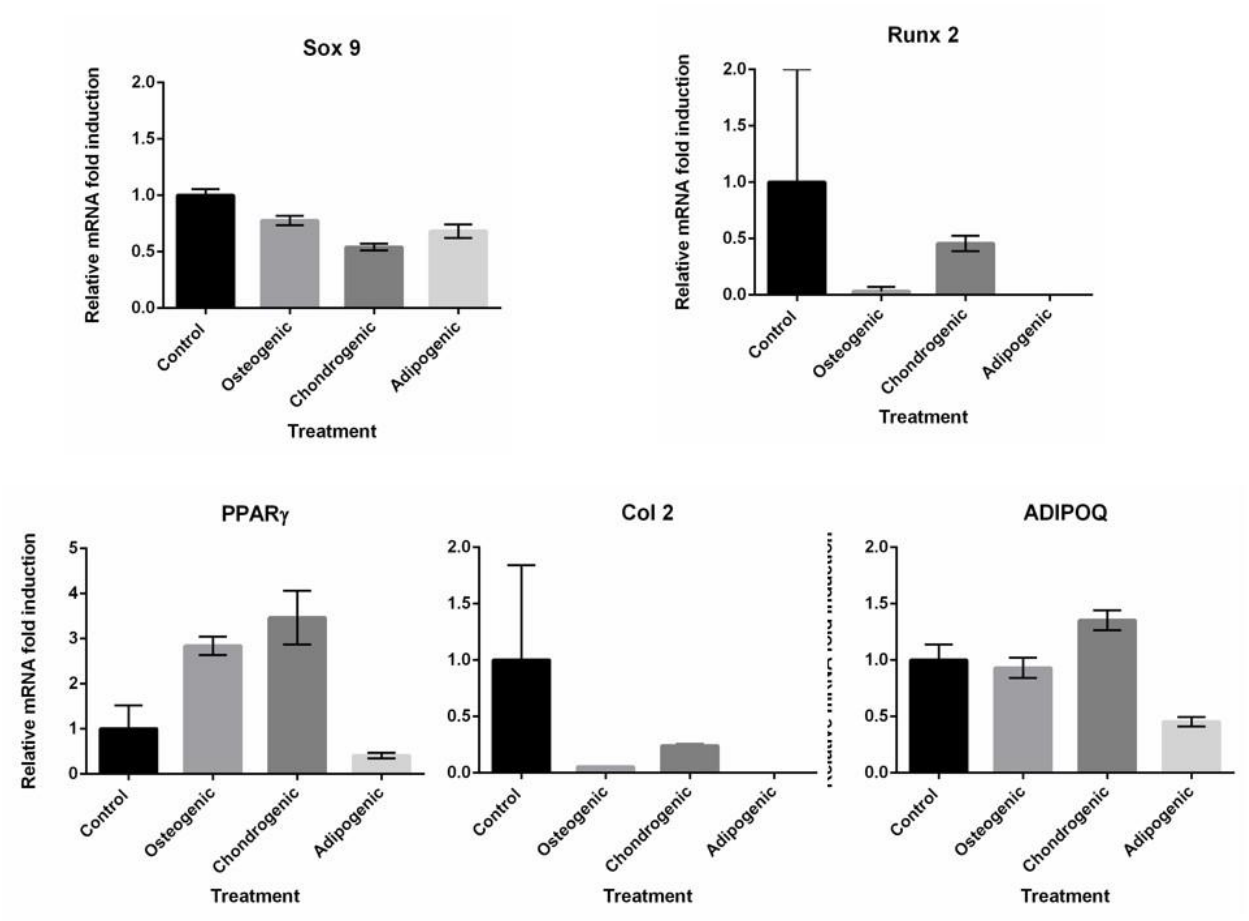

Quantitative PCR was performed at the end of the tri-lineage differentiation. Due to low sample numbers, significance cannot be calculated. However the overall trend seems to indicate that for all treatments, controls displayed higher expression levels of differentiation markers compared to cells treated with differentiation media. A possible explanation could be that the cell population is highly heterogenous in nature contain low numbers of progenitors. When undergoing differentiation, amount of gene expression is limited to the number of progenitors that are available to differentiate. Cells in the control wells were incubated in MSC expansion media and at no point, were the cells passaged during the differentiation period. It is likely that a base level

of spontaneous differentiation will occur. Despite the loss of progenitors due to spontaneous differentiation, it is possible that existing progenitor cells replenish lost cells which can subsequently undergo spontaneous differentiation as well. The overall effect is a higher level of differentiation expression compared to treated cells.

Appendix B: MRI Sample Preparation

Ex vivo sample preparation

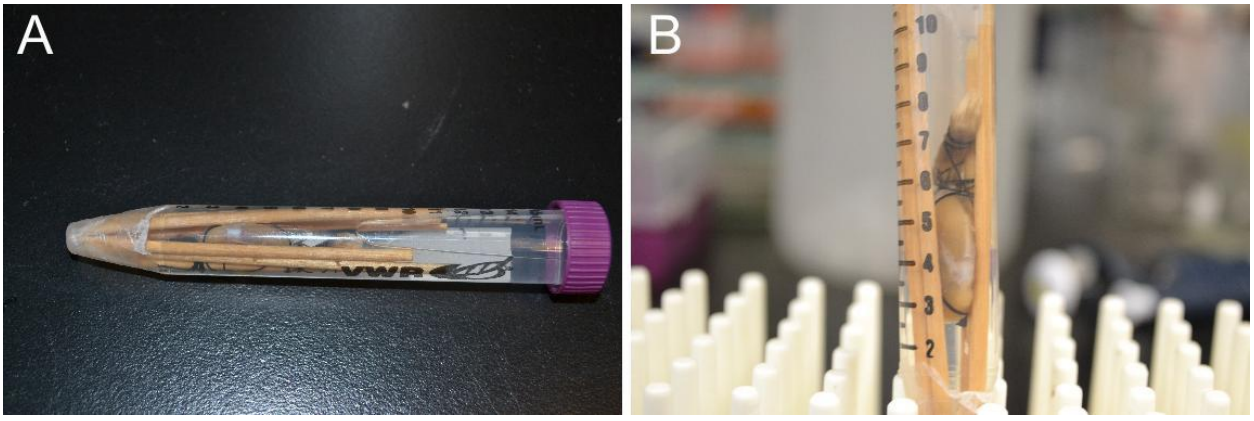

Wooden splints were attached to sample of interest using silk sutures and the splinted sample was placed inside a 15ml falcon tube (A,B). Additional wooden supports were strategically placed in the tube such that the sample was fixed, centred and knee was as close to the inner surface of the tube as possible without being compressed. The tube was then filled with Fluorinert (3M) and care was taken to minimize air bubbles.

***In vivo* sample preparation**

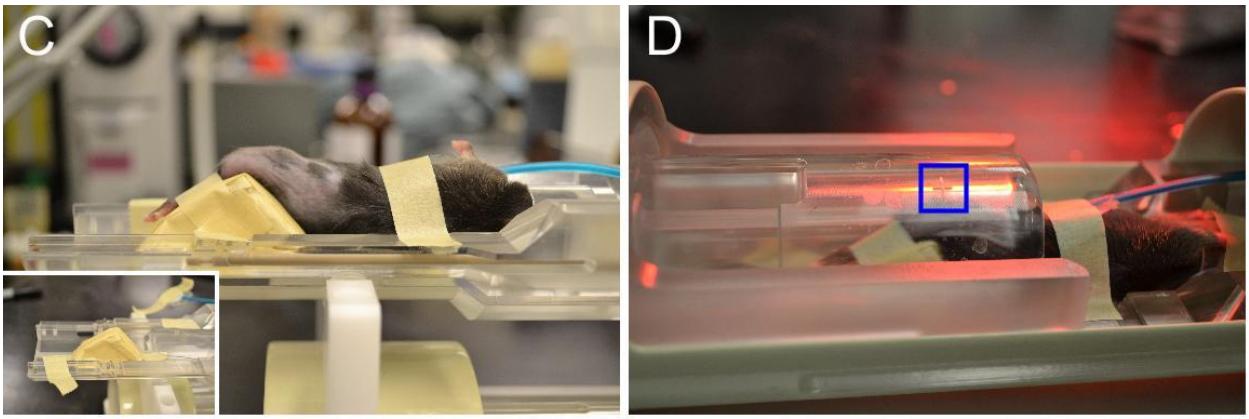

The animal is placed in a supine position on the animal bed with the knee of interest resting on a foam block. The block, with a height of approximately 2 cm, base length of 5 cm, and base width of 1 cm, was used to elevate the knee such that the joint could be as close to the surface coil as possible without compression. Angle of flexion was determined to be 110° (C). Knee had to centred according to the crosshair (D, highlighted in blue square) and the knee joint had to be positioned as close to the surface as possible without compression.

Appendix C: Setup for Intra-articular Injections

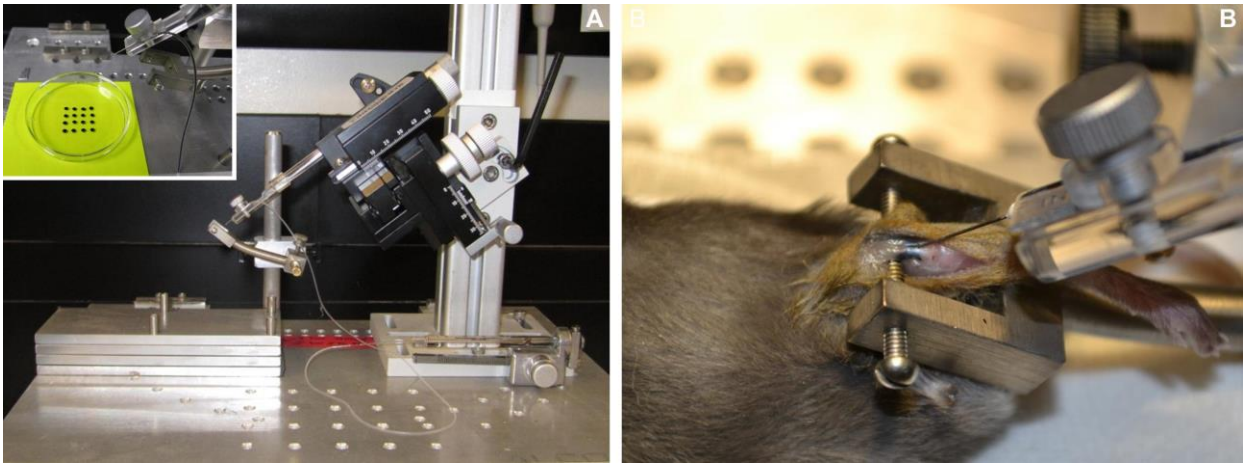

Injection apparatus (A) was provided by Dr. Paul Salo. Inset picture illustrates the accuracy of each 1 µL dispensed. Setup consists of custom-made knee holder, silicone tubing used to connect a 30G needle to a 50 µL Hamilton microliter syringe (model # 705), a 1 µL dispensing Hamilton repeating dispenser and a three axis micromanipulator was used to adjust the entry angle of the needle. Intra-articular injection of india ink was performed initially to confirm successful injection (B).

Appendix D: Positive and Negative controls for Sca-1, F4/80 and c-Kit

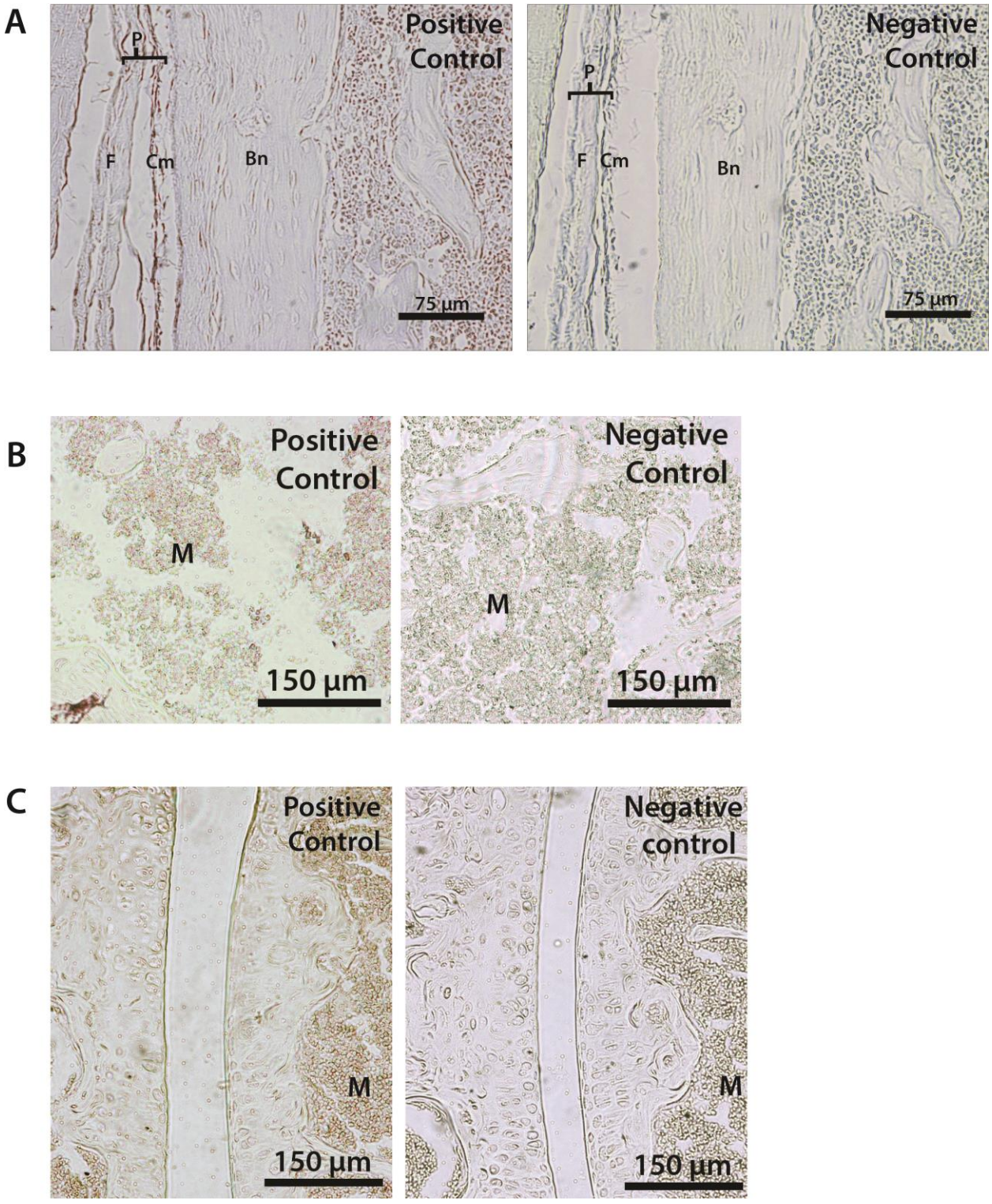

Periosteum (A) was used as the positive control for Sca-1 as it has been previously published that the periosteum (P) expressed Sca-1 [103]. The periosteum consists of two layers: fibrous (F) and cambium (Cm). Positive staining (brown color) was detected in the cambium layer only. Staining was absent in the negative control.

Bone marrow was used as the positive control for c-Kit (B). Positive staining is seen in the marrow (M) but absent in the negative control.

Bone marrow was also used as the positive control for F4/80 (C). Positive staining is seen the marrow (M) but is absent in the negative control.

References

1. Roelofs, a J., Rocke, J. P. J. & De Bari, C. Cell-based approaches to joint surface repair: a research perspective. *Osteoarthritis Cartilage* (2013). doi:10.1016/j.joca.2013.04.008

2. Vasiliadis, H. S. *et al.* Autologous Chondrocyte Implantation in Cartilage Lesions of the Knee: Long-term Evaluation With Magnetic Resonance Imaging and Delayed Gadolinium-Enhanced Magnetic Resonance Imaging Technique. *Am. J. Sports Med.* **38,** 943–949 (2010).

3. *Cartilage Repair Strategies*. (Humana Press, 2007).

4. Benjamin, M. in *Biol. Synovial Jt.* (Archer, C. W., Caterson, B., Benjamin, M. & Ralphs, J. R.) 1–9 (Harwood Academic Publishers, 1999).

5. Foster, J. E. *et al.* Structural periodicity in human articular cartilage: comparison between magnetic resonance imaging and histological findings. *Osteoarthritis Cartilage* **7,** 480–5 (1999).

6. Jeffrey, D. R. Imaging hyaline cartilage. *Br. J. Radiol.* **76,** 777–787 (2003).

7. Buckwalter, J. A. & Hunziker, E. B. in *Biol. Synovial Jt.* (Archer, C. W., Caterson, B., Benjamin, M. & Ralphs, J. R.) 75–100 (Harwood Academic Publishers, 1999).

8. Khan, I. M., Williams, R. & Archer, C. W. One Flew over the Progenitor's Nest: Migratory Cells Find a Home in Osteoarthritic Cartilage. *Cell Stem Cell* **4,** 282–284 (2009).

9. Flik, K., Verma, N., Cole, B. & Bach Jr., B. in *Cartil. Repair Strateg. SE - 1* (Williams III, R.) 1–12 (Humana Press, 2007). doi:10.1007/978-1-59745-343-1_1

10. Bilge, O. *et al.* in *Sport. Inj. SE - 92* (Doral, M. N.) 693–700 (Springer Berlin Heidelberg, 2012). doi:10.1007/978-3-642-15630-4_92

11. Edwards, J. C. W. in *Biol. Synovial Jt.* (Archer, C. W., Caterson, B., Benjamin, M. & Ralphs, J. R.) 225–233 (Harwood Academic Publishers, 1999).

12. Levick, J. R. & Architecture, M. Microvascular architecture and exchange in synovial joints. *Microcirculation* **2,** 217–33 (1995).

13. Mason, R. M., Levick, J. R., Coleman, P. J. & Scott, D. in *Biol. Synovial Jt.* (Archer, C. W., Caterson, B., Benjamin, M. & Ralphs, J. R.) 253–264 (Harwood Academic Publishers, 1999).

14. Harting, M. T. in *Progenit. Cell Ther. Neurol. Inj.* (Charles, S.) 1–18 (Humana Press, 2011). doi:10.1007/978-1-60761-965-9

15. Scadden, D. T. The stem-cell niche as an entity of action. *Nature* **441,** 1075–9 (2006).

16. Lilly, A. J., Johnson, W. E. & Bunce, C. M. The haematopoietic stem cell niche: new insights into the mechanisms regulating haematopoietic stem cell behaviour. *Stem Cells Int.* **2011,** 274564 (2011).

17. Ghaemi, S. R., Harding, F. J., Delalat, B., Gronthos, S. & Voelcker, N. H. Exploring the mesenchymal stem cell niche using high throughput screening. *Biomaterials* **34,** 7601–15 (2013).

18. Frenette, P. S., Pinho, S., Lucas, D. & Scheiermann, C. *Mesenchymal stem cell: keystone of the hematopoietic stem cell niche and a stepping-stone for regenerative medicine. Annu. Rev. Immunol.* **31,** 285–316 (2013).

19. Chen, F.-M., Wu, L.-A., Zhang, M., Zhang, R. & Sun, H.-H. Homing of endogenous stem/progenitor cells for in situ tissue regeneration: Promises, strategies, and translational perspectives. *Biomaterials* **32,** 3189–209 (2011).

20. Bielby, R., Jones, E. & McGonagle, D. The role of mesenchymal stem cells in maintenance and repair of bone. *Injury* **38 Suppl 1,** S26–32 (2007).

21. Sada, A. & Tumbar, T. in *Int. Rev. Cell Mol. Biol.* (Biology, K. W. J. B. T.-I. R. of C. and M.) **Volume 300,** 1–50 (Academic Press, 2013).

22. De Bari, C., Kurth, T. B. & Augello, A. Mesenchymal stem cells from development to postnatal joint homeostasis, aging, and disease. *Birth defects Res. Part C Embryo today Rev.* **90,** 257–271 (2010).

23. Dominici, M. *et al.* Minimal criteria for defining multipotent mesenchymal stromal cells. The International Society for Cellular Therapy position statement. *Cytotherapy* **8,** 315–7 (2006).

24. Djouad, F. *et al.* Research article Transcriptional profiles discriminate bone marrow-derived and synovium-derived mesenchymal stem cells. **7,** 1304–1315 (2005).

25. Sakaguchi, Y., Sekiya, I., Yagishita, K. & Muneta, T. Comparison of Human Stem Cells Derived From Various Mesenchymal Tissues Superiority of Synovium as a Cell Source. *Arthritis Rheum.* **52,** 2521–2529 (2005).

26. Baksh, D., Yao, R. & Tuan, R. S. Comparison of proliferative and multilineage differentiation potential of human mesenchymal stem cells derived from umbilical cord and bone marrow. *Stem cells Dayt. Ohio* **25,** 1384–92 (2007).

27. Panepucci, R. a *et al.* Comparison of gene expression of umbilical cord vein and bone marrow-derived mesenchymal stem cells. *Stem Cells* **22,** 1263–78 (2004).

28. Wegmeyer, H. *et al.* Mesenchymal stromal cell characteristics vary depending on their origin. *Stem Cells Dev.* **22,** 2606–18 (2013).

29. Pittenger, M. F. *et al.* Multilineage Potential of Adult Human Mesenchymal Stem Cells. *Science (80-.).* **284,** 143–147 (1999).

30. Zuk, P. A. *et al.* Human Adipose Tissue Is a Source of Multipotent Stem Cells. *Mol. Biol. Cell* **13,** 4279–4295 (2002).

31. Bari, C. De & Dell'Accio, F. Multipotent mesenchymal stem cells from adult human synovial membrane. *Arthritis Rheum.* **44,** 1928–1942 (2001).

32. Nakahara, H. *et al.* In vitro differentiation of bone and hypertrophic cartilage from periosteal-derived cells. *Exp. Cell Res.* **195,** 492–503 (1991).

33. Johnson, K. *et al.* A Stem Cell–Based Approach to Cartilage Repair. *Science (80-.).* **336,** 717–721 (2012).

34. Qi, Y., Feng, G. & Yan, W. Mesenchymal stem cell-based treatment for cartilage defects in osteoarthritis. *Mol. Biol. Rep.* **39,** 5683–9 (2012).

35. Holmes, B., Castro, N. J., Li, J., Keidar, M. & Zhang, L. G. Enhanced human bone marrow mesenchymal stem cell functions in novel 3D cartilage scaffolds with hydrogen treated multi-walled carbon nanotubes. *Nanotechnology* **24,** 365102 (2013).

36. Orozco, L. *et al.* Treatment of knee osteoarthritis with autologous mesenchymal stem cells: a pilot study. *Transplantation* **95,** 1535–41 (2013).

37. El-Denshary, E. S. M., Rashed, L. a & Elhussiny, M. Mesenchymal stromal cells versus betamethasone can dampen disease activity in the collagen arthritis mouse model. *Clin. Exp. Med.* (2013). doi:10.1007/s10238-013-0248-3

38. Williams, R. *et al.* Identification and clonal characterisation of a progenitor cell sub-population in normal human articular cartilage. *PLoS One* **5,** e13246 (2010).

39. Jones, B. A., Pei, M. & Ph, D. Synovium-Derived Stem Cells : A Tissue-Specific Stem Cell for Cartilage Engineering and Regeneration. **18,** (2012).

40. Kurth, T. B. *et al.* Functional mesenchymal stem cell niches in adult mouse knee joint synovium in vivo. *Arthritis Rheum.* **63,** 1289–300 (2011).

41. Hunziker, E. B. & Rosenberg, L. C. Repair of partial-thickness defects in articular cartilage: cell recruitment from the synovial membrane. *J. Bone Joint Surg. Am.* **78,** 721–33 (1996).

42. Hunziker, E. B. Growth-factor-induced healing of partial-thickness defects in adult articular cartilage. *Osteoarthritis Cartilage* **9,** 22–32 (2001).

43. Yoshimura, H. *et al.* Comparison of rat mesenchymal stem cells derived from bone marrow, synovium, periosteum, adipose tissue, and muscle. *Cell Tissue Res.* **327,** 449–62 (2007).

44. Koelling, S. *et al.* Migratory chondrogenic progenitor cells from repair tissue during the later stages of human osteoarthritis. *Cell Stem Cell* **4,** 324–335 (2009).

45. Murphy, J. M., Fink, D. J., Hunziker, E. B. & Barry, F. P. Stem cell therapy in a caprine model of osteoarthritis. *Arthritis Rheum.* **48,** 3464–74 (2003).

46. Sato, M. *et al.* Direct transplantation of mesenchymal stem cells into the knee joints of Hartley strain guinea pigs with spontaneous osteoarthritis. *Arthritis Res. Ther.* **14,** R31 (2012).

47. Ahern, B. J., Parvizi, J., Boston, R. & Schaer, T. P. Preclinical animal models in single site cartilage defect testing: a systematic review. *Osteoarthr. Cartil.* **17,** 705–713 (2009).

48. Clark, L. D., Clark, R. K. & Heber-Katz, E. A new murine model for mammalian wound repair and regeneration. *Clin. Immunol. Immunopathol.* **88,** 35–45 (1998).

49. Gourevitch, D. *et al.* Matrix metalloproteinase activity correlates with blastema formation in the regenerating MRL mouse ear hole model. *Dev. Dyn.* **226,** 377–87 (2003).

50. Fitzgerald, J. *et al.* Evidence for articular cartilage regeneration in MRL/MpJ mice. *Osteoarthritis Cartilage* **16,** 1319–26 (2008).

51. Bari, C. De *et al.* Multipotent mesenchymal stem cells from adult human synovial membrane. *Arthritis Rheum.* **44,** 1928–1942 (2001).

52. Jones, E. a *et al.* Synovial fluid mesenchymal stem cells in health and early osteoarthritis: detection and functional evaluation at the single-cell level. *Arthritis Rheum.* **58,** 1731–40 (2008).

53. Pessler, F. *et al.* The synovitis of ‘‘ non-inflammatory ’’ orthopaedic arthropathies : a quantitative histological and immunohistochemical analysis. **68,** 1184–1187 (2008).

54. Cleland, L. G. & James, M. J. Osteoarthritis. Omega-3 fatty acids and synovitis in osteoarthritic knees. *Nat. Rev. Rheumatol.* **8,** 314–5 (2012).

55. Fan, J., Varshney, R. R., Ren, L., Cai, D. & Wang, D.-A. Synovium-derived mesenchymal stem cells: a new cell source for musculoskeletal regeneration. *Tissue Eng. Part B. Rev.* **15,** 75–86 (2009).

56. Soleimani, M. & Nadri, S. A protocol for isolation and culture of mesenchymal stem cells from mouse bone marrow. *Nat. Protoc.* **4,** 102–106 (2009).

57. Valorani, M. G., Germani, A., Otto, W. R. & Harper, L. Hypoxia increases Sca-1/CD44 co-expression in murine mesenchymal stem cells and enhances their adipogenic differentiation potential. *Cell Tissue Res* **341,** 111–120 (2010).

58. Morikawa, S. *et al.* Prospective identification, isolation, and systemic transplantation of multipotent mesenchymal stem cells in murine bone marrow. *J. Exp. Med.* **206,** 2483–2496 (2009).

59. Nimura, A. *et al.* Increased proliferation of human synovial mesenchymal stem cells with autologous human serum: comparisons with bone marrow mesenchymal stem cells and with fetal bovine serum. *Arthritis Rheum.* **58,** 501–10 (2008).

60. Boxall, S. a & Jones, E. Markers for characterization of bone marrow multipotential stromal cells. *Stem Cells Int.* **2012,** 975871 (2012).

61. Morikawa, S. *et al.* Prospective identification, isolation, and systemic transplantation of multipotent mesenchymal stem cells in murine bone marrow. *J. Exp. Med.* **206,** 2483–2496 (2009).

62. Uezumi, A., Fukada, S., Yamamoto, N., Takeda, S. & Tsuchida, K. Mesenchymal progenitors distinct from satellite cells contribute to ectopic fat cell formation in skeletal muscle. *Nat. Cell Biol.* **12,** 143–52 (2010).

63. Diekman, B. O. *et al.* Intra-articular delivery of purified mesenchymal stem cells from C57BL/6 or MRL/MpJ superhealer mice prevents post-traumatic arthritis. *Cell Transplant.* (2012). doi:10.3727/096368912X653264

64. Joe, A. W. B. *et al.* Muscle injury activates resident fibro/adipogenic progenitors that facilitate myogenesis. *Nat. Cell Biol.* **12,** 153–63 (2010).

65. Heldin, C. H., Ostman, a & Rönnstrand, L. Signal transduction via platelet-derived growth factor receptors. *Biochim. Biophys. Acta* **1378,** F79–113 (1998).

66. Ball, S. G., Shuttleworth, C. A. & Kielty, C. M. Inhibition of platelet-derived growth factor receptor signaling regulates Oct4 and Nanog expression, cell shape, and mesenchymal stem cell potency. *Stem cells Dayt. Ohio* **30,** 548–60 (2012).

67. Holmes, C. & Stanford, W. L. Concise review: stem cell antigen-1: expression, function, and enigma. *Stem Cells* **25,** 1339–47 (2007).

68. Kiel, M. J. *et al.* Haematopoietic stem cells do not asymmetrically segregate chromosomes or retain BrdU. *Nature* **449,** 238–42 (2007).

69. Futami, I., Ishijima, M., Kaneko, H., Tsuji, K. & Ichikawa-tomikawa, N. Isolation and Characterization of Multipotential Mesenchymal Cells from the Mouse Synovium. **7,** (2012).

70. Schatteman, G. C., Morrison-Graham, K., Van Koppen, a, Weston, J. a & Bowen-Pope, D. F. Regulation and role of PDGF receptor alpha-subunit expression during embryogenesis. *Dev. Cambridge Engl.* **115,** 123–31 (1992).

71. Rubin, K. *et al.* Expression of platelet-derived growth factor receptors is induced on connective tissue cells during chronic synovial inflammation. *Scand. J. Immunol.* **27,** 285–94 (1988).

72. Lee, J. I., Sato, M., Kim, H. W. & Mochida, J. Transplantatation of scaffold-free spheroids composed of synovium-derived cells and chondrocytes for the treatment of cartilage defects of the knee. *Eur. Cell. Mater.* **22,** 275–90; discussion 290 (2011).

73. Warnock, J. J., Fox, D. B., Stoker, A. M. & Cook, J. L. Evaluation of in vitro growth factor treatments on fibrochondrogenesis by synovial membrane cells from osteoarthritic and nonosteoarthritic joints of dogs. *Am. J. Vet. Res.* **72,** 500–11 (2011).

74. Mohyeldin, A., Garzón-Muvdi, T. & Quiñones-Hinojosa, A. Oxygen in stem cell biology: a critical component of the stem cell niche. *Cell Stem Cell* **7,** 150–61 (2010).

75. Fujita, H. *et al.* Necrotic and apoptotic cells serve as nuclei for calcification on osteoblastic differentiation of human mesenchymal stem cells in vitro. *Cell Biochem. Funct.* (2013). doi:10.1002/cbf.2974

76. Li, Z. *et al.* Epigenetic dysregulation in mesenchymal stem cell aging and spontaneous differentiation. *PLoS One* **6,** e20526 (2011).

77. Berniakovich, I. & Giorgio, M. Low oxygen tension maintains multipotency, whereas normoxia increases differentiation of mouse bone marrow stromal cells. *Int. J. Mol. Sci.* **14,** 2119–34 (2013).

78. Krinner, a, Zscharnack, M., Bader, a, Drasdo, D. & Galle, J. Impact of oxygen environment on mesenchymal stem cell expansion and chondrogenic differentiation. *Cell Prolif.* **42,** 471–84 (2009).

79. Basciano, L. *et al.* Long term culture of mesenchymal stem cells in hypoxia promotes a genetic program maintaining their undifferentiated and multipotent status. *BMC Cell Biol.* **12,** 12 (2011).

80. Gerter, R., Kruegel, J. & Miosge, N. New insights into cartilage repair — The role of migratory progenitor cells in osteoarthritis. *Matrix Biol. J. Int. Soc. Matrix Biol.* **31,** 1–8 (2012).

81. Ward, B. D. *et al.* Absence of posttraumatic arthritis following intraarticular fracture in the MRL/MpJ mouse. *Arthritis Rheum.* **58,** 744–53 (2008).

82. Holmes, C. & Stanford, W. L. Concise review: stem cell antigen-1: expression, function, and enigma. *Stem Cells* **25,** 1339–47 (2007).

83. Yasuda, A. *et al.* The stem cell factor/c-kit receptor pathway enhances proliferation and invasion of pancreatic cancer cells. *Mol. Cancer* **5,** 46 (2006).

84. Reber, L., Da Silva, C. a & Frossard, N. Stem cell factor and its receptor c-Kit as targets for inflammatory diseases. *Eur. J. Pharmacol.* **533,** 327–40 (2006).

85. Berenbaum, F. Osteoarthritis as an inflammatory disease (osteoarthritis is not osteoarthrosis!). *Osteoarthritis Cartilage* **21,** 16–21 (2013).

86. Lewis, J. S. *et al.* Genetic and cellular evidence of decreased inflammation associated with reduced incidence of posttraumatic arthritis in MRL/MpJ mice. *Arthritis Rheum.* **65,** 660–70 (2013).

87. Harris, Q. *et al.* Monocyte chemotactic protein-1 inhibits chondrogenesis of synovial mesenchymal progenitor cells: an in vitro study. *Stem Cells* **31,** 2253–65 (2013).

88. Eltawil, N. M., De Bari, C., Achan, P., Pitzalis, C. & Dell'accio, F. A novel in vivo murine model of cartilage regeneration. Age and strain-dependent outcome after joint surface injury. *Osteoarthritis Cartilage* **17,** 695–704 (2009).

89. Eltawil, N. M., De Bari, C., Achan, P., Pitzalis, C. & Dell'Accio, F. A novel in vivo murine model of cartilage regeneration. Age and strain-dependent outcome after joint surface injury. *Osteoarthr. Cartil.* **17,** 695–704 (2009).

90. Weishaupt, D., Köchli, V. D. & Marincek, B. *How does MRI work?* (Springer Berlin Heidelberg, 2003). doi:10.1007/978-3-662-07805-1

91. Goodwin, D. W., Wadghiri, Y. Z., Dunn, J. F., Density, P. & Effect, A. Micro-imaging of articular cartilage: T2, proton density, and the magic angle effect. *Acad. Radiol.* **5,** 790–798 (1998).

92. Niitsu, M. *Magnetic Resonance Imaging of the Knee*. *Am. J. ...* 200 (Springer Berlin Heidelberg, 2013). doi:10.1007/978-3-642-17893-1

93. Sokolove, J. & Lepus, C. M. Role of inflammation in the pathogenesis of osteoarthritis: latest findings and interpretations. *Ther. Adv. Musculoskelet. Dis.* **5,** 77–94 (2013).

94. Etich, J. *et al.* PECAM1(+)/Sca1(+)/CD38(+) vascular cells transform into myofibroblast-like cells in skin wound repair. *PLoS One* **8,** e53262 (2013).

95. Bulman, S. E., Barron, V., Coleman, C. M. & Barry, F. Enhancing the Mesenchymal Stem Cell Therapeutic Response : Cell Localization. **19,** 58–68 (2013).

96. Meirelles, L. D. S., Fontes, A. M., Covas, D. T. & Caplan, A. I. Mechanisms involved in the therapeutic properties of mesenchymal stem cells. *Cytokine Growth Factor Rev.* **20,** 419–27 (2009).

97. Da Silva Meirelles, L., Caplan, A. I. & Nardi, N. B. In search of the in vivo identity of mesenchymal stem cells. *Stem Cells* **26,** 2287–99 (2008).

98. Lee, K. B. L., Hui, J. H. P., Song, I. C., Ardany, L. & Lee, E. H. Injectable mesenchymal stem cell therapy for large cartilage defects--a porcine model. *Stem Cells* **25,** 2964–71 (2007).

99. Murphy, M. B., Moncivais, K. & Caplan, A. I. Mesenchymal stem cells: environmentally responsive therapeutics for regenerative medicine. *Exp. Mol. Med.* **45,** e54 (2013).

100. Evans, C. H. Advances in regenerative orthopedics. *Mayo Clin. Proc.* **88,** 1323–39 (2013).

101. Horie, M. *et al.* Intra-articular Injected synovial stem cells differentiate into meniscal cells directly and promote meniscal regeneration without mobilization to distant organs in rat massive meniscal defect. *Stem Cells* **27,** 878–87 (2009).

102. Toupet, K. *et al.* Long-term detection of human adipose-derived mesenchymal stem cells after intraarticular injection in SCID mice. *Arthritis Rheum.* **65,** 1786–94 (2013).

103. Park, J. *et al.* Transgene-activated mesenchymal cells for articular cartilage repair: a comparison of primary bone marrow-, perichondrium/periosteum- and fat-derived cells. *J. Gene Med.* **8,** 112–25 (2006).